Two-Dimensional Computation of the Outer Matching-Data in Resistive Stability Studies

A thesis submitted for the degree
of Doctor of Philosophy of
the Australian National University

Alexander Pletzer

May 14, 1992

This thesis is the fruit of my own original research. Contributions from others are explicitely acknowledged as such.

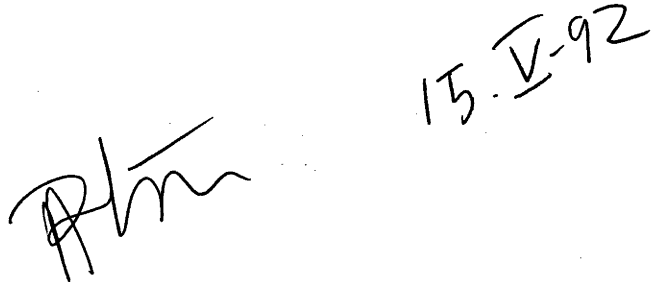

15. V. 92

Aknowledgements

I am greatly indebted to Dr R.L. Dewar, my supervisor, who has largely contributed to this work through his devoted support and by providing continual inspiration.

I would also like to thank Dr B.A. Robson for giving me the opportunity to pursue my PhD in the multi-disciplinary environment of the Department of Theoretical Physics.

The implementation of the matching-data variational method into the PEST code was facilitated by the help of Dr J. Manickam who also supplied me with equilibrium input files for the numerical test-cases. Dr J.M. Greene has played an important role in stimulating the quest for an energy principle.

This work was supported by an ANU scholarship and a stipend from the Fond National Suisse de la Recherche.

Abstract

The purpose of this thesis is to investigate the linear-stability properties of magnetically confined plasmas in the low-resistivity limit, with particular emphasis on toroidal and finite-β effects. It is well-known that, in this limit, the asymptotic matching method [Kerkovian & Cole (1981)] applies so that one is entitled to use the zero-resistivity approximation everywhere but in thin layers comprising the rational surfaces, where resistivity and other non-ideal effects dominate.

The problem of stability can be shown in some models [Glasser *et al.* (1975)], to reduce to the one of determining the data needed to match the asymptotic solutions arising in the outer region, with those emerging from the resistive layers [Greene (1976)]. The conditions for matching yield a dispersion relation. In the simplest case of a one-dimensional plasma, the outer matching-data are given by a single coefficient called Δ', which, if negative [Furth *et al.* (1963)], ensures stability with respect to tearing modes. The inclusion of finite-pressure and toroidal effects, however, leads to the introduction of additional matching-data which are responsible for the coupling of tearing modes with resistive interchange-modes.

To overcome the difficulty encountered in toroidal geometry by the emergence of regular solutions which modify the global solution behaviour near the rational surfaces without affecting the matching data, we have adapted and further developed a scheme by Miller & Dewar (1986), which expresses the matching data as a bilinear contcomitant jump at the rational surfaces. Using a relation similar to Green's theorem, we have been able to attach a symmetric functional to the definition of the matching data which leads to a variational principle.

We have implemented the variational algorithm into the finite-element stability code PEST, and applied successfully this method to test the tearing stability in

a range of cylindrical and toroidal plasmas, including finite-pressure equilibria. In addition to the inherent robustness of the variational principle, the method has a rich physical content, allowing easy demonstration of reciprocity relations between modes coupling different rational surfaces. Convergence rate proportional to the inverse number of mesh nodes were achieved for all cases.

The symmetric, energy-like expression of the concomitant jump has prompted further investigations, to determine whether an energy principle can exist, and under which conditions, in dissipative stability problems. From first principles, we find that for "causal" systems, a symmetric functional of the form of an energy can be defined as a Lyapunov functional. The definiteness of the time derivative of the energy yields a necessary and sufficient stability condition, subject to the causality condition being satisfied.

Contents

Chapter 1

Review of resistive instabilities

Since the works of Suydam (1958) and Newcomb (1960), the problem of stability of magnetically confined plasmas has been a subject of prime interest. This chapter is dedicated to reviewing the tools commonly used in analyzing the stability properties.

Stability analysis was first performed using the magnetohydrodynamics (MHD) approximation which has proven very successful in treating both ideal and resistive instabilities [Bateman (1978)]. It is thus natural to start in § 1.1 by introducing the set of equations that govern the motion of a conducting fluid in the presence of a magnetic field. In § 1.2, we restrict our attention to equilibrium solutions, or stationary solutions of the MHD equations, whereas the small-perturbation approximation is used in § 1.3 to linearize the plasma motion as it departs from equilibrium. The stability equations are applied in § 1.4 to a resistive slab-plasma with the aim of rederiving the tearing-stability criterion $\Delta' < 0$. Finally, the implications of extending the Furth *et al.* (1963) model to compressible-toroidal plasmas [Glasser *et al.* (1975)] are discussed in § 1.5.

1.1 MHD model

In the one-fluid approximation, the plasma obeys the Navier-Stokes equation

$$\partial_t(\rho \mathbf{v}) = -\boldsymbol{\nabla}\cdot\left[\rho \mathbf{v}\mathbf{v} - \mathbf{B}\mathbf{B} + \left(p + \frac{B^2}{2}\right) \mathsf{I}\,,\right] \tag{1.1}$$

written here in conservative form, with ρ being the density, $\mathbf{v}$ the macroscopic velocity (or flow) of the plasma, p the pressure and I the identity tensor. The magnetic field $\mathbf{B}$ (in rationalized e.m. units where $\mu_0 = 1$) evolves according to Faraday's law

$$\partial_t \mathbf{B} = -\nabla\cdot(\mathbf{vB} - \mathbf{Bv}) - \nabla\times(\eta\nabla\times\mathbf{B}), \tag{1.2}$$

with the right-hand side being $-\nabla\times\mathbf{E}$, the curl of the electric field, which has been replaced in favour of $\mathbf{B}$ after using Ohm's law, $\nabla\times\mathbf{B} = \eta^{-1}(\mathbf{E} + \mathbf{v}\times\mathbf{B})$. Only the last term in (1.2) is affected by the resistivity η. Note that $\partial_t\nabla\cdot\mathbf{B} = 0$ is implicitly satisfied in (1.2) whereas

$$\nabla\cdot\mathbf{B} = 0 \tag{1.3}$$

must be used as an additional constraint when employing the diffusive form of (1.2), $\partial_t\mathbf{B} = \eta\nabla^2\mathbf{B} + \nabla\times(\mathbf{v}\times\mathbf{B})$ (assuming $\nabla\eta = 0$).

The system of Eqs.(1.1) and (1.2) is closed with the mass-conservation equation

$$\partial_t\rho = -\nabla\cdot(\rho\mathbf{v}) \tag{1.4}$$

and the entropy-conservation equation

$$(\partial_t + \mathbf{v}\cdot\nabla)\left[\frac{p}{\rho^\Gamma}\right] = 0, \tag{1.5}$$

written in a form neglecting heat conduction, where $\Gamma = 5/3$ is the ratio of specific heats.

1.2 Equilibrium

The equilibrium equations are found by setting $\partial_t = 0$ in Eqs.(1.1)–(1.5). For the flowless case, $\mathbf{v} = 0$, (1.1) reduces to

$$\nabla p = (\nabla\times\mathbf{B})\times\mathbf{B}. \tag{1.6}$$

In order to satisfy (1.3), it is convenient to express the magnetic field in arbitrary geometry as

$$\mathbf{B} = \nabla\alpha\times\nabla\psi \tag{1.7}$$

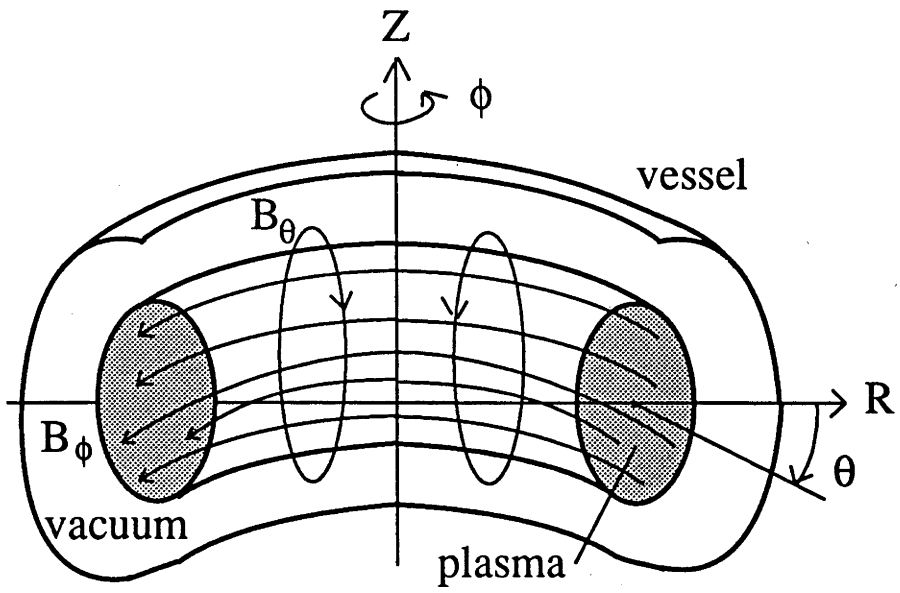

Figure 1.1: Toroidal coordinate-system.

with

$$\psi = \frac{1}{(2\pi)^2} \int d\tau \mathbf{B}\cdot\nabla\theta \tag{1.8}$$

representing the *poloidal-flux* coordinate and θ being the poloidal angle shown in Fig. 1.1. Rather than working with an orthogonal system of coordinates, we find it preferable from an analytical and numerical viewpoint to choose the second independent coordinate to be $\zeta \equiv \phi - q(\psi)\delta(\psi,\theta)$, where ϕ is the toroidal angle increasing by 2π after completing a turn along the toroidal direction [see Fig. 1.1]. The function $\delta(\psi,\theta)$, periodic in θ, is chosen such that the field lines of $\mathbf{B}$ be straight in the (θ,ζ)-coordinate representation with the ratio

$$\frac{\mathbf{B}\cdot\nabla\zeta}{\mathbf{B}\cdot\nabla\theta} \equiv q(\psi) \tag{1.9}$$

defining the *safety factor*. The safety factor plays a crucial role in resistive stability; the ψ-surfaces where q takes a rational value, henceforth called *rational surfaces*, are vulnerable to resistive instabilities as will be seen subsequently in § 1.4 and § 1.5.

Equation (1.9) is satisfied for

$$\alpha = \zeta - q(\psi)\theta \tag{1.10}$$

which can then be substituted into (1.7) to give $\mathbf{B} = [\nabla\zeta - q(\psi)\nabla\theta]\times\nabla\psi$. This magnetic field representation will be used in Ch. 4 to derive the ideal-stability equation.

Another useful representation of $\mathbf{B}$ in axisymmetric-toroidal geometry is

$$\mathbf{B} = \nabla\phi\times\nabla\psi + g(\psi)\nabla\phi, \tag{1.11}$$

as (1.11) leads to an elliptic equation for the ψ-flux, [Bateman (1978), Grimm *et al.* (1983)]

$$\Delta^*\psi = -R^2p'(\psi) - g(\psi)g'(\psi), \tag{1.12}$$

called the Grad-Shafranov equation with

$$\Delta^*\psi \equiv R^2\nabla\cdot\left(\frac{1}{R^2}\nabla\psi\right). \tag{1.13}$$

1.3 Linear perturbations

The complexity of Eqs.(1.1)–(1.5) is intractable except in the simplest geometry. One is thus led to introduce approximations in order to be able to describe the dynamical regime of the plasma as it moves from the initial equilibrium. There are two issues of interest regarding the stability of plasmas against these perturbations: firstly, one may be interested in determining whether the plasma spectrum admits unstable, growing modes and secondly, if so, whether the evolution of these instabilities will ultimately disrupt the confinement (disruptive instabilities), or on the contrary saturate and possibly even disappear. The determination of the long-time evolution requires a non-linear MHD description of the model, this has been the object of studies by Parker *et al.* (1990), Parker & Dewar (1989), and others who used the so called reduced-MHD equations [Strauss *et al.* (1976)] which discard two- and higher-dimensional effects. The approach taken in the present work focuses on the initial regime with particular emphasis on two-dimensional effects. Equations (1.1)–(1.5) can then be reduced, in the small perturbation limit $\epsilon \ll 1$, to a set of

linear equations

$$\left.\begin{array}{rcl} \mathbf{B} & \mapsto & \mathbf{B} + \epsilon \mathbf{b} \exp(\gamma t) \\ \mathbf{v} & \mapsto & \epsilon \mathbf{v} \exp(\gamma t) \\ \rho & \mapsto & \rho + \epsilon(\delta\rho) \exp(\gamma t) \\ p & \to & p + \epsilon(\delta p) \exp(\gamma t) \end{array}\right\}, \tag{1.14}$$

for the perturbed quantities $\mathbf{b}$, $\mathbf{v}$, $\delta\rho$ and δp. Henceforth, we adopt the convention that lower-case symbols and symbols preceded by a δ designate the small, time-dependent perturbations, while $\mathbf{B}$, ρ and p denote the equilibrium quantities which are assumed to be either static or else evolve on a much longer time-scale than $\mathbf{b}$, $\mathbf{v}$, $\delta\rho$ and δp respectively. Equation (1.6) is recovered at order ϵ^0. One finds at next order in ϵ using Eqs.(1.1)–(1.5):

$$\rho \partial_t \mathbf{v} = \nabla \cdot [\mathbf{b}\mathbf{B} + \mathbf{B}\mathbf{b} - (\delta p + \mathbf{B}\cdot\mathbf{b})\, \mathsf{I}\,], \tag{1.15}$$

$$\partial_t \mathbf{b} = \nabla \times (\mathbf{v} \times \mathbf{B}) - \nabla \times (\eta \nabla \times \mathbf{b}), \tag{1.16}$$

and

$$\partial_t \delta\rho = -\mathbf{v}\cdot\nabla\rho - \rho \nabla\cdot\mathbf{v} \tag{1.17}$$

$$\partial_t \delta p = -\mathbf{v}\cdot\nabla p - \Gamma p \nabla\cdot\mathbf{v}. \tag{1.18}$$

In the limit of $\eta \to 0$, (1.16) simplifies to

$$\mathbf{b} = \nabla \times (\boldsymbol{\xi} \times \mathbf{B}). \tag{1.19}$$

This is the limit where magnetic-field lines are "frozen" to the displacement field $\boldsymbol{\xi} \equiv \partial_t \mathbf{v}$. Equation (1.19) can then be used to eliminate $\mathbf{b}$ in (1.15).

1.4 Tearing modes

As a result of ionization, the conductivity $\sigma \equiv \eta^{-1}$ of the plasma is usually very high

$$\sigma \approx 1.5 \times 10^{-2} \ln \Lambda^{-1} T^{3/2} \quad \Omega^{-1} m^{-1} \tag{1.20}$$

[Spitzer (1962)] and increases further with temperature T in $^\circ K$. ($\ln \Lambda$ is of the order of 10 for most plasmas.) This justifies the widely used approximation of infinite conductivity, or $\eta \to 0$ used to derive (1.19) from (1.2), yet experiments have

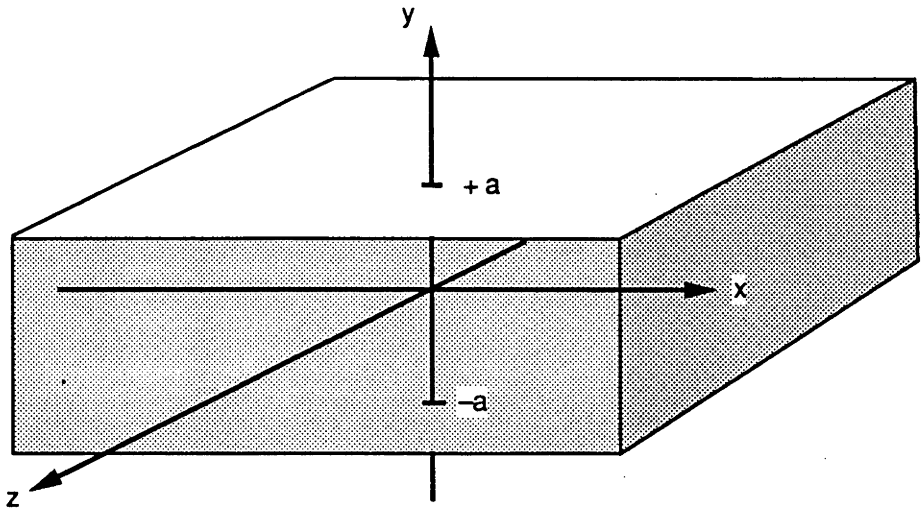

Figure 1.2: Slab geometry.

shown that plasmas that should be stable according to the ideal assumption can nevertheless exhibit instabilities characterized by very small growth-rates compared to the ideal modes. Furth *et al.* (1963) have suggested that resistive instabilities could account for these experimental observations.

Let us rederive here the stability criterion for resistive modes in the most simple case of a plasma in slab geometry, as shown in Fig. 1.2, and furthermore restrict ourselves in this first approach to the problem of "tearing" modes only, despite the existence of two other types of modes referred to by Furth *et al.* (1963) as the "rippling" and the "g-interchange" instabilities. The g-interchange mode is driven by finite-pressure gradients and will be discussed in § 1.5. The rippling mode is discarded here because it is driven by gradients of the resistivity which we neglect,

$$\eta = \text{const} \tag{1.21}$$

will be assumed in the regions of magnetic reconnection.

For simplicity, pressure and flow are chosen zero so that (1.6) reduces to

$$\mathbf{B}''(y) = 0 \tag{1.22}$$

in the slab, with $\mathbf{B}(y) = B_x\mathbf{e}_x + B_z\mathbf{e}_z$. One then obtains by taking $\mathbf{e}_y \cdot \nabla \times \nabla \times$ of (1.15)

$$k^2\rho\partial_t v - \partial_y\left[\rho\partial_y\partial_t v\right] = -\mathbf{B}\cdot i\mathbf{k}(\partial_y{}^2 - k^2)b \tag{1.23}$$

and dotting $\mathbf{e}_y$ with (1.16)

$$\partial_t b = \eta \left[\partial_y{}^2 b - k^2\right] + \mathbf{B}\cdot i\mathbf{k}v, \tag{1.24}$$

where

$$\begin{aligned} b &\equiv \mathbf{b}\cdot\mathbf{e}_y \\ v &\equiv \mathbf{v}\cdot\mathbf{e}_y \end{aligned} \tag{1.25}$$

are the perturbations having the $\exp i(k_x x + k_z z)$ dependence with

$$k^2 \equiv k_x^2 + k_y^2. \tag{1.26}$$

In (1.23), the incompressibility condition $\nabla\cdot\mathbf{v} = 0$ is used to decouple the motion of p and ρ, rendering Eqs.(1.17) and (1.18) superfluous. The incompressibility assumption drastically simplifies the system of equations since the components of $\mathbf{b}$ and $\mathbf{v}$ normal to $\mathbf{B}$ decouple from those lying in the plane of $\mathbf{B}$ in the slab.

It is convenient to normalize all quantities so as to become dimensionless: define

$$\left.\begin{aligned} \Psi &\equiv b/B \\ F &\equiv \mathbf{B}\cdot\mathbf{k}/Bk \\ \zeta &\equiv y/a \\ \alpha &\equiv ka \\ r &\equiv \rho/\bar{\rho} \end{aligned}\right\} \tag{1.27}$$

where $\bar{\rho}$ is a measure of the density and a is the height of the slab as shown in Fig. 1.2. The time t is rescaled

$$s \equiv \frac{t}{\tau_R} \tag{1.28}$$

with respect to the resistive diffusion time

$$\tau_R \equiv a^2/\eta \ll \tau_A \tag{1.29}$$

which is much longer than the typical transit-time of ideal MHD

$$\tau_A \equiv a\bar{\rho}^{1/2}/B, \tag{1.30}$$

that is the Alfvén time-scale. Introducing the Lundquist (magnetic Reynold's) number

$$S \equiv \tau_R/\tau_A \gg 1 \tag{1.31}$$

and

$$w \equiv -ik\tau_R v, \tag{1.32}$$

Eqs.(1.23) and (1.24) lead to

$$\begin{aligned} \alpha^2 r\partial_s w - \partial_\zeta\left[r\partial_s\partial_\zeta w\right] &= S^2\alpha^2 F\left[\alpha^2\Psi - \partial_\zeta{}^2\Psi\right] \\ &= -F(\zeta)S^2\alpha^2\left[\partial_s\Psi + Fw\right] \end{aligned} \tag{1.33}$$

and

$$\partial_s\Psi = \partial_\zeta{}^2\Psi - \alpha^2\Psi - Fw. \tag{1.34}$$

The limit of $\eta \to 0$ is readily recovered by taking $S \to \infty$ in (1.33), yielding the frozen magnetic-field relation

$$\partial_s\Psi = -Fw \tag{1.35}$$

of (1.19), as well as the ideal equation

$$\partial_\zeta{}^2\Psi - \alpha^2\Psi = 0. \tag{1.36}$$

Equation (1.36) may be thought of as the stability equation for the outer region without, however, exhibiting the well-known singularity at $F = 0$ that characterizes Newcomb's equation [Newcomb (1960)]. The reason for this lies in the slab-geometry and $\eta = \text{const}$ assumptions, for one can show that the Newcomb equation takes the form [Furth *et al.* (1973)]

$$\partial_\zeta{}^2\Psi - \left[\frac{g_0}{\zeta^2} + \frac{g_1}{\zeta} + g_2 + \mathcal{O}(\zeta)\right]\Psi = 0 \tag{1.37}$$

in cylindrical geometry, with g_0 being proportional to the pressure gradient and $g_1 = F''/F$ [Furth *et al.* (1963)]. Both g_0 and g_1 vanish here due to the zero-pressure hypothesis and due to (1.22). [In Furth *et al.* (1963) $F'' = -\eta' F'/\eta$, where $\eta' \equiv d\eta/dy$, is nonvanishing because of the peculiar choice of the resistivity profile.] We are not interested here in finding a rigorous description of the outer region, leaving this task to Ch. 4 where the outer-region equation will be derived in toroidal geometry. This section focuses instead on the region where F is approximately zero.

We may choose conveniently the value of ζ where $F = 0$ to be $\zeta = 0$ so that, in the inner layer, the region of interest where the right-hand side of (1.33) is of the same order as the left-hand side, we have $\zeta \sim \epsilon$ and $F = F_0'\epsilon\zeta + \mathcal{O}(\epsilon^2)$ where

$$\epsilon \sim (S\alpha)^{-2}F_0'^{-1} \ll 1 \tag{1.38}$$

is the inner-layer width. Assuming $F_0' \sim r \sim q \sim 1$, one can choose the inner-layer width to be

$$\epsilon \equiv \left(\frac{qr}{S^2 \alpha^2 F_0'^2} \right)^{\frac{1}{4}} \tag{1.39}$$

with q denoting the normalized growth-rate $[\partial_s u(\zeta, s) \equiv qu(\zeta, s),\ u \in \{w, \Psi\}]$. Defining

$$\begin{aligned} \theta &\equiv \zeta/\epsilon \\ V &\equiv \epsilon w, \end{aligned} \tag{1.40}$$

then (1.33) and (1.34) reduce to

$$V''(\theta) - \theta^2 V = \frac{q}{F_0'} \theta \Psi \tag{1.41}$$

$$\Psi''(\theta) - q\Psi = F_0' \theta V, \tag{1.42}$$

with the terms proportional to ϵ^2 discarded as $F_0' \sim \alpha^2 \sim 1$ are assumed to be of same order.

It is clear from the symmetry property of Eqs.(1.41) and (1.42) under reflection $\theta \mapsto -\theta$ that V and Ψ must be of opposite parity. Expanding

$$\begin{aligned} \Psi &= \Psi_0 + \zeta \Psi_1 + \cdots \\ &= \Psi_0 + \theta \epsilon \Psi_1 + \cdots \end{aligned} \tag{1.43}$$

in ϵ around $\zeta = 0$, it is found that Ψ is predominantly even so that one may use the constant-Ψ approximation, $\Psi = \Psi_0$, everywhere in Eqs.(1.41) and (1.42) except where Ψ appears in the form of a derivative, as in the left-hand side of (1.42). The latter equation can be integrated to yield

$$\Delta(q) \equiv \frac{1}{\Psi_0} \int_{-\infty}^{+\infty} d\theta \Psi''(\theta) \tag{1.44}$$

the jump of derivative in the inner layer. A corresponding quantity can be defined in the outer region,

$$\Delta' \equiv \frac{1}{\Psi_0} \lim_{\zeta \to 0+} \left[\partial_\zeta \Psi(\zeta) - \partial_\zeta \Psi(-\zeta) \right], \tag{1.45}$$

ensuring the smooth matching between outer and inner solutions when

$$\Delta' = \epsilon \Delta(q). \tag{1.46}$$

The technique for calculating $\Delta(q)$ consists in expanding

$$\begin{aligned} V &= \sum_{n=0}^{\infty} V_n \exp(-\tfrac{1}{2}\theta^2) H_{2n+1}(\theta) \\ \Psi &= \sum_{n=0}^{\infty} \Psi_n \exp(-\tfrac{1}{2}\theta^2) H_{2n}(\theta) \end{aligned} \tag{1.47}$$

in Hermite polynomials $H_n(\theta)$ which satisfy $d^2H_n(\theta)/d\theta^2 - [\theta^2 + 2n + 1]H_n(\theta) = 0$ and form a complete set of eigenfunctions subject to the orthogonality relation

$$\int_{-\infty}^{\infty} d\theta \exp(-\theta^2) H_n(\theta) H_m(\theta) = 2^n \sqrt{\pi} n!\, \delta_{nm}. \tag{1.48}$$

Introducing (1.47) into Eqs.(1.41) and (1.42) gives

$$\begin{aligned} \Delta(q) = q\pi^{-\frac{1}{2}} \sum_{n=0}^{\infty} \frac{4^{-n}}{\Gamma(2n+1)} \Bigg\{ \Bigg[\int_{-\infty}^{\infty} d\theta \exp(-\theta^2) H_{2n}(\theta) \Bigg]^2 \\ - \frac{1}{2(4n+3)(2n+1)} \Bigg[\int_{-\infty}^{\infty} d\theta \exp(-\theta^2) \theta H_{2n+1}(\theta) \Bigg]^2 \Bigg\}, \end{aligned} \tag{1.49}$$

which can be further reduced using [Gradshteyn & Ryzhik (1980)]

$$\int_{-\infty}^{\infty} d\theta \exp(-\tfrac{1}{2}\theta^2) H_{2n}(\theta) = \sqrt{2\pi} \frac{\Gamma(2n+1)}{\Gamma(n+1)} \tag{1.50}$$

and the recurrence relation $\theta H_{2n+1}(\theta) = (2n+1)H_{2n}(\theta) + \frac{1}{2}H_{2n+2}(\theta)$, to

$$\Delta(q) = \frac{q}{2} \sum_{n=0}^{\infty} \frac{\Gamma(n+\frac{1}{2})}{(n+\frac{3}{4})\, n!}. \tag{1.51}$$

This series can in turn be easily expressed in terms of the hypergeometric function ${}_2F_1(\frac{1}{2}, \frac{3}{4}, \frac{7}{4}|1)$ of argument one, yielding

$$\Delta(q) = 2\pi q \frac{\Gamma(\frac{3}{4})}{\Gamma(\frac{1}{4})}. \tag{1.52}$$

Therefore, $\Delta(q)$ possesses the sign of the normalized growth-rate q; but since q is positive in virtue of (1.39) it is found that no matching between inner-layer and outer-region solutions is possible when Δ' of (1.45) is negative. The stability criterion can then be written using (1.46) as

$$\Delta' < 0. \tag{1.53}$$

There also exists an analytical expression for Δ' in this example, in fact using (1.36) one finds that $\Delta' = -2\alpha$, but as it was already pointed out, this result is

not expected to hold in any realistic configuration in which geometrical effects such as curvature play a dominant role [or even a y dependence of η is shown in Parker & Dewar (1989) to violate (1.53)]. In the inner region, however, the slab geometry may well be a satisfactory model for describing the tearing-mode evolution in that most quantities can be taken to be constant in the limit of small ϵ, so that the quest to determine stability essentially reduces to computing Δ' in the outer region. This is the main object of this thesis. We refer the reader to Chapters 6–8 for the detailed exposition of a variational scheme for the accurate computation of Δ' in toroidal geometry.

1.5 Finite-compressibility effects

As already pointed out, the assumption of incompressibility has the merit of simplifying considerably the resistive equations. Removing this assumption gives rise to the coupling between all components of both $\mathbf{b}$ and $\mathbf{v}$ so that additional assumptions must be introduced in order to close the system of equations. One may use in this regard (1.31) to show that the sum of the plasma pressure and magnetic pressure perturbation

$$\delta p + \mathbf{B}\cdot\mathbf{b} \approx 0 \tag{1.54}$$

approximately balances on the Alfvén time scale τ_A, several orders of magnitude shorter that the diffusion time τ_R. As a consequence, the total-pressure contribution in (1.15) is recessive although each term composing (1.54) may in fact dominate individually over the remaining contributions in (1.15). This is the prime difficulty in tackling the equations for the finite-pressure case. One way to overcome this difficulty was suggested by Coppi *et al.* (1966) and consists in employing an "annihilator", that is, an operator that kills the total pressure contribution in (1.15).

Avoiding here the further development of machinery for the derivation of the resistive equations, let us instead reproduce the low-resistivity equations (9), (22) and (23) of Glasser *et al.* (1975). Using the notation of the authors, these equations,

$$\dot{\Psi} + X\dot{\Xi} - H\Upsilon' - \Psi'' = 0, \tag{1.55}$$

$$-\ddot{\Xi}'' + X\dot{\Psi} + X^2\dot{\Xi} + H\Psi' - (E+F)\Upsilon = 0 \tag{1.56}$$

and

$$-KH\ddot{\Psi}' + (KE - G)\ddot{\Xi} + (G + KF)\ddot{\Upsilon} - \dot{\Upsilon}'' + X\Psi + X^2\Upsilon = 0, \qquad (1.57)$$

are valid in toroidal geometry. Equations (1.55)–(1.57) govern the motion of the following rescaled fields: Ψ is the magnetic-field normal to the rational surface (resistive layer), Ξ the normal displacement field and Υ the contribution of the magnetic-field along the equilibrium field. Primes denote derivation with respect to the normal coordinate X and "dots" derivation with respect to the rescaled time: e.g. $\dot{\Psi} \equiv Q\Psi$ where Q is the growth rate. Note that the definition of Ψ used in Eqs.(1.55)–(1.57) has opposite sign to the Ψ defined in Glasser *et al.* (1975), this in order to be consistent with earlier equations and in particular with those of Furth *et al.* (1963) [see (1.42)]. For the exact definition of the coefficients involved in Eqs.(1.55)–(1.57) we refer to Glasser *et al.* (1975). We need however, to demystify the role of some coefficients: H is a measure of the toroidicity which, combined with E and F, forms the Mercier parameter

$$D_I \equiv E + F + H - \tfrac{1}{4} \qquad (1.58)$$

whose sign determines stability, $D_I < 0$, towards localized ideal-modes. Similarly the parameter

$$D_R \equiv E + F + H^2 \qquad (1.59)$$

bears a stability criterion as will be shown shortly, against resistive-interchange modes [Glasser *et al.* (1975)].

There are two limiting cases of interest; first set $H = 0$ in Eqs.(1.55)–(1.57) to obtain the cylindrical limit. Equation (1.55) is then recognized as having the same form as (1.42) with Eqs.(1.55)–(1.57) corresponding to Eqs.(60)–(62) of Coppi *et al.* (1966) while $G \equiv B^2/(\Gamma p)$ is proportional to β^{-1}, the ratio of magnetic to plasma pressure. Therefore the terms containing G become increasingly dominant as $p \to 0$. Expanding

$$\left.\begin{aligned} \Psi &= \Psi^{(0)} + \epsilon\Psi^{(1)} + \epsilon^2\Psi^{(2)} + \cdots \\ \Xi &= \Xi^{(0)} + \epsilon\Xi^{(1)} + \epsilon^2\Xi^{(2)} + \cdots \\ \Upsilon &= \Upsilon^{(0)} + \epsilon\Upsilon^{(1)} + \epsilon^2\Upsilon^{(2)} + \cdots \end{aligned}\right\} \qquad (1.60)$$

in the small parameter $\epsilon \ll 1$ representing the inverse aspect-ratio (small toroidicity) and taking $H \sim \epsilon$ and $G \sim \epsilon^{-1}$, (1.57) then reduces at lowest order to

$$\Upsilon^{(0)} = \Xi^{(0)}, \tag{1.61}$$

whereas Eqs.(1.55)–(1.56) simplify to [dropping the superscripts (0)]

$$\left.\begin{aligned} \dot{\Psi} + X\dot{\Xi} - \Psi'' &= 0 \\ -\ddot{\Xi}'' + X\dot{\Psi} + X^2\dot{\Xi} - D_R\Xi &= 0 \end{aligned}\right\}. \tag{1.62}$$

Equations (1.62) are Eqs.(42) and (43) of Johnson *et al.* (1963) for slow-interchange modes.

To investigate the asymptotic behaviour of the solutions as $|X| \to \infty$, consider as *ansatz*

$$\left.\begin{aligned} \Psi &= X^{\alpha+1}\left(b_0 + b_1/X + b_2/X^2 \cdots\right) \\ \Xi &= X^{\alpha}\left(c_0 + c_1/X + c_2/X^2 \cdots\right) \\ \Upsilon &= X^{\alpha}\left(d_0 + d_1/X + d_2/X^2 \cdots\right) \end{aligned}\right\}. \tag{1.63}$$

Substituting (1.63) into Eqs.(1.55)–(1.57) and (1.62) gives

$$\left.\begin{aligned} c_0 &= d_0 = -b_0 \\ c_1 &= d_1 = -b_1 \end{aligned}\right\} \tag{1.64}$$

at lowest order and at next order in X^{α}, these coefficients are otherwise arbitrary. At the following order one obtains

$$\alpha = -\tfrac{1}{2} \pm \sqrt{-D_I}, \tag{1.65}$$

a result that is consistent with the asymptotic behaviour of the solutions arising in the outer region [c.f. Ch. 4]. Requiring α of (1.65) to be real one gets the local criterion against ideal modes [Suydam (1958)]

$$D_I < 0. \tag{1.66}$$

Other solutions of Eqs.(1.55)–(1.57) and (1.62) include exponentially large and small solutions which cannot be matched to outer solutions and thus must be set to zero at the matching interface, that is the coefficient of the large solution is zero whereas the small coefficient is arbitrary. These solutions are not without physical implications as they give rise to interchange instabilities which are subject to the

criterion (1.72) which bears similarity to (1.66). Focusing on modes of power-like asymptotic behaviour, Eqs.(1.64) provide sufficient degree of freedom for matching to the outer region. One may for this purpose rewrite (1.63)

$$\begin{aligned}\Xi &= C_+\left(|X|^{\alpha^{(b)}} + \Delta_+(Q)|X|^{\alpha^{(s)}} + \Delta_-(Q)|X|^{\alpha^{(s)}}\mathrm{sgn}X\right) \\ &\quad + C_-\left(|X|^{\alpha^{(b)}}\mathrm{sgn}X + \Delta_-(Q)|X|^{\alpha^{(s)}} + \Delta_+(Q)|X|^{\alpha^{(s)}}\mathrm{sgn}X\right), \quad (1.67)\end{aligned}$$

in terms of "dominant", $\alpha^{(s)} \equiv -\frac{1}{2} + \sqrt{-D_I}$, and "recessive", $\alpha^{(b)} \equiv -\frac{1}{2} - \sqrt{-D_I}$ solutions of even and odd parity. [Note that the designation of dominant and recessive relies in the inner layer on how fast the solutions decrease at infinity whereas we will term small and big, respectively, the corresponding solutions arising in the outer region, where a small exponent gives rise to a weaker singularity.] Assuming a similar expansion for the outer solutions in $x \equiv \epsilon X$, $\epsilon \ll 1$ being the width of the layer, matching is accomplished provided the following dispersion relation

$$\Delta_+(Q)\Delta_-(Q) + \tfrac{1}{2}\epsilon\left[\Delta_+(Q) + \Delta_-(Q)\right]\Delta' + \mathcal{O}(\epsilon^2) = 0 \quad (1.68)$$

given by Eq.(94) of Glasser *et al.* (1984), also reproduced here by (6.15), is satisfied. Equation (1.68) is a generalization of (1.46) to finite-pressure modes. As ϵ vanishes in the limit of $\eta \to 0$, these modes are characterized by $\Delta_+(Q) \ll \Delta_-(Q)$ for the *tearing* parity and $\Delta_+(Q) \gg \Delta_-(Q)$ for the *interchange* parity.

The value of

$$\Delta_-(Q) = a(H)Q^{\frac{5}{4}} - D_R b(H)Q^{-\frac{1}{4}} \quad (1.69)$$

is calculated in Glasser *et al.* (1975); for $H = 0$,

$$\begin{aligned}a(0) &= 2\pi\frac{\Gamma(\frac{3}{4})}{\Gamma(\frac{1}{4})} \\ b(0) &= \pi^2\frac{\Gamma(\frac{3}{4})}{\Gamma(\frac{1}{4})}.\end{aligned} \quad (1.70)$$

Glasser *et al.* (1975) use a Nyquist-plot argument to discuss the stability of the solution of Eqs.(1.68)–(1.70); provided $a(H)$ and $b(H)$ are positive in the regime of $H \approx 0$ we are interested in, it is apparent from Figs.1.3 and 1.4 that the sign of D_R determines stability as there exists no root (tearing-stability condition) to

$$\Delta_-(Q) = 0 \quad (1.71)$$

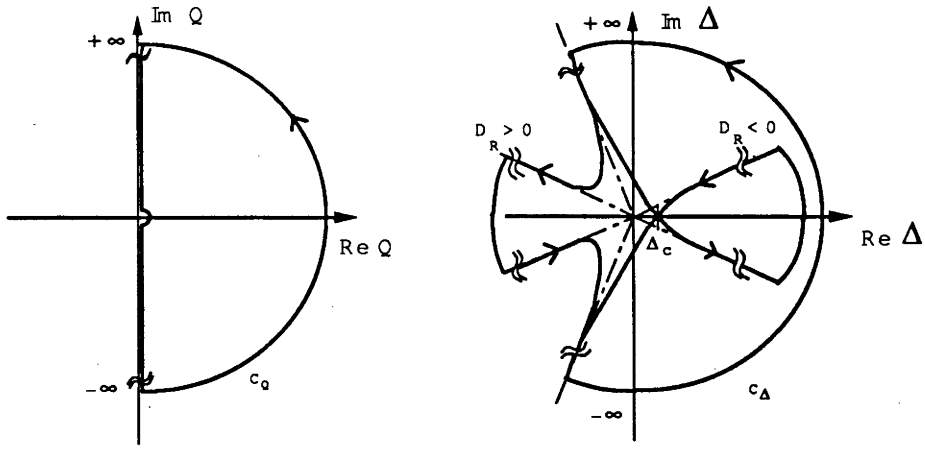

Figure 1.3: Nyquist plot: the number of times C_Δ encircles the origin gives the number of zeros minus the number of poles of $\Delta_-(Q)$ inside the contour C_Q. Here, C_Q is chosen to circumscribe the unstable half-plane $\mathrm{Re}Q > 0$ where $\Delta_-(Q)$ is analytic (no poles). Note that changing the sign of D_R causes the map: $Q \to \Delta_-(Q)$ to bifurcate. For $D_R < 0$, $\Delta_-(Q) - C = 0$, where C is any constant, possesses a root only for $C > \Delta_c > 0$.

for

$$D_R < 0 \tag{1.72}$$

while on the other hand there is always a growth rate Q such that (1.71) is satisfied for $D_R > 0$. Note that this is in disagreement with the results of Glasser *et al.* (1975) where the dispersion relation is expressed as (1.46) instead of (1.68), thus conflicting with the idea that matching can be achieved for any $\Delta_-(Q)$ but those for which

$$\Delta_-(Q) = \mathcal{O}(\epsilon). \tag{1.73}$$

In this picture, it is at least questionable whether the critical Δ_c of Fig. 1.3 is meaningful except, perhaps for $D_R = \mathcal{O}(\epsilon)$. Greene (1992) agrees about (1.73) but argues that despite the restriction imposed by (1.73), there are also experiments that confirm the existence of magnetic reconnection in highly conductive plasmas. This may be the result of ϵ being not always as small as expected, $\epsilon \sim \eta^{\frac{1}{3}}$ in real machines. However, he also points to the need to refine the existing model which exhibits anomalies especially as $Q \to 0$ which translate into an extreme sensitivity of Δ_-, arising simultaneously the issue whether the widely used zero-frequency approximation for the outer solutions is still appropriate in this limit.

Rosenau (1983) suggested that the singularity of the dispersion relation is the re-

sult of neglecting other slow-growth effects such as viscosity and transport [Dobrott *et al.* (1977)] for instance, which could alter substantially the scaling. However, introducing high-order effects may not prove always satisfactory especially if the resulting modes exhibit growth rates which scale higher in the resistivity, as the distinction between a slowly evolving equilibrium and an exponentially growing instability may well become fuzzy. In this regime of $Q \to 0$, modes may not be subjected to exponential growth so that a non-linear treatment becomes imperative to account for power-like growth behaviours. We see this problem already emerging between the interchange modes, characterized by growth rates scaling as $\gamma \sim \eta^{\frac{1}{3}}$, and tearing modes which have $\gamma \sim \eta^{\frac{3}{5}}$.

Finally, let us mention the results of Iacono & Bhattacharjee (1992) who came to the conclusion that finite-β growth-rates are undiscernible from zero-β growth-rates except for $S > 10^7$. This is also the regime where the growth rate scales as S^{-1} (proportional to the resistivity!) instead of $\gamma \sim S^{-3/5}$ for $S < 10^7$. To conclude, we may state that the regime where Δ_c has a sensible effect corresponds to high Lundquist numbers and is associated with extremely slow growth rates for which linear stability may not apply. For $S < 10^7$, the stability criterion (1.53) is necessary and sufficient and remains sufficient for $S \geq 10^7$ for Δ_c is positive.

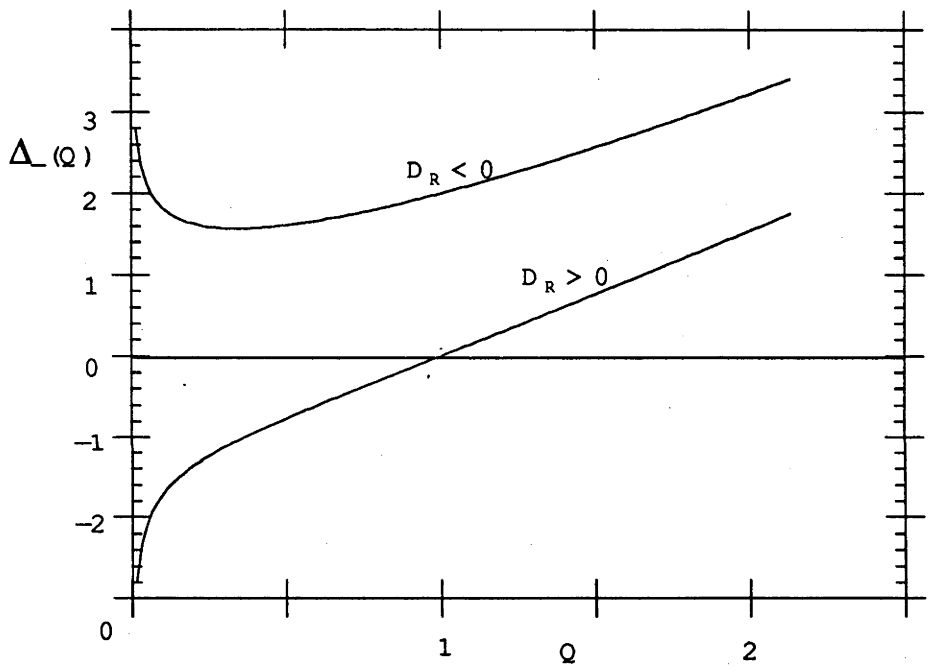

Figure 1.4: Role of D_R in the dispersion relation $\Delta_-(Q) = 0$ for $a = |D_R b| = 1$.

Chapter 2

Energy principles for dissipative systems

Testing the stability of a system usually requires the computation of the growth rates; if the most positive, or *dominant* growth rate $\hat{\gamma}$ has a positive real part then the system is said to be *unstable*. This is often a laborious task since it consists in solving the equations governing the evolution of the modes. In some cases, however, the knowledge of the growth rates, or spectrum, is not required if one can show that stability depends upon the definiteness of a functional, and furthermore that this functional is bound to decrease, for instance, in time for all *stable and unstable modes*. Such a functional is called a Lyapunov functional [Saaty & Bram (1964)]; we will derive a Lyapunov functional which possesses all the expected properties of an energy and for this reason we will refer to it as the *energy functional*. In this case we will also say that we have an *energy principle*.

The existence of an energy principle for ideal, non-resistive, modes is well-known since Bernstein *et al.* (1958), and has found numerous applications, especially in high-dimensional geometry as the energy principle reduces the complexity of determining stability to the one of analyzing the definiteness of a functional which is quadratic in the normal displacement-field [see Newcomb (1960) for the cylindrical case and Bineau (1962) for the two-dimensional case]. The question of existence of an energy principle for resistive modes, however, has been considered in works including Furth *et al.* (1973), Adler *et al.* (1980), Bondeson & Sobel (1984),

Tasso (1990) and more recently Wesson (1991). In the pressureless case of a one-dimensional plasma, Furth *et al.* (1963) derived a stability criterion $\Delta' < 0$ for tearing modes, with Δ' playing a similar role in tearing stability to the energy functional in ideal stability. Adler *et al.* (1980) have shown that, within the approximation of the reduced equations, Δ' is proportional to the non-linear increase of magnetic energy in the resistive layer. [See also White (1986) for a summary of the non-linear energy balance discussion.] Bondeson & Sobel (1984) extended this result to take into account asymmetric layers and Tasso (1990) derived a sufficient stability-criterion against purely growing modes in arbitrary geometry by means of a functional dispersion-relation. The aim of this chapter is to provide tools for the construction of the energy functional, from which *necessary and sufficient* stability criteria can be extracted provided some "causality" conditions are satisfied. A large class of problems, including those which are time-reversible, do fulfill these conditions. However, the non-Hermitian property of some operators in resistive MHD destroys the causality conditions and therefore the stability criterion do not apply except for the restricted class of real growth-rates.

We adopt the approach of field theory in § 2.1 to derive the set of Euler-Lagrange equations that leave the action stationary. The originality of the approach resides in the fact that the equations we seek are not self-adjoint, so that the variation of the action must be performed with respect to the solutions and the adjoint solutions, both treated as independent of one another. Thus, the Lagrangian ought to be a bilinear form of the solutions and their adjoint rather than the quadratic form which is more common in the literature [Itzykson & Zuber (1980)] and which is proper only to self-adjoint systems. The same remark applies to the Hamiltonian functional which is shown in § 2.2 to be conserved; for this reason it can clearly not represent the energy of a dissipative system. In order to define the energy functional, we replace the adjoint solution in the Hamiltonian by the solution, or indeed any test function, so as to construct a *quadratic energy.* A further condition requires the energy to be real, this is achieved in § 2.4 in the usual way by adding the Hermitian adjoint. These two conditions, which can be applied to any functional, define the notion of observable similarly to the prescription in quantum mechanics.

It should be added that the arbitrariness involved in the choice of deciding which of the solutions is the adjoint and conversely, can often be overcome by requiring the Lagrangian and the energy to satisfy the causal properties, defined in § 2.5, which guarantee that the energy observable decrease in time (for isolated systems), in agreement with intuition.

Because of the dissipative nature of the system, the notion of stability is redefined independently from the concept of potential energy. The system is stable if the energy remains bounded for all perturbations of the equilibrium (Lyapunov's theorem), and unstable if its energy can be released. We then find that the condition that the energy ultimately relax to the the initial energy (that is stability) requires a positive-definite energy. This allows us to write a necessary and sufficient criterion for causal-dissipative systems in § 2.6, similar to the ideal stability criterion, using the definiteness of the zero-frequency energy.

2.1 Lagrangian and Euler-Lagrange equations

Consider the linear system composed of N continuous vector fields $\boldsymbol{z}_i$, $i = 1, \cdots N$. Without loss of generality, we may attach to any linear system a Lagrangian functional

$$\mathcal{L} \equiv \int_\Omega d\tau L[\mathbf{z}^+; \mathbf{z}], \tag{2.1}$$

which is bilinear in the vector fields

$$\mathbf{z} \equiv \begin{pmatrix} \boldsymbol{z}_1 \\ \vdots \\ \boldsymbol{z}_N \end{pmatrix} \tag{2.2}$$

and

$$\mathbf{z}^{+\dagger} \equiv (\mathbf{z}^{+*})^{\mathsf{T}} \equiv \left(\boldsymbol{z}_1^+, \ \cdots, \ \boldsymbol{z}_N^+\right)^*, \tag{2.3}$$

with * denoting the complex conjugate and $\mathbf{z}^{\mathsf{T}}$ the transpose of $\mathbf{z}$. The role of the superscript $^+$ is to discriminate the adjoint solution $\mathbf{z}^+$ against $\mathbf{z}$, for the system may not necessarily be self-adjoint. In fact, we are in particular interested in the case where $\mathbf{z}^+ \neq \mathbf{z}$, so that $\mathbf{z}^+$ must be perceived as being independent from $\mathbf{z}$.

If, however, the system turns out to be self-adjoint, then we will find $\mathsf{z}^+ = \mathsf{z}$ *a posteriori*, demonstrating the generality of (2.1).

We do not wish to be too specific about the components of z^+ and z, so let us assume that each component $\boldsymbol{z}_i^+$ and $\boldsymbol{z}_i$, $i = 1, \cdots N$, is a *spatial vector*. The inner product between two such components will be denoted by, say $\boldsymbol{z}_i^+ \cdot \boldsymbol{z}_i$, whereas the inner product between two "sets of vectors" by

$$\mathsf{y}^\dagger \cdot \mathsf{z} \equiv \sum_{i=1}^{N} \boldsymbol{y}_i^* \cdot \boldsymbol{z}_i. \tag{2.4}$$

The following assumptions are made regarding the form of $L[\mathsf{z}^+; \mathsf{z}]$ in (2.1): firstly, $L[\mathsf{z}^+; \mathsf{z}]$ depends on time t only through the field variables; secondly, by $[\mathsf{z}^+; \mathsf{z}]$ we mean that L is a *bilinear* combination of $\mathsf{z}^{+\dagger}$, $\boldsymbol{\nabla}\mathsf{z}^{+\dagger} \equiv \left(\boldsymbol{\nabla}\boldsymbol{z}_1^+ \ \cdots \ \boldsymbol{\nabla}\boldsymbol{z}_N^+\right)^*$, $\dot{\mathsf{z}}^{+\dagger} \equiv \left(\dot{\boldsymbol{z}}_1^+ \ \cdots \ \dot{\boldsymbol{z}}_N^+\right)^*$, $\boldsymbol{\nabla}\dot{\mathsf{z}}^{+\dagger}$, $\boldsymbol{\nabla}\mathsf{z}$, $\dot{\mathsf{z}}$ and $\boldsymbol{\nabla}\dot{\mathsf{z}}$ only, with $\dot{\mathsf{z}} \equiv \partial_t \mathsf{z}$ and excluding higher-order derivatives so that we consider only *second-order* systems in space and time.

The equations for the $\boldsymbol{z}_i$ are the Euler-Lagrange equations that leave the action

$$\mathcal{S} \equiv \int_{\mathrm{T}} dt \mathcal{L} \tag{2.5}$$

stationary with respect to variations of $\mathsf{z}^{+\dagger}$:

$$\frac{\delta \mathcal{S}}{\delta \mathsf{z}^{+\dagger}} = 0, \tag{2.6}$$

which yields, according to the convention that the derivative of a row vector is a column vector, the set of N second-order differential equations

$$\left.\begin{array}{c} -\boldsymbol{\nabla}\cdot\partial_t \frac{\partial L}{\partial \boldsymbol{\nabla}\dot{\boldsymbol{z}}_1^{+*}} + \boldsymbol{\nabla}\cdot\frac{\partial L}{\partial \boldsymbol{\nabla}\boldsymbol{z}_1^{+*}} + \partial_t \frac{\partial L}{\partial \dot{\boldsymbol{z}}_1^{+*}} - \frac{\partial L}{\partial \boldsymbol{z}_1^{+*}} \\ \vdots \\ -\boldsymbol{\nabla}\cdot\partial_t \frac{\partial L}{\partial \boldsymbol{\nabla}\dot{\boldsymbol{z}}_N^{+*}} + \boldsymbol{\nabla}\cdot\frac{\partial L}{\partial \boldsymbol{\nabla}\boldsymbol{z}_N^{+*}} + \partial_t \frac{\partial L}{\partial \dot{\boldsymbol{z}}_N^{+*}} - \frac{\partial L}{\partial \boldsymbol{z}_N^{+*}} \end{array}\right\} \equiv \mathsf{L}\cdot\mathsf{z} = 0 \tag{2.7}$$

(provided the boundary of Ω, $\partial\Omega$, and T, ∂T, are chosen such that $\delta\mathsf{z}^+$ vanishes there). Requiring

$$\frac{\delta \mathcal{S}}{\delta \mathsf{z}} = 0, \tag{2.8}$$

leads to the Euler-Lagrange equations for z^+, $(\tilde{\mathsf{L}}\cdot\mathsf{z}^+ = 0)^\dagger$, or

$$\left.\begin{array}{c} -\boldsymbol{\nabla}\cdot\partial_t \frac{\partial L}{\partial \boldsymbol{\nabla}\dot{\boldsymbol{z}}_1} + \boldsymbol{\nabla}\cdot\frac{\partial L}{\partial \boldsymbol{\nabla}\boldsymbol{z}_1} + \partial_t \frac{\partial L}{\partial \dot{\boldsymbol{z}}_1} - \frac{\partial L}{\partial \boldsymbol{z}_1} \\ \vdots \\ -\boldsymbol{\nabla}\cdot\partial_t \frac{\partial L}{\partial \boldsymbol{\nabla}\dot{\boldsymbol{z}}_N} + \boldsymbol{\nabla}\cdot\frac{\partial L}{\partial \boldsymbol{\nabla}\boldsymbol{z}_N} + \partial_t \frac{\partial L}{\partial \dot{\boldsymbol{z}}_N} - \frac{\partial L}{\partial \boldsymbol{z}_N} \end{array}\right\} \equiv \tilde{\mathsf{L}}\cdot\mathsf{z}^+ = 0 \tag{2.9}$$

which are the adjoint equations to (2.7) written as a column vector, i.e. Eqs.(2.9) can be derived by acting $\mathsf{z}^{+\dagger}\cdot$ onto $\mathsf{L}\cdot\mathsf{z}$, integrating the ∇ and ∂_t operators of L by parts so as to have $(\tilde{\mathsf{L}}\cdot\mathsf{z}^{+})^{\dagger}\cdot\mathsf{z}$ and neglecting the endpoint contributions.

2.2 Conservation laws

It is well known form Noether's theorem [Fonda & Ghirardi (1970)] that systems described by a Lagrangian density that does not depend explicitly on time, possess fundamental symmetries with respect to temporal translations $t \rightarrow t+T$. Invariance under such translations gives rise to a conservation law for the Hamiltonian:

$$\nabla\cdot\mathbf{S} + \partial_t H = 0, \tag{2.10}$$

where $\mathbf{S}$ is the Hamiltonian flux and H the Hamiltonian. We can convince ourselves that (2.10) is satisfied for

$$\mathbf{S}[\mathsf{z}^{+},\mathsf{z}] \equiv \ddot{\mathsf{z}}^{+\dagger}\cdot\frac{\partial L}{\partial\nabla\dot{\mathsf{z}}^{+\dagger}} + \dot{\mathsf{z}}^{+\dagger}\cdot\frac{\partial L}{\partial\nabla\mathsf{z}^{+\dagger}} + \frac{\partial L}{\partial\nabla\dot{\mathsf{z}}}\cdot\ddot{\mathsf{z}} + \frac{\partial L}{\partial\nabla\mathsf{z}}\cdot\dot{\mathsf{z}} \tag{2.11}$$

and

$$H[\mathsf{z}^{+},\mathsf{z}] = \dot{\mathsf{z}}^{+\dagger}\cdot\left(\frac{\partial L}{\partial\dot{\mathsf{z}}^{+\dagger}} - \nabla\cdot\frac{\partial L}{\partial\nabla\dot{\mathsf{z}}^{+\dagger}}\right) + \left(\frac{\partial L}{\partial\dot{\mathsf{z}}} - \nabla\cdot\frac{\partial L}{\partial\nabla\dot{\mathsf{z}}}\right)\cdot\dot{\mathsf{z}} - L, \tag{2.12}$$

for we have

$$\begin{aligned}
\nabla\cdot\mathbf{S}[\mathsf{z}^{+};\mathsf{z}] + \partial_t H[\mathsf{z}^{+};\mathsf{z}] \;=\; & \dot{\mathsf{z}}^{+\dagger}\cdot\left[-\partial_t\nabla\cdot\frac{\partial L}{\partial\nabla\dot{\mathsf{z}}^{+\dagger}} + \nabla\cdot\frac{\partial L}{\partial\nabla\mathsf{z}^{+\dagger}} + \partial_t\frac{\partial L}{\partial\dot{\mathsf{z}}^{+\dagger}}\right] \\
& + (\nabla\ddot{\mathsf{z}}^{+})^{\dagger}:\frac{\partial L}{\partial\nabla\dot{\mathsf{z}}^{+\dagger}} + (\nabla\dot{\mathsf{z}}^{+})^{\dagger}:\frac{\partial L}{\partial\nabla\mathsf{z}^{+\dagger}} + \ddot{\mathsf{z}}^{+\dagger}\cdot\frac{\partial L}{\partial\dot{\mathsf{z}}^{+\dagger}} \\
& + \left[-\partial_t\nabla\cdot\frac{\partial L}{\partial\nabla\dot{\mathsf{z}}} + \nabla\cdot\frac{\partial L}{\partial\nabla\mathsf{z}} + \partial_t\frac{\partial L}{\partial\dot{\mathsf{z}}}\right]\cdot\dot{\mathsf{z}} \\
& + \frac{\partial L}{\partial\nabla\dot{\mathsf{z}}}:\nabla\ddot{\mathsf{z}} + \frac{\partial L}{\partial\nabla\mathsf{z}}:\nabla\dot{\mathsf{z}} + \frac{\partial L}{\partial\dot{\mathsf{z}}}\cdot\ddot{\mathsf{z}} - \partial_t L[\mathsf{z}^{+};\mathsf{z}] \\
=\; & \dot{\mathsf{z}}^{+\dagger}\cdot(\mathsf{L}\cdot\mathsf{z}) + \left(\tilde{\mathsf{L}}\cdot\mathsf{z}^{+}\right)^{\dagger}\cdot\dot{\mathsf{z}}.
\end{aligned} \tag{2.13}$$

[Where : denotes the tensorial product between spatial tensor, e.g. $\boldsymbol{z}_1\boldsymbol{z}_2:\boldsymbol{z}_3\boldsymbol{z}_4 \equiv (\boldsymbol{z}_1\cdot\boldsymbol{z}_4)(\boldsymbol{z}_2\cdot\boldsymbol{z}_3)$.] Equation (2.13) vanishes provided $\mathsf{L}\cdot\mathsf{z} = 0$ and $\tilde{\mathsf{L}}\cdot\mathsf{z}^{+} = 0$ are satisfied. In this formalism,

$$\frac{\partial L}{\partial\dot{\mathsf{z}}_i} - \nabla\cdot\frac{\partial L}{\partial\nabla\dot{\mathsf{z}}_i} \equiv \boldsymbol{\pi}_i^{+*} \tag{2.14}$$

plays the role of momentum conjugate to z_i, allowing us to rewrite (2.12) in the more familiar form

$$H[\mathsf{z}^+;\mathsf{z}] = \sum_{i=1}^{N} \left(z_i^{+*} \cdot \pi_i + \pi_i^{+*} \cdot z_i \right) - L \tag{2.15}$$

representing two times the kinetic energy minus the potential energy. Integrating (2.12) over an arbitrary volume Ω' which is a subset of the entire universe Ω, to obtain the *global Hamiltonian*

$$\mathcal{E}[\mathsf{z}^+;\mathsf{z}] \equiv \int_{\Omega'} d\tau H[\mathsf{z}^+;\mathsf{z}], \tag{2.16}$$

we find that $\mathcal{E}[\mathsf{z}^+;\mathsf{z}]$ is invariant, except for a boundary term

$$\frac{d}{dt}\mathcal{E}[\mathsf{z}^+;\mathsf{z}] = -\int_{\partial\Omega'} d\boldsymbol{\sigma} \cdot \mathbf{S}[\mathsf{z}^+;\mathsf{z}]. \tag{2.17}$$

We must be careful not to interpret (2.16) as the energy of the system and (2.17) as the corresponding radiation losses, for it is clear that the conservation property (2.10) is the consequence of time-invariance. We shall come back to the question of constructing the "proper energy" in § 2.4. Equation (2.10) may yield, however, important information about the time behaviour of the solution knowing the adjoint solution or *vice versa*. We see that if one component, z^+ say, is exponentially growing in time and the other component, z, is decaying at the same rate then this will give rise to a time-invariant Lagrangian. On the other hand, the situation where z^+ and z possess identical growth rates cannot be excluded on the grounds that the different contributions forming the Hamiltonian may cancel. This will be the case for non-dissipative systems in particular where kinetic and potential energies are balanced.

The conservation of the global momentum follows the invariance property of $L[\mathsf{z}^+;\mathsf{z}]$ with respect to translation of the space coordinates. Provided $L[\mathsf{z}^+;\mathsf{z}]$ depends on the space coordinates *only* through z^+ and z, we can show by following a similar path to (2.10) and (2.13) that the momentum $\int_\Omega d\tau \mathbf{p}[\mathsf{z}^+;\mathsf{z}]$ with

$$\mathbf{p}[\mathsf{z}^+;\mathsf{z}] \equiv (\boldsymbol{\nabla}\mathsf{z}^+)^\dagger \cdot \left(-\boldsymbol{\nabla} \cdot \frac{\partial L}{\partial \boldsymbol{\nabla}\dot{\mathsf{z}}^{+\dagger}} + \frac{\partial L}{\partial \dot{\mathsf{z}}^{+\dagger}} \right) + \left(-\boldsymbol{\nabla} \cdot \frac{\partial L}{\partial \boldsymbol{\nabla}\dot{\mathsf{z}}} + \frac{\partial L}{\partial \dot{\mathsf{z}}} \right) \cdot \boldsymbol{\nabla}\mathsf{z} \tag{2.18}$$

and

$$\mathsf{T}[\mathsf{z}^+;\mathsf{z}] = (\boldsymbol{\nabla}\dot{\mathsf{z}}^+)^\dagger \cdot \frac{\partial L}{\partial \boldsymbol{\nabla}\dot{\mathsf{z}}^{+\dagger}} + (\boldsymbol{\nabla}\mathsf{z}^+)^\dagger \cdot \frac{\partial L}{\partial \boldsymbol{\nabla}\mathsf{z}^{+\dagger}} + \frac{\partial L}{\partial \boldsymbol{\nabla}\dot{\mathsf{z}}} \cdot \boldsymbol{\nabla}\dot{\mathsf{z}} + \frac{\partial L}{\partial \boldsymbol{\nabla}\mathsf{z}} \cdot \boldsymbol{\nabla}\mathsf{z} - L\,\mathsf{I} \tag{2.19}$$

are conserved,

$$\nabla\cdot\mathsf{T}[z^+;z] + \partial_t \mathsf{p}[z^+;z] = (\mathsf{L}\cdot z)^\dagger\cdot\nabla z^+ + \left(\tilde{\mathsf{L}}\cdot z^+\right)^{\mathsf{T}}\cdot\nabla z, \tag{2.20}$$

where T is the stress tensor and I the identity tensor. Equations (2.11), (2.12), (2.18) and (2.19) form the 16 components of the stress-energy tensor [Morse & Feshbach (1953)].

2.3 The concomitant invariant

We introduce here quantities whose physical interpretation may appear at first sight obscure, but which will be of interest in the subsequent stability analysis as performed in Chapters 3 and 6. Let

$$U_+[z^+;z] \equiv z^{+\dagger}\cdot\left(\frac{\partial L}{\partial \dot{z}^{+\dagger}} - \nabla\cdot\frac{\partial L}{\partial \nabla\dot{z}^{+\dagger}}\right) \tag{2.21}$$

and

$$U_-[z^+;z] \equiv -\left(\frac{\partial L}{\partial \dot{z}} - \nabla\cdot\frac{\partial L}{\partial \nabla\dot{z}}\right)\cdot z \tag{2.22}$$

be two bilinear densities, with

$$\mathbf{P}_+[z^+;z] \equiv \dot{z}^{+\dagger}\cdot\frac{\partial L}{\partial \nabla\dot{z}^{+\dagger}} + z^{+\dagger}\cdot\frac{\partial L}{\partial \nabla z^{+\dagger}} \tag{2.23}$$

and

$$\mathbf{P}_-[z^+;z] \equiv -\frac{\partial L}{\partial \nabla\dot{z}}\cdot\dot{z} - \frac{\partial L}{\partial \nabla z}\cdot z \tag{2.24}$$

being the fluxes corresponding to (2.21) and (2.22). Equations (2.21) and (2.23) result from integrating by parts $(z^+)^\dagger\cdot(\mathsf{L}\cdot z)$ of (2.7) in space and time, and (2.22) and (2.24) from applying a similar procedure onto $-(\tilde{\mathsf{L}}\cdot z^+)^\dagger\cdot z$, which yields

$$\begin{aligned} z^{+\dagger}\cdot(\mathsf{L}\cdot z) \;=\; & \nabla\cdot\mathbf{P}_+[z^+;z] + \partial_t U_+[z^+;z] - z^{+\dagger}\cdot\frac{\partial L}{\partial z^{+\dagger}} \\ & - (\nabla z^+)^\dagger : \frac{\partial L}{\partial \nabla z^{+\dagger}} - \dot{z}^{+\dagger}\cdot\frac{\partial L}{\partial \dot{z}^{+\dagger}} \\ & - (\nabla \dot{z}^+)^\dagger : \frac{\partial L}{\partial \nabla \dot{z}^{+\dagger}} \end{aligned} \tag{2.25}$$

$$\begin{aligned} -(\tilde{\mathsf{L}}\cdot z^+)^\dagger\cdot z \;=\; & \nabla\cdot\mathbf{P}_-[z^+;z] + \partial_t U_-[z^+;z] + \frac{\partial L}{\partial z}\cdot z \\ & + \frac{\partial L}{\partial \nabla z} : \nabla z + \frac{\partial L}{\partial \dot{z}}\cdot\dot{z} \\ & + \frac{\partial L}{\partial \nabla \dot{z}} : \nabla \dot{z}. \end{aligned} \tag{2.26}$$

Since the right-hand side of (2.25) and (2.26) is equal to $\nabla\cdot\mathbf{P}_+ + \partial_t U_+ - L[\mathsf{z}^+;\mathsf{z}]$ and $\nabla\cdot\mathbf{P}_- + \partial_t U_+ + L[\mathsf{z}^+;\mathsf{z}]$ respectively, adding (2.25) and (2.26) leads to a third conservation law

$$\nabla\cdot\mathbf{P}[\mathsf{z}^+;\mathsf{z}] + \partial_t U[\mathsf{z}^+;\mathsf{z}] = \mathsf{z}^{+\dagger}\cdot(\mathsf{L}\cdot\mathsf{z}) - (\tilde{\mathsf{L}}\cdot\mathsf{z}^+)^\dagger\cdot\mathsf{z}, \tag{2.27}$$

with

$$U[\mathsf{z}^+;\mathsf{z}] \equiv U_+[\mathsf{z}^+;\mathsf{z}] + U_-[\mathsf{z}^+;\mathsf{z}] \tag{2.28}$$

and

$$\mathbf{P}[\mathsf{z}^+;\mathsf{z}] \equiv \mathbf{P}_+[\mathsf{z}^+;\mathsf{z}] + \mathbf{P}_-[\mathsf{z}^+;\mathsf{z}]. \tag{2.29}$$

Equation (2.27) is a direct consequence of the bilinearity of L, i.e. the linearity of Eqs.(2.7) and (2.9). To grasp the significance of (2.27), suppose we take $\mathsf{z}^+ = \mathsf{z}$ with $\mathsf{L}\cdot\mathsf{z} = 0$, then (2.27) is a measure of the non-self-adjointness of L. Comparing Eqs.(2.12) with (2.21) and (2.22) and assuming a single Fourier-mode dependence of $\mathsf{z} \propto \exp\gamma t$ and $\mathsf{z}^+ \propto \exp\gamma_+ t$, we find that the Hamiltonian density

$$H[\mathsf{z}^+;\mathsf{z}] = \gamma_+^* \mathcal{U}_+[\mathsf{z}^+;\mathsf{z}] - \gamma\mathcal{U}_-[\mathsf{z}^+;\mathsf{z}] \tag{2.30}$$

is proportional to $\mathcal{U}$ provided $\gamma = -\gamma_+^*$, which defines in § 2.5 the subclass of dissipative systems which are time-reversible. Equation (2.30) also points to $\mathcal{U}$ having the dimensions of an "action density", which also plays an important role in the Vlasov-Maxwell theory of wave propagation [Kull *et al.* (1989)].

On the other hand, choose an L that is self-adjoint and let z^+ and z be two solutions of $\mathsf{L}\cdot\mathsf{y} = \tilde{\mathsf{L}}\cdot\mathsf{y} = 0$, then $\int_\Omega d\tau U[\mathsf{z}^+;\mathsf{z}]$ can be seen from (2.27) to be a constant of motion. Because of the minus sign occurring in (2.27), $\int_\Omega d\tau U[\mathsf{z}^+;\mathsf{z}]$ is also a constant of motion if z^+ and z are linearly dependent. Equations (2.28) and (2.29) generalize what is called the *bilinear concomitant* [Morse & Feshbach (1953)].

The importance of the concomitant concept arises also for self-adjoint operators acting on the space coordinates. We see in particular that, when integrating (2.27) over the finite volume $\Omega' \subset \Omega$ while assuming that $U = 0$ (i.e. the Lagrangian density does not contain any $\dot{\mathsf{z}}$ nor $\dot{\mathsf{z}}^+$ dependence), $\mathbf{P}$ may contribute at the endpoints $\partial\Omega'$ even though $\mathsf{L} = \tilde{\mathsf{L}} = \mathsf{L}^\dagger$, violating the relation $\int_{\Omega'} d\tau \mathsf{z}_i^\dagger\cdot(\mathsf{L}\cdot\mathsf{z}_j) = \int_{\Omega'} d\tau(\mathsf{L}\cdot\mathsf{z}_i)^\dagger\cdot\mathsf{z}_j$

which defines Hermiticity. For homogeneous Dirichlet-boundary conditions $\mathbf{P}$ vanishes at $\partial\Omega'$. These are the zero-flux boundary conditions

$$\left[\frac{\partial L}{\partial \nabla \dot{\mathsf{z}}}\cdot\dot{\mathsf{z}} + \frac{\partial L}{\partial \nabla \mathsf{z}}\cdot\mathsf{z}\right]_{\partial\Omega'} = 0. \tag{2.31}$$

We will refer to (2.31) as the zero-flux boundary conditions in subsequent chapters with the terminology motivated by the similarity exhibited by Eqs.(2.23) and (2.24) as compared to (2.11). In this chapter and the following we will concentrate on systems satisfying the zero-flux boundary condition with exception of § 3.3. The recurrence of the bilinear concomitant in Ch. 6 will be at the basis of our scheme to calculate the matching data.

2.4 Energy and other observables

The distinction between Hamiltonian and energy is intrinsic to non-conservative systems, where the Hamiltonian is conserved [c.f. (2.13)] but the energy is in general not. It is also clear that the Hamiltonian defined by (2.16) cannot correspond to any physical reality, being merely a mathematical trick which allowed us to treat dissipative systems on the same footing as conservative systems; the reason being that the state of a system must be defined from z, and z alone, or alternatively from z^+ only *but not from both* since they are independent functions of t. Therefore, it is natural in a linear theory to postulate that only functionals which depend *quadratically* in z can give rise to measurable quantities which we refer to as *observables.* Furthermore, we shall require these observables to be *real.* This is achieved in quantum mechanics by associating observables with Hermitian operators. However, we find it preferable to use the following, more general prescription; let

$$\mathcal{A}[\mathsf{z}_i;\mathsf{z}_j] \equiv (\mathsf{z}_i, \mathsf{A}\cdot\mathsf{z}_j) \tag{2.32}$$

be any bilinear functional, where

$$(\mathsf{z}_i,\mathsf{z}_j) \equiv \int_{\Omega'} d\tau \mathsf{z}_i^\dagger\cdot\mathsf{z}_j \tag{2.33}$$

defines the inner product in the volume $\Omega' \subseteq \Omega$ of two states z_i and z_j in the Hilbert space $\mathcal{H}$ with positive norm $\| \mathsf{z} \|^2 \equiv (\mathsf{z},\mathsf{z}) > 0$, $\mathsf{z} \in \mathcal{H}$. A functional $\mathcal{A}$ is *symmetric*

if

$$\mathcal{A}[\mathsf{z}_i;\mathsf{z}_j] \equiv \mathcal{A}[\mathsf{z}_j;\mathsf{z}_i]^* \quad \forall\ \mathsf{z}_i,\mathsf{z}_j \in \mathcal{H}. \tag{2.34}$$

Such a functional satisfies the requirements of an observable which we denote with the subscript r: $\mathcal{A}_r[\mathsf{z}_i;\mathsf{z}_j] \equiv \mathcal{A}[\mathsf{z}_i;\mathsf{z}_j]$. However, if (2.34) is not fulfilled we construct the symmetric form

$$\begin{aligned}\mathcal{A}_r[\mathsf{z}_i;\mathsf{z}_j] &\equiv \tfrac{1}{2}\left(\mathsf{z}_i, \mathsf{A}\cdot\mathsf{z}_j\right) + \tfrac{1}{2}\left(\mathsf{A}\cdot\mathsf{z}_i, \mathsf{z}_j\right)\\ &\equiv \tfrac{1}{2}\left(\mathsf{z}_i, \mathsf{A}\cdot\mathsf{z}_j\right) + \text{h.c.},\end{aligned} \tag{2.35}$$

where h.c. denotes the Hermitian conjugate of the matrix $\mathcal{A}[\mathsf{z}_i;\mathsf{z}_j]$, in order that $\mathcal{A}_r[\mathsf{z},\mathsf{z}]$ be real. The lack of symmetry may be due to $\mathsf{A} \neq \mathsf{A}^\dagger$ [here † denotes the Hermitian adjoint in the domain Ω: $\int_\Omega d\tau \mathsf{z}_i^\dagger\cdot(\mathsf{A}\cdot\mathsf{z}_j) \equiv \int_\Omega d\tau(\mathsf{A}^\dagger\cdot\mathsf{z}_i)^\dagger\cdot\mathsf{z}_j$ with z_i and z_j satisfying homogeneous boundary conditions at $\partial\Omega$] or may result from inhomogeneous boundary conditions of z_i and z_j at $\partial\Omega'$ indicating the interaction of the system with a "reservoir" for instance.

2.5 Causality condition

According to (2.35), the energy takes the form

$$\mathcal{E}_r[\mathsf{z}_i;\mathsf{z}_j] \equiv \tfrac{1}{2}\int_{\Omega'} d\tau H[\mathsf{z}_i;\mathsf{z}_j] + \text{h.c.} \tag{2.36}$$

and the energy flux becomes

$$\mathbf{S}_r[\mathsf{z}_i;\mathsf{z}_j] \equiv \tfrac{1}{2}\mathbf{S}[\mathsf{z}_i;\mathsf{z}_j] + \text{h.c.} \tag{2.37}$$

so that, from (2.13),

$$\begin{aligned}\frac{d}{dt}\mathcal{E}_r[\mathsf{z}_i;\mathsf{z}_j] &= \tfrac{1}{2}\int_{\Omega'} d\tau\left\{\boldsymbol{\nabla}\cdot\mathbf{S}_r[\mathsf{z}_i;\mathsf{z}_j] + \partial_t H_r[\mathsf{z}_i;\mathsf{z}_j]\right\}\\ &= \tfrac{1}{2}\left(\dot{\mathsf{z}}_i, \left[\mathsf{L}+\tilde{\mathsf{L}}\right]\cdot\mathsf{z}_j\right) + \text{h.c.}\end{aligned} \tag{2.38}$$

We see from (2.38) that dissipation is given by the non-self-adjointness of L. Expressing L in the generic form of the damped oscillator

$$\mathsf{L} \equiv \mathsf{M}\partial_t^2 + \mathsf{D}\partial_t + \mathsf{V}, \tag{2.39}$$

with the adjoint operator to L being

$$\tilde{\mathsf{L}} \equiv \mathsf{M}^\dagger \partial_t^2 - \mathsf{D}^\dagger \partial_t + \mathsf{V}^\dagger, \tag{2.40}$$

and writing

$$\begin{aligned} \mathsf{M}_H &\equiv \tfrac{1}{2}(\mathsf{M} + \mathsf{M}^\dagger), \quad \mathsf{D}_H \equiv \tfrac{1}{2}(\mathsf{D} + \mathsf{D}^\dagger), \quad \mathsf{V}_H \equiv \tfrac{1}{2}(\mathsf{V} + \mathsf{V}^\dagger), \\ \mathsf{M}_A &\equiv \tfrac{1}{2}(\mathsf{M} - \mathsf{M}^\dagger), \quad \mathsf{D}_A \equiv \tfrac{1}{2}(\mathsf{D} - \mathsf{D}^\dagger), \quad \mathsf{V}_A \equiv \tfrac{1}{2}(\mathsf{V} - \mathsf{V}^\dagger), \end{aligned} \tag{2.41}$$

in terms of Hermitian and anti-Hermitian parts respectively, which involve differential operators acting on space variables only, we find from (2.38)

$$\frac{d}{dt}\mathcal{E}_r[\mathsf{z}_i; \mathsf{z}_j] = (\dot{\mathsf{z}}_i, \mathsf{M}_H \cdot \ddot{\mathsf{z}}_j + \mathsf{V}_H \cdot \mathsf{z}_j) + \text{h.c.}, \tag{2.42}$$

which can be integrated over t to give (up to a constant of integration)

$$\mathcal{E}_r[\mathsf{z}_i; \mathsf{z}_j] = (\dot{\mathsf{z}}_i, \mathsf{M}_H \cdot \dot{\mathsf{z}}_j) + (\mathsf{z}_i, \mathsf{V}_H \cdot \mathsf{z}_j), \tag{2.43}$$

provided the concomitant of (2.29) vanishes at $\partial\Omega'$, that is (2.39) obeys the boundary conditions of (2.31). Equation (2.43) can be shown to be consistent with definition (2.36).

It is our intention to discuss now the various degrees of freedom one is confronted with, as one goes through the procedure of constructing the Lagrangian density L. It is well-known that for conservative systems, $L = T - V$, where T is the kinetic energy and V the potential energy. As T is a positive-definite quantity, the sign of the action (2.5), and therefore the sign L, is determined by $T > 0$, this regardless of the fact that the Euler-Lagrange equations (2.7) and (2.9) are insensitive to $L \mapsto -L$. We will see that for a number of dissipative systems, such that D is non-vanishing, the definiteness of D determines which of z^+ and z should be chosen as representing the physical state of the system in the sense of observable as defined in § 2.4.

For dissipative systems, we shall arrange the Euler-Lagrange equations, whenever possible, in such a way that the kinetic contribution be positive-definite. That is the term quadratic in $\dot{\mathsf{z}}$ in (2.43),

$$(\dot{\mathsf{z}}, \mathsf{M}_H \cdot \dot{\mathsf{z}}) \geq 0 \tag{2.44}$$

$\forall\ \dot{\mathsf{z}} \in \mathcal{H}$. We then postulate that the physically relevant states are such that the the sign of dissipation be positive, which corresponds to the decrease of $\mathcal{E}_r$ in time,

$$\begin{aligned} \frac{d}{dt}\mathcal{E}_r[\mathsf{z};\mathsf{z}] &= -2\,(\dot{\mathsf{z}}, \mathsf{D}_H{\cdot}\dot{\mathsf{z}}) - [(\dot{\mathsf{z}}, \mathsf{M}_A{\cdot}\ddot{\mathsf{z}}) + (\dot{\mathsf{z}}, \mathsf{V}_A{\cdot}\mathsf{z}) + \text{c.c.}] \\ &\leq 0 \end{aligned} \tag{2.45}$$

and which is obtained from (2.38) by writing $\tilde{\mathsf{L}} = \mathsf{L} - 2\mathsf{M}_A\partial_t^2 - 2\mathsf{D}_H\partial_t - 2\mathsf{V}_H$, for z solution of $\mathsf{L}{\cdot}\mathsf{y} = 0$. The first term on the right-hand side of (2.45) being quadratic, we write the *causality condition* as

$$(\mathsf{z}, \mathsf{D}_H{\cdot}\mathsf{z}) \geq 0 \qquad \forall\ \mathsf{z} \in \mathcal{H} \tag{2.46}$$

which expresses the fact that the energy is bound to decrease, provided the two terms $(\dot{\mathsf{z}}, \mathsf{M}_A{\cdot}\ddot{\mathsf{z}}) + (\dot{\mathsf{z}}, \mathsf{V}_A{\cdot}\mathsf{z}) + \text{c.c.}$ vanish. If either $\mathsf{M}_A \neq 0$ or $\mathsf{V}_A \neq 0$, then the causality condition (2.45) only holds in general for real growth-rates. It is interesting to note that the condition M_A and V_A vanishing is in particular satisfied for time-reversible systems where z^+ is the "advanced" solution and z the "retarded" solution with $\mathsf{z}^+(t) = \mathsf{z}(-t)$.

2.6 Stability criteria

We shall address in this section the issue of stability for dissipative systems using the causality condition introduced in the previous section. For conservative systems, it is well known since Bernstein *et al.* (1958) that stability is given by the positive definiteness of the potential energy, however, it is far from obvious how this criterion generalizes to the dissipative case. One reason for this is due to the concept itself of potential energy which becomes rather meaningless in the dissipative case. Thus, one is led to use a more general definition of stability, consistent with the linear perturbation approximation, such as: *a system is unstable when there exists the possibility for the system to lower its energy exponentially.* In other words, an equilibrium is stable when it is a minimum energy state. Suppose the zero-energy state is the equilibrium state, any infinitesimal perturbation that elevates the energy gives rise to a positive energy and, conversely, any perturbation that lowers the energy produces a negative energy. As the system evolves in time, the energy is

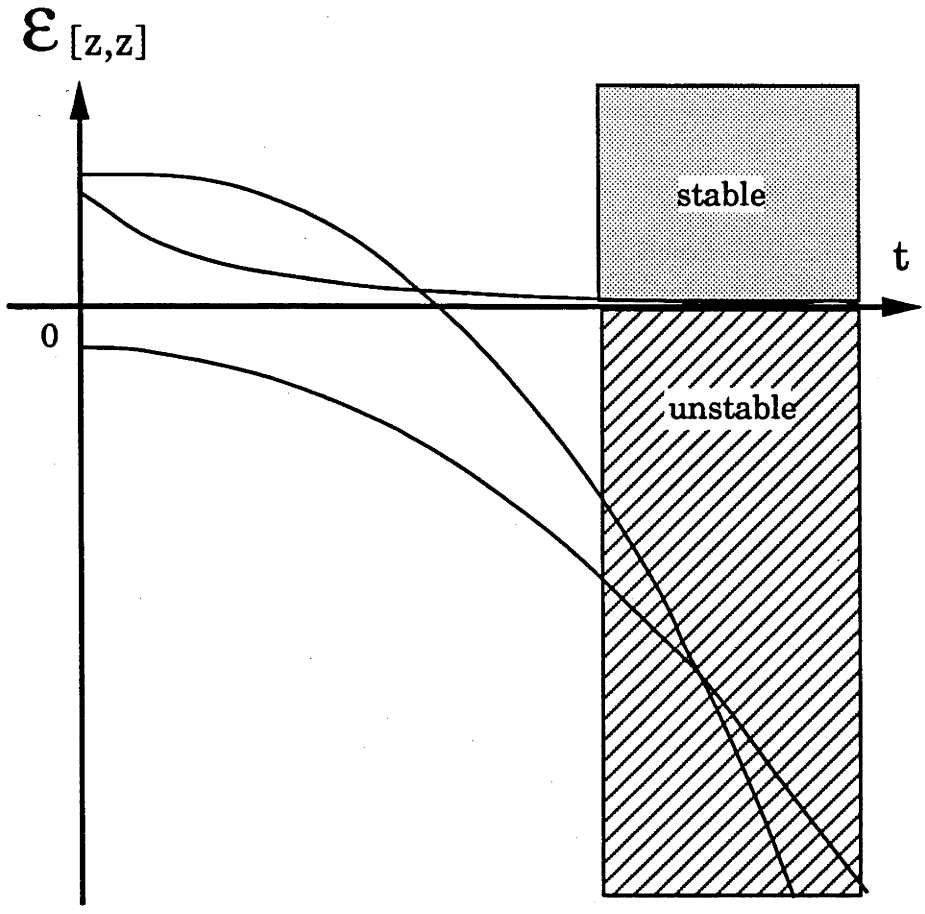

Figure 2.1: Evolutionary path followed by the energy observable as the system relaxes. For stable modes, the system relaxes to its anterior state, whereas for unstable modes, the energy departs exponentially from the initial state as $t \to \infty$.

bound to decrease for both positive and negative energies if the causality principle (2.46) holds. This situation is exposed in Fig. 2.1. Thus, negative energies depart exponentially from the zero-energy state, $\mathcal{E}_r = 0$ as time passes by, whereas positive energies have the choice between relaxing to $\mathcal{E}_r = 0$, or else crossing the $\mathcal{E}_r = 0$ axis and joining the negative energy states. Since we have not specified the origin of time $t = 0$, the latter case corresponds in essence to a negative initial energy which is translated in time (with positive energy for $t < 0$). Thus, requiring

$$\mathcal{E}_r[\mathsf{z};\mathsf{z}] \geq 0 \quad \forall\ \mathsf{z} \in \mathcal{H} \tag{2.47}$$

for causal systems [satisfying (2.46)] provides a *necessary* and *sufficient* criterion to ensure stability; if (2.47) is satisfied $\mathcal{E}_r$ is necessarily positive at all times, and this is sufficient to prohibit the system from diverging exponentially from $\mathcal{E}_r = 0$ as

$t \to \infty$.

We now discuss the connection between criterion (2.47) and the sign of the dominant growth rate $\hat{\gamma}$. Figure 2.1 suggests that stable modes must be decaying. This is, however, best seen from Eqs.(2.42), (2.43) and (2.46) which reduces

$$\frac{d}{dt}\mathcal{E}_r = 2\mathrm{Re}\{\hat{\gamma}\}\mathcal{E}_r \tag{2.48}$$

as $t \to \infty$. Equation (2.48) shows that $\mathcal{E}_r > 0$ corresponds to $\mathrm{Re}\{\hat{\gamma}\} < 0$, and $\mathcal{E}_r < 0$ to $\mathrm{Re}\{\hat{\gamma}\} > 0$.

Since (2.47) is valid for all initial perturbations, including those with $\dot{\mathsf{z}}$ initially zero, we can rewrite (2.47) as

$$W[\mathsf{z};\mathsf{z}] \equiv (\mathsf{z}, \mathsf{V}_H{\cdot}\mathsf{z}) \geq 0 \quad \forall\ \mathsf{z} \in \mathcal{H}. \tag{2.49}$$

without loss of generality *if* $(\mathsf{z}, \mathsf{M}_H{\cdot}\mathsf{z})$ is positive-definite. Criterion (2.49) is equivalent to (2.47) in that $\mathcal{E}_r[\mathsf{z};\mathsf{z}]$ is positive-definite if $W[\mathsf{z};\mathsf{z}]$ is positive-definite, and there always exists an $\mathcal{E}_r < 0$ if $W < 0$.

Equations (2.47) and (2.49) are the main results of this chapter. The procedure to test stability is the following: first, we must ensure that the equations are presented in causal form, meaning that (2.46) is satisfied for all states $\mathsf{z} \in \mathcal{H}$. We speculate that most physical systems can be put in causal form since intuitively all systems are dissipative (the complex conjugate in the definiton of the inner product ensuring that no reactive power can alter the causal behaviour). Fortunately, this is the case of all three examples considered in Ch. 3. The next impediment is encountered when either of M_A or V_A is non-vanishing, as it is the case for the unreduced set of resistive equations (see § 3.1). This reduces the range of applicability of the energy principle (2.47) to perturbations having real growth-rates only.

Chapter 3

Resistive stability

The purpose of the present chapter is to utilize the machinery developed in Ch. 2, that is to derive the energy observable, apply the causality principle and obtain, when possible a stability criterion. First, we focus in § 3.1 on the full set of resistive equations which are shown to dissipate at a rate proportional to the resistivity. However, the presence of an anti-Hermitian part in the V operator prevents us from obtaining a causal relation for all but real growth-rates. This anti-Hermitian contribution is attributed to the work performed by the diffusing magnetic field which can only be balanced by introducing a source term, indicating that this set of equations is propitious to linear-stability studies, only in the limit of short time-scale with respect to the equilibrium evolution-time.

Tasso's stability criterion [Tasso (1983) and Tasso (1990)], which applies to purely growing modes, is shown in § 3.1 to be necessary *and* sufficient without introducing a limiting scaling. We next turn our attention to the set of equations of Glasser *et al.* (1975), discussed in § 1.5, which describes the evolution of tearing and interchange modes in toroidal plasmas. As for the previous case, the operator D of § 2.4 exhibits the proper symmetry, its positive-definiteness ensuring dissipation. However, the problem of anti-Hermiticity of V recurs here too; it is only in the limit of the Coppi *et al.* (1966) equations that V becomes Hermitian. In the large aspect-ratio limit, we are able to recover the resistive-interchange criterion of § 3.2 by requiring the zero-frequency energy to be positive-definite. Finally, we apply in § 3.3 the concomitant formulae of § 2.3 to show that the logarithmic jump

$\Delta(Q)$ introduced §§ 1.4 and 1.5, which defines the inner matching-data, increases monotonically with the growth rate Q. The condition that the outer matching data $\Delta' < 0$ is then found to be a sufficient criterion, in agreement with the results of § 1.4.

3.1 Resistive equations

The resistive model with $\eta = \text{const}$ is considered here in arbitrary geometry [to generalize this case to $\eta \neq \text{const}$ we refer to the work of Tasso (1990)]. The Lagrangian density takes the form

$$\begin{aligned} L \;=\; \tfrac{1}{2}\Big[&\rho\dot{\boldsymbol{\xi}}^{+}\cdot\dot{\boldsymbol{\xi}} - 2w(\boldsymbol{\xi}^{+},\boldsymbol{\xi}) - \boldsymbol{\nabla}\times\mathbf{a}^{+}\cdot\boldsymbol{\nabla}\times\mathbf{a} + \frac{1}{2\eta}\left(\dot{\mathbf{a}}^{+}\cdot\mathbf{a} - \mathbf{a}^{+}\cdot\dot{\mathbf{a}}\right) \\ &- \mathbf{Q}^{+}\cdot\boldsymbol{\nabla}\times\mathbf{a} - \boldsymbol{\nabla}\times\mathbf{a}^{+}\cdot\mathbf{Q} + \boldsymbol{\xi}^{+}\cdot\mathbf{J}\times(\boldsymbol{\nabla}\times\mathbf{a})\Big] \end{aligned} \tag{3.1}$$

for the motion of the virtual displacement field $\boldsymbol{\xi}$ and the correction $\mathbf{a}$. This choice of variable is appropriate for taking the limit of $\eta \to 0$, for $\mathbf{a}$ represents the correction to the ideal vector potential $\boldsymbol{\xi}\times\mathbf{B}$; the total magnetic field perturbation being

$$\mathbf{b} \equiv \mathbf{Q} + \boldsymbol{\nabla}\times\mathbf{a}, \tag{3.2}$$

where

$$\mathbf{Q} \equiv \boldsymbol{\nabla}\times(\boldsymbol{\xi}\times\mathbf{B}). \tag{3.3}$$

Since (3.1) is not a symmetric form, we must discriminate $\{\boldsymbol{\xi}, \mathbf{a}\}$ against the adjoint solutions $\{\boldsymbol{\xi}^{+}, \mathbf{a}^{+}\}$ as in (2.1) of Ch. 2. In (3.1), $\mathbf{J} \equiv \boldsymbol{\nabla}\times\mathbf{B}$ is the equilibrium current-density and

$$2w(\boldsymbol{\xi}^{+},\boldsymbol{\xi}) \equiv (\mathbf{Q}^{+} + \xi_n^{+}\mathbf{J}\times\mathbf{n})\cdot(\mathbf{Q} + \xi_n\mathbf{J}\times\mathbf{n}) + \boldsymbol{\nabla}\cdot\boldsymbol{\xi}^{+}\Gamma p\boldsymbol{\nabla}\cdot\boldsymbol{\xi} - 2U\xi^{+}\xi \tag{3.4}$$

represents the ideal potential energy when integrated over the volume of the plasma. The derivation of (3.4) will be discussed in more detail in Ch. 4. Here, ψ is the poloidal magnetic flux-coordinate of § 1.2, $\xi_n \equiv \boldsymbol{\xi}\cdot\mathbf{n}$ and $\xi \equiv \boldsymbol{\xi}\cdot\boldsymbol{\nabla}\psi = \xi_n|\boldsymbol{\nabla}\psi|$. For a complete description of the terms involved in the Hermitian operator U in (3.4) we further refer the reader to Ch. 4.

Following § 2.2, we form the vector

$$\mathsf{z} \equiv \begin{pmatrix} \boldsymbol{\xi} \\ \mathbf{a} \end{pmatrix} \tag{3.5}$$

allowing us to write the linear, resistive equations in the form of (2.39), with

$$\mathsf{M} = \tfrac{1}{2}\begin{pmatrix} \rho & 0 \\ 0 & 0 \end{pmatrix}, \tag{3.6}$$

$$\mathsf{D} = \tfrac{1}{2}\begin{pmatrix} 0 & 0 \\ 0 & 1/\eta \end{pmatrix}, \tag{3.7}$$

$$\mathsf{V}_H = \tfrac{1}{2}\begin{pmatrix} -\mathsf{F} & +\mathbf{B}\times[\nabla\times(\nabla\times\mathsf{I})] - \tfrac{1}{2}\mathbf{J}\times(\nabla\times\mathsf{I}) \\ -\nabla\times[\nabla\times(\mathbf{B}\times\mathsf{I}) + \tfrac{1}{2}\nabla\times(\mathbf{J}\times\mathsf{I}) & \nabla\times(\nabla\times\mathsf{I}) \end{pmatrix} \tag{3.8}$$

and

$$\mathsf{V}_A = \tfrac{1}{2}\begin{pmatrix} 0 & -\tfrac{1}{2}\mathbf{J}\times(\nabla\times\mathsf{I}) \\ -\tfrac{1}{2}\nabla\times(\mathbf{J}\times\mathsf{I}) & 0 \end{pmatrix}, \tag{3.9}$$

and where

$$\begin{aligned} \mathsf{F}\cdot\boldsymbol{\xi} \;=\; & -\mathbf{B}\times[\nabla\times(\mathbf{Q} + \xi_n\mathbf{J}\times\mathbf{n})] \\ & + \nabla[\Gamma p\nabla\cdot\boldsymbol{\xi}] - \mathbf{n}\mathbf{J}\times\mathbf{n}\cdot(\mathbf{Q} + \xi_n\mathbf{J}\times\mathbf{n}) + 2U\boldsymbol{\xi}\nabla\psi \end{aligned} \tag{3.10}$$

is the force operator of Bernstein *et al.* (1958) [see for instance Bineau (1962) for the original derivation of the present expression]. The cross product of a vector and the unit dyadic, e.g. $\mathbf{J}\times\mathsf{I}$ in (3.8), is, by definition, the dyadic $\mathbf{J}\times\mathsf{I} \equiv \sum_i \mathbf{J}\times\mathbf{e}_i\mathbf{e}_i$, where $\{\mathbf{e}_i\}$ is any orthonormal basis.

The adjoint equation (2.40) can be derived by means of (2.27), or alternatively from (2.9).

Using (2.11), we find

$$\begin{aligned} \mathsf{S}_r[\mathsf{z}_i;\mathsf{z}_j] \;=\; & \tfrac{1}{4}\big[(\mathbf{Q} + \xi_n\mathbf{J}\times\mathbf{n})_i^*\cdot\mathbf{B}\dot{\boldsymbol{\xi}}_j - \mathbf{B}(\mathbf{Q} + \xi_n\mathbf{J}\times\mathbf{n})_i^*\cdot\dot{\boldsymbol{\xi}}_j - \nabla\cdot\boldsymbol{\xi}_i^*\Gamma p\dot{\boldsymbol{\xi}}_j \\ & - \mathbf{B}\nabla\times\mathbf{a}_i^*\cdot\dot{\boldsymbol{\xi}}_j + \nabla\times\mathbf{a}_i^*\cdot\mathbf{B}\dot{\boldsymbol{\xi}}_j \\ & + (\nabla\times\mathbf{a} + \mathbf{Q} - \tfrac{1}{2}\boldsymbol{\xi}\times\mathbf{J})_i^*\times\dot{\mathbf{a}}_j\big] + \text{h.c.} \end{aligned} \tag{3.11}$$

and, with the help of (2.43),

$$\begin{aligned}\mathcal{E}_\tau[\mathsf{z}_i;\mathsf{z}_j] &= \tfrac{1}{2}\left(\rho\dot{\boldsymbol{\xi}}_i,\dot{\boldsymbol{\xi}}_j\right)+\tfrac{1}{2}\left(\nabla\times\mathbf{a}_i,\nabla\times\mathbf{a}_j\right)\\ &\quad+\tfrac{1}{2}\int_{\Omega'}d\tau\left[2w(\boldsymbol{\xi}_i{}^*,\boldsymbol{\xi}_j)+\nabla\times\mathbf{a}_i{}^*\cdot(\mathbf{Q}_j-\tfrac{1}{2}\boldsymbol{\xi}_j\times\mathbf{J})\right.\\ &\quad\left.+(\mathbf{Q}_i-\tfrac{1}{2}\boldsymbol{\xi}_i\times\mathbf{J})^*\cdot\nabla\times\mathbf{a}_j\right],\end{aligned}\tag{3.12}$$

which is in agreement with (2.12).

The zero-flux-boundary conditions of (2.31) become

$$\begin{aligned}[(\mathbf{Q}+\xi_n\mathbf{J}\times\mathbf{n}+\nabla\times\mathbf{a}_i)_i\cdot\mathbf{B}\xi_j]_{\partial\Omega'} &= 0\\ \left[\nabla\psi\cdot(\nabla\times\mathbf{a}+\mathbf{Q}^+-\tfrac{1}{2}\boldsymbol{\xi}^+\times\mathbf{J})_i\times(\mathbf{a}_j)\right]_{\partial\Omega'} &= 0\end{aligned}\tag{3.13}$$

where $\partial\Omega'$ is a $\psi=$ const surface, i.e. $\mathbf{B}\cdot\nabla\psi=0$ [§ 1.2]. The boundary conditions of (3.13) correspond to the presence of an infinitely conducting wall at $\partial\Omega$, but can be easily extended to incorporate an interface between plasma and vacuum as shown in Ch. 4.

Substituting (3.7) into (2.46), we find

$$\frac{d}{dt}\mathcal{E}_\tau=-\frac{1}{\eta}\parallel\dot{\mathbf{a}}\parallel^2-(\mathsf{V}_A\cdot\mathsf{z},\dot{\mathsf{z}})-(\mathsf{z},\mathsf{V}_A\cdot\dot{\mathsf{z}}),\tag{3.14}$$

with the first term in the right-hand side being negative-definite. Disregarding first the case of complex growth-rates, we find that (3.14) satisfies (2.46) and is therefore causal, and furthermore that the rate of dissipation $\parallel\mathbf{a}\parallel^2/\eta\sim\eta$ is in the order of η since

$$\mathbf{a}\sim\eta\tag{3.15}$$

as $\eta\to 0$. It can be shown that the momentum conjugate to $\mathbf{a}$ is $\partial L/\partial\dot{\mathbf{a}}^+=\mathbf{a}/2\eta$, that is the momentum is of order η^0 and, surprisingly, proportional to $\mathbf{a}$ itself. This is characteristic of a diffusion equation, which cannot for this reason be put into Hamiltonian form. Note also that expression (3.12) for $\mathcal{E}_\tau$ is invariant under the gauge transformations $\mathbf{a}\mapsto\mathbf{a}+\nabla\phi$ since $\mathcal{E}_\tau$ depends only upon the magnetic-field perturbation $\nabla\times\mathbf{a}$ [Chu *et al.* (1990a)].

As M is positive-definite, we may apply the necessary and sufficient criterion of (2.49),

$$(\mathsf{z},\mathsf{V}_H\cdot\mathsf{z})\geq 0,\qquad\forall\ \mathsf{z}\in\mathcal{H},\tag{3.16}$$

for purely growing modes γ, $\mathsf{z} \propto \exp\gamma t$. This criterion is in essence equivalent to the criterion of Tasso (1990) which derives from the dispersion relation

$$(\mathsf{z}, \mathsf{M}\cdot\ddot{\mathsf{z}}) + (\mathsf{z}, \mathsf{D}\cdot\dot{\mathsf{z}}) + (\mathsf{z}, \mathsf{V}\cdot\mathsf{z}) = 0. \tag{3.17}$$

As a consequence of the positive-definiteness of the kinetic term $\gamma^2(\mathsf{z}, \mathsf{M}\cdot\mathsf{z})$ and since the dissipative term $\gamma(\mathsf{z}, \mathsf{D}\cdot\mathsf{z})$ has the sign of the growth rate, it is readily seen that (3.17) does not admit any positive root $\gamma > 0$ if $(\mathsf{z}, \mathsf{V}\cdot\mathsf{z})$ is positive-definite. Clearly, Tasso's criterion is only sufficient since, following his argument, the case where all the roots γ are negative (stable) with $(\mathsf{z}, \mathsf{V}\cdot\mathsf{z})$ being indefinite, or even possibly negative-definite cannot *a priori* be excluded. On the other hand, the existence of a negative-definite Lyapunov-functional $\frac{d}{dt}\mathcal{E}_r = 2\gamma\mathcal{E}_r$ given by (3.14) shows independently that a positive γ corresponds to a negative $\mathcal{E}_r$ and conversely, hence demonstrating that requiring $\mathcal{E}_r = (\dot{\mathsf{z}}, \mathsf{M}\cdot\dot{\mathsf{z}}) + (\mathsf{z}, \mathsf{V}_H\cdot\mathsf{z})$ to be positive-definite is a necessary and sufficient criterion for stability. The positive-definiteness of $(\dot{\mathsf{z}}, \mathsf{M}\cdot\dot{\mathsf{z}})$ reduces then this criterion to the zero-frequency form (3.16) without loss of generality.

The limit of zero-resistivity is straight-forward, setting $\mathbf{a} = 0$ in (3.5), we find the familiar energy principle of [Berstein *et al.* (1958)]

$$\begin{aligned} W[\boldsymbol{\xi};\boldsymbol{\xi}] &= -\tfrac{1}{2}(\boldsymbol{\xi}, \mathsf{F}\cdot\boldsymbol{\xi}) \\ &= \int_\Omega d\tau w(\boldsymbol{\xi},\boldsymbol{\xi}) \geq 0, \end{aligned} \tag{3.18}$$

$\forall\ \boldsymbol{\xi} \in \mathcal{H}$, which is the global-stability criterion against ideal modes.

3.2 Interchange modes

Our prime interest, of course, is to investigate the existence of criteria for the case where η is small but non-zero. The criterion of (1.72) against fast resistive-interchange modes appears suitable for this task, for these modes are known to be localized; they do not need to be matched to outer region solutions and thus we may apply the simpler formalism developed in § 2.4 which is only valid for solutions satisfying Hermitian, or zero-flux boundary conditions. The case where energy

fluxes play a dominant role, as for tearing modes, will be discussed in § 3.3. The Lagrangian density corresponding to Eqs.(1.55)–(1.57) is

$$\begin{aligned} L \;=\; & \tfrac{1}{4}\Big\{-\Psi^{+}\dot{\Psi}+\dot{\Psi}^{+}\Psi-\Psi^{+}X\dot{\Xi}+\dot{\Psi}^{+}X\Xi+\Psi^{+}H\Upsilon'-\Psi^{+\prime}H\Upsilon \\ & -2\Psi^{+\prime}\Psi'+2\dot{\Xi}^{+\prime}\dot{\Xi}'-\Xi^{+}X\dot{\Psi}+\dot{\Xi}^{+}X\Psi-\Xi^{+}X^{2}\dot{\Xi}+\dot{\Xi}^{+}X^{2}\Xi \\ & -\Xi^{+}H\Psi'+\Xi^{+\prime}H\Psi+2\Xi^{+}(E+F)\Upsilon-\dot{\Upsilon}^{+}KH\dot{\Psi}'+\dot{\Upsilon}^{+\prime}KH\dot{\Psi} \\ & +2\dot{\Upsilon}^{+}(KE-G)\dot{\Xi}+2\dot{\Upsilon}^{+}(G+KF)\dot{\Upsilon}-\Upsilon^{+\prime}\dot{\Upsilon}'+\dot{\Upsilon}^{+\prime}\Upsilon'-2\Upsilon^{+}X\Psi \\ & -2\Upsilon^{+}X^{2}\Upsilon\Big\}. \end{aligned} \tag{3.19}$$

Constructing the solution vector

$$\mathsf{z}\equiv\begin{pmatrix}\Psi\\ \Xi\\ \Upsilon\end{pmatrix}, \tag{3.20}$$

(3.19) yields $\mathsf{L}\mathsf{z}=0$ with L given by (2.39). The matrix-operators of (2.39) are

$$\mathsf{M}=\tfrac{1}{2}\begin{pmatrix}0 & 0 & 0\\ 0 & -\partial_X^2 & 0\\ -KH\partial_X & KE-G & G+KF\end{pmatrix}, \tag{3.21}$$

$$\mathsf{D}=\tfrac{1}{2}\begin{pmatrix}1 & X & 0\\ X & X^2 & 0\\ 0 & 0 & -\partial_X^2\end{pmatrix} \tag{3.22}$$

and

$$\mathsf{V}=\tfrac{1}{2}\begin{pmatrix}-\partial_X^2 & 0 & -H\partial_X\\ H\partial_X & 0 & -E-F\\ X & 0 & X^2\end{pmatrix}. \tag{3.23}$$

We find from (3.22) that

$$\begin{aligned} 2(\mathsf{z},\mathsf{D}\cdot\mathsf{z}) \;&=\; \int_{-\infty}^{\infty}dX\left(|\Psi-X\Xi|^2+|\Upsilon'|^2\right)\\ &\geq\; 0 \end{aligned} \tag{3.24}$$

is causal, in the sense defined by (2.46). The fact, however, that V of (3.23) is non-Hermitian means that the stability considerations must be restricted, as in § 3.1, to real growth-rates in spite of the existence of overstable modes [Glasser *et al.*

(1975)]. More problematic is the non-Hermiticity of (3.21) which contradicts the positive definiteness (2.44) of the kinetic component. From the point of view of (2.43), the physical meaning of a non-definite kinetic energy remains obscure. This may well underline the inconsistencies of Eqs.(1.55)–(1.57) which were discussed in § 1.5. It is clear that the lack of symmetry exhibited by the matrix-operators (3.21)–(3.23) forms an obstacle that prohibits us to proceed further without introducing simplifying assumptions.

We then turn to Eqs.(1.62), which are obtained from Eqs.(1.55)–(1.57) after using the large aspect-ratio expansion (1.60). Defining in this limit

$$\mathsf{z} \equiv \begin{pmatrix} \Psi \\ \Xi \end{pmatrix}. \tag{3.25}$$

Equations (1.62) possess the appropriate form

$$\mathsf{M} = \tfrac{1}{2} \begin{pmatrix} 0 & 0 \\ 0 & -\partial_X^2 \end{pmatrix}, \tag{3.26}$$

$$\mathsf{D} = \tfrac{1}{2} \begin{pmatrix} 1 & X \\ X & X^2 \end{pmatrix} \tag{3.27}$$

and

$$\mathsf{V} = \tfrac{1}{2} \begin{pmatrix} -\partial_X^2 & 0 \\ 0 & -D_R \end{pmatrix}, \tag{3.28}$$

exhibiting the desired symmetry at the expense of reducing the order of the system, possessing nonetheless asymptotic solutions with exponentially small behaviour as $X \to \pm\infty$ [Johnson *et al.* (1963)]. The energy observable is given from (2.43) in § 2.6,

$$\mathcal{E}_r = \tfrac{1}{2} \int_{-\infty}^{\infty} dX \left(|\dot{\Xi}'|^2 - D_R |\Xi|^2 + |\Psi'|^2 \right). \tag{3.29}$$

It is apparent that stability ($\mathcal{E}_r \geq 0$) relies in (3.29) entirely upon having

$$D_R < 0, \tag{3.30}$$

the sufficient criterion towards slow-interchange modes mentioned in § 1.5. This result is consistent with the discussion of § 1.5, and has been derived for a set of equations similar to Eqs.(3.26)–(3.28) in Johnson *et al.* (1963), by means of a

quadratic functional that bears resemblence to the energy functional (3.29). The fact that a functional possessing the properties of an energy has been used to obtain this result is new.

The energy-functional approach also clarifies some questions related to the fundamental properties that the system must satisfy in order to be of dissipative nature. The method fails nonetheless to yield a simple stability-condition for every model but the simplest; even for systems which satisfy the causality conditions, the definiteness of V_H is not expected to rely in general upon the sign of a unique matrix element such as D_R in (3.28).

3.3 Tearing modes

In the previous section, we excluded the possibility for z to be non-vanishing at $\partial\Omega'$. Inhomogenuous boundary conditions can be perceived as being the consequence of energy fluxes interacting between the resistive layer and the outer region. Recall that, Eqs.(1.62) also admit the power-like asymptotic solutions of (1.63) with leading exponents given by (1.65).

Let us give for convenience the Lagrangian density,

$$\begin{aligned} L \;=\; & \tfrac{1}{2}\Big\{\tfrac{1}{2}\left(\dot\Psi^+ + X\dot\Xi^+\right)\left(\Psi + X\Xi\right) - \tfrac{1}{2}\left(\Psi^+ + X\Xi^+\right)\left(\dot\Psi + X\dot\Xi\right) \\ & + \dot\Xi^{+\prime}\dot\Xi' - \Psi^{+\prime}\Psi' + \Xi^+ D_R \Xi\Big\}. \end{aligned} \tag{3.31}$$

As for § 3.2, we seek a quadratic form which involves the solutions Ψ and Ξ at $X \to \pm\infty$. To do so, we may use the conservation law for the concomitant (2.25),

$$\partial_X P_+[\mathsf{z};\mathsf{z}] + \partial_t U_+[\mathsf{z};\mathsf{z}] = L[\mathsf{z};\mathsf{z}] \tag{3.32}$$

or alternatively, one could also take (2.26),

$$\partial_X P_-[\mathsf{z};\mathsf{z}] + \partial_t U_-[\mathsf{z};\mathsf{z}] = \left(\dot\Psi^+ + X\dot\Xi^+\right)\left(\Psi + X\Xi\right) - L[\mathsf{z};\mathsf{z}], \tag{3.33}$$

assuming we have $\mathsf{L}\mathsf{z} = 0$ with L given by the matrices (3.26)–(3.28). Taking the former choice, we find

$$P_+[\mathsf{z};\mathsf{z}] = \tfrac{1}{2}\left(\dot\Xi^*\dot\Xi' - \Psi^*\Psi'\right) \tag{3.34}$$

and

$$U_+[z;z] = \tfrac{1}{2}\left(\tfrac{1}{2}|\Psi + X\Xi|^2 - \Xi^*\dot{\Xi}''\right) \tag{3.35}$$

from (2.23) and (2.21). Inserting Eqs.(3.34) and (3.35) into (3.32) and integrating over the layer, we then get

$$\begin{aligned}\tfrac{1}{2}\left[\Psi^*\Psi' + \Xi^*\ddot{\Xi}'\right]_{-\infty}^{\infty} &= W[z;z] \\ &\quad + \tfrac{1}{2}\int_{-\infty}^{\infty} dX\left\{\Xi'^*\ddot{\Xi}' + (\Psi + X\Xi)^*\left(\dot{\Psi} + X\dot{\Xi}\right)\right\},\end{aligned} \tag{3.36}$$

with $W[z;z]$ being the zero-frequency energy (2.49). Considering real growth-rates $Q^* = Q$, the right-hand side of (3.36) is composed of a positive-definite term by assumption of (3.30), and a term that possesses the sign of the growth rate, i.e. which is positive if $Q > 0$ and negative otherwise. Equation (3.36) shows that, in the constant-Ψ approximation [see also (1.43)] where

$$\left.\begin{aligned}\Psi &= \Psi_0 + \epsilon X\Psi_1 + \cdots \\ \Xi &= \Xi_0/(\epsilon X) + \Xi_1 + \cdots\end{aligned}\right\}, \tag{3.37}$$

the outer quantity corresponding to the left-hand side of (3.36),

$$[\Psi^*\Psi']_{-\infty}^{\infty} = \epsilon\Psi_0^2\Delta(Q) \tag{3.38}$$

of (1.52). Therefore, the inner matching data $\Delta(Q)$ is a monotonic function of Q which tends to zero in the limit of $Q \to 0$ at the marginal point of slow-interchange stability $W[z;z] = 0$. We see that $Q < 0$ is necessary in (3.36) in order to have a negative inner-matching data, so that the sign of the outer-matching data provides a sufficient stability criterion in agreement with (1.46).

Chapter 4

Two-dimensional equation for the outer solution

It is known from §§ 1.4 and 1.5 that the problem of determining stability essentially reduces to the one of calculating the outer-region data needed for the matching between inner and outer solution, as this yields a dispersion relation of the form given by (1.68) in the finite-β case, and (1.46) for the case of $\beta = 0$.

In cylindrical and toroidal geometry, there exists in general no analytic expression for the outer-matching data, thus creating the need to compute the outer solution using a numerical scheme. The purpose of this chapter is to present the derivation of the two-dimensional scalar-equation governing the plasma motion in the outer region, where resistivity and inertia may be neglected. It is well known from Newcomb (1960) and Bineau (1962) that the force-balance equation $\mathsf{F}\cdot\boldsymbol{\xi} = 0$ can be reduced in the marginal ($\gamma = 0$) limit, by solving for the components within a magnetic surface, to an equation for a scalar dependent-variable ξ proportional to the displacement normal to a magnetic surface.

Following the work of Dewar & Pletzer (1990), Bineau's scalar reduction [Bineau (1962)] of the force-balance equation will be rederived in § 4.2 using the straight-field-line coordinate-system defined in § 4.1, which is equally applicable to toroidal and helically symmetric plasmas. We refer to the outer stability equation as the *Generalized Newcomb Equation* (GNE) because of its similar structure to Newcomb's original equation. We then discuss in § 4.3 the different, equivalent forms

of the GNE that can be generated from the group of symplectic transformations. A particular transformation is used in § 4.4 to reduce the GNE to Newcomb's form in the cylindrical limit. The usefulness of symplectic transformations, which are shown to be intimately connected to the canonical transformations occurring in Hamiltonian theory, will further become apparent in Ch. 5.

4.1 Universal system of coordinates

We work in the (ψ, θ, ζ) curvilinear coordinate-system of § 1.2 [see e.g. Dewar & Glasser (1983)], in which ψ is a surface flux-function, θ is a poloidal-angle variable and ζ is the corresponding toroidal angle such that the field lines appear straight when graphed in the (θ, ζ) space. We take θ to increase by 2π once around the short way, and ζ to increase by 2π over one toroidal field period (see Fig. 1.1), or once around the long way in the case of axisymmetry, as in § 1.2. In this coordinate system the magnetic field $\mathbf{B}$ of (1.7) is represented using (1.10) by

$$\mathbf{B} = \nabla\zeta \times \nabla\psi + q(\psi)\nabla\psi \times \nabla\theta, \tag{4.1}$$

so that

$$\mathbf{B}\cdot\nabla = \mathcal{J}^{-1}(\partial_\theta + q\partial_\zeta), \tag{4.2}$$

with

$$\mathcal{J} \equiv (\nabla\psi \times \nabla\theta \cdot \nabla\zeta)^{-1} \tag{4.3}$$

being the Jacobian of the transformation from Cartesian coordinates to (ψ, θ, ζ) coordinates.

Equation (4.1) is valid even for a fully three-dimensional equilibrium provided it has perfect, nested magnetic-surfaces. However, to simplify some of the later equations we further assume the existence of a continuous symmetry in the equilibrium (i.e. toroidal axisymmetry as in a tokamak, or helical symmetry as in an idealized "straight" stellarator). As a consequence of this assumption, we can and do specify that all equilibrium scalar quantities depend only on ψ and θ, i.e. that ζ is ignorable. In the axisymmetric toroidal case, this means that $2\pi\psi$ is the poloidal magnetic-flux, while in the case of helical symmetry $2\pi\psi$ is the flux threading a

helical ribbon over one field period. In the axisymmetric case, the surface function $q(\psi)$ in (4.1) is the "safety factor", while in the helical symmetry case it is $(\iota/2\pi - 1/l)^{-1}$ where ι is the rotational transform per field period and the integer l is the degree of symmetry of the cross section. In the following, the only geometric assumption we shall make is the ignorability of ζ — the results will apply equally to axisymmetric and helically symmetric equilibria, which is the reason we call the coordinates "universal". [See Dewar *et al.* (1984) for a detailed exposition of all the results in this section, as well as details of how to calculate the quantities defined in terms of a primitive set of equilibrium quantities which are stored on disc and used by the PEST2 stability program.]

We resolve vectors onto the physically important directions $\mathbf{B}$, $\nabla\psi$ and

$$\mathbf{s} \equiv \frac{\nabla\psi\times\mathbf{B}}{|\nabla\psi|^2}, \tag{4.4}$$

which is orthogonal to $\mathbf{B}$ and lies within a magnetic surface. The ψ derivative of q, $q'(\psi)$, measures the global shear in the magnetic field, while the quantity $S \equiv -\mathbf{s}\cdot\nabla\times\mathbf{s}$ measures the local magnetic-shear. Since we can write $\mathcal{J}S = q' + \mathcal{R}_\theta$, where the subscript θ represents the partial derivative with respect to θ, and

$$\mathcal{R} \equiv \frac{q\nabla\psi\cdot\nabla\theta - \nabla\psi\cdot\nabla\zeta}{|\nabla\psi|^2}, \tag{4.5}$$

we call $\mathcal{R}$ the integrated residual-shear.

Another important geometric quantity is the field-line curvature,

$$\begin{aligned}\boldsymbol{\kappa} &\equiv (\mathbf{B}/B)\cdot\nabla(\mathbf{B}/B) \\ &= \kappa_\psi\nabla\psi + \kappa_s\mathbf{s},\end{aligned} \tag{4.6}$$

where κ_ψ is the normal curvature and κ_s is the geodesic curvature.

By integrating the condition that there be no component of the equilibrium current $\mathbf{J}$ normal to a magnetic surface, using the ignorability of ζ, it can be shown [Dewar *et al.* (1984)] that

$$\mathbf{s}\cdot\nabla\theta = -\frac{g(\psi)}{\mathcal{J}|\nabla\psi|^2}, \tag{4.7}$$

where $g(\psi)$, of (1.11), arises as a constant of integration. An equilibrium can be specified by giving the boundary shape and the profile functions $p(\psi)$ and $q(\psi)$, or by specifying $p(\psi)$ and $g(\psi)$ [as in (1.12)].

The equilibrium current $\mathbf{J}$ can be written

$$\mathbf{J} = \sigma\mathbf{B} - \frac{|\nabla\psi|^2 p'(\psi)\mathbf{s}}{B^2}, \tag{4.8}$$

where

$$\sigma \equiv \frac{\mathbf{J}\cdot\mathbf{B}}{B^2} = -g' - \frac{gp'}{B^2} \tag{4.9}$$

measures the parallel current.

4.2 Generalized Newcomb equation

We are concerned with the solution of the linearized MHD-force-balance equation [Bernstein *et al.* (1958)]

$$\begin{aligned} \mathsf{F}\cdot\boldsymbol{\xi} \;=\; & -\mathbf{B}\times[\nabla\times(\mathbf{Q}+\xi_n\mathbf{J}\times\mathbf{n})] - \mathbf{n}\mathsf{j}\times\mathbf{n}\cdot(\mathbf{Q}+\xi_n\mathbf{J}\times\mathbf{n}) \\ & + 2U\nabla\psi\,\boldsymbol{\xi}\cdot\nabla\psi + \nabla(\Gamma p\nabla\cdot\boldsymbol{\xi}) = 0, \end{aligned} \tag{4.10}$$

for the ideal displacement-field $\boldsymbol{\xi}$, where $\mathbf{n} \equiv \nabla\psi/|\nabla\psi|$ is the unit normal to the magnetic surface, $\xi_n \equiv \mathbf{n}\cdot\boldsymbol{\xi}$, $\mathbf{Q} \equiv \nabla\times(\boldsymbol{\xi}\times\mathbf{B})$ and

$$U \equiv \frac{\mathbf{J}\times\mathbf{n}\cdot(\mathbf{B}\cdot\nabla\mathbf{n})}{|\nabla\psi|^2}. \tag{4.11}$$

A more physically meaningful expression for U is given by Dewar *et al.* (1984)

$$2U = 2p'\kappa_\psi + \sigma^2|\mathbf{s}|^2 + \sigma S, \tag{4.12}$$

which shows the potentially destabilizing effects of field-line curvature and parallel current.

Owing to the assumed continuous symmetry we take the ζ dependence of $\boldsymbol{\xi}$ to be that of the single-Fourier mode $\exp(-in\zeta)$, where n is the toroidal-mode number, which we assume to be non-zero. This allows us to solve the magnetic differential-equation $\mathbf{B}\cdot\nabla(\Gamma p\nabla\cdot\boldsymbol{\xi}) = 0$, obtained when we dot (4.10) with $\mathbf{B}$, to give the incompressibility condition

$$\nabla\cdot\boldsymbol{\xi} \equiv 0 \tag{4.13}$$

as an exact result. It also allows us to write

$$\mathcal{J}\mathbf{B}\cdot\nabla\boldsymbol{\xi} = \mathcal{D}_\theta\boldsymbol{\xi}, \tag{4.14}$$

where

$$\mathcal{D}_\theta \equiv \partial_\theta - inq. \tag{4.15}$$

Equation (4.13) eliminates the parallel component of $\boldsymbol{\xi}$ from (4.10). To eliminate the other component of $\boldsymbol{\xi}$ lying within a magnetic surface in favour of the covariant ψ-component

$$\xi \equiv \boldsymbol{\xi}\cdot\nabla\psi \tag{4.16}$$

we dot (4.10) with s and obtain [Grimm *et al.* (1983)], again assuming $n \neq 0$,

$$\mathbf{Q} + \xi_n \mathbf{J}\times\mathbf{n} = \frac{\nabla\psi(\mathbf{B}\cdot\nabla\xi)}{|\nabla\psi|^2} + \nabla_s(\mathcal{G}\mathcal{P}\xi). \tag{4.17}$$

Here ∇_s is the surface gradient operator (I $-$ **nn**)$\cdot\nabla$, I being the unit dyadic, $\mathcal{G}$ is the surface Green's function operator

$$\mathcal{G} \equiv -(\nabla\cdot\nabla_s)^{-1}\mathcal{J}^{-1}, \tag{4.18}$$

and $\mathcal{P}\xi$ is defined by

$$\mathcal{P}\xi \equiv \mathcal{J}\nabla\cdot\left(\frac{\nabla\psi\,\mathbf{B}\cdot\nabla\xi - \mathbf{J}\times\nabla\psi\,\xi)}{|\nabla\psi|^2}\right). \tag{4.19}$$

In terms of the quantities defined in the previous section, we write the operator $\mathcal{P}$ more explicitly as

$$\mathcal{P} = \mathcal{D}_\theta\partial_\psi + \mathcal{Q}, \tag{4.20}$$

where

$$\begin{aligned}\mathcal{Q} \equiv\ & \mathcal{D}_\theta\frac{\nabla\psi\cdot\nabla\theta}{|\nabla\psi|^2}\mathcal{D}_\theta + \mathcal{D}_\theta\left(\frac{p'}{B^2} - \frac{g\sigma}{|\nabla\psi|^2} + in\mathcal{R}\right)\\ & - in(\mathcal{J}|\mathbf{s}|^2\sigma + q' + \mathcal{R}_\theta),\end{aligned} \tag{4.21}$$

the operators ∂_ψ and ∂_θ (in $\mathcal{D}_\theta$) acting on everything to their right (including the ψ and θ variation in the equilibrium quantities). The surface Green's function is the inverse of the operator

$$\begin{aligned}\mathcal{G}^{-1} =\ & n^2\mathcal{J}|\nabla_s\zeta|^2 + in(\mathcal{J}\nabla_s\theta\cdot\nabla_s\zeta)\partial_\theta + in\partial_\theta(\mathcal{J}\nabla_s\theta\cdot\nabla_s\zeta)\\ & - \partial_\theta(\mathcal{J}|\nabla_s\theta|^2)\partial_\theta,\end{aligned} \tag{4.22}$$

in which form it is seen that there is no ∂_ψ operator in $\mathcal{G}$.

Rather than Fourier analyzing in θ, as is done in the PEST2 code [Grimm *et al.* (1983)], it is more convenient for the purposes of the discussion to remain in θ space at the expense of working with operators which may not necessarily commute, but avoiding the matrices which occur in Fourier space. We define, for arbitrary 2π-periodic f and g, the surface inner product

$$< f, g > \equiv \frac{1}{2\pi} \int_0^{2\pi} d\theta f^*(\theta) g(\theta), \tag{4.23}$$

with respect to which $\mathcal{G}$ is an Hermitian operator, as is seen from (4.22).

Substituting (4.17) in (4.10) we obtain the *Generalized Newcomb Equation* (GNE)

$$\mathcal{J} \frac{\nabla\psi \cdot (\mathsf{F} \cdot \boldsymbol{\xi})}{|\nabla\psi|^2} \equiv L\xi = 0 \tag{4.24}$$

where

$$L\xi = -(\partial_\psi \mathcal{D}_\theta + \mathcal{Q}^\dagger)\mathcal{G}(\mathcal{D}_\theta \partial_\psi + \mathcal{Q})\xi + \mathcal{K}\xi, \tag{4.25}$$

is the GNE operator, with $(\cdot)^\dagger$ denoting the Hermitian conjugate of $(\cdot)$ (e.g. $\mathcal{D}_\theta^\dagger = -\mathcal{D}_\theta$), and $\mathcal{K}$ is an Hermitian operator defined by

$$\mathcal{K} \equiv 2\mathcal{J}U + \mathcal{J}\mathbf{B}\cdot\nabla \frac{1}{|\nabla\psi|^2} \mathbf{B}\cdot\nabla. \tag{4.26}$$

Using (4.12) we obtain the form

$$\mathcal{K} = 2p'\mathcal{J}\kappa_\psi + \mathcal{J}\sigma^2|\mathsf{s}|^2 + \sigma(q' + \mathcal{R}_\theta) + \mathcal{D}_\theta \frac{1}{\mathcal{J}|\nabla\psi|^2} \mathcal{D}_\theta. \tag{4.27}$$

4.3 Hamiltonian form of the GNE and symplectic transformations

Equation (4.24) has a similar one-dimensional (with respect to ψ) Sturm-Liouville structure to Eq.(23) of Newcomb (1960), except for the $\mathcal{Q}$ terms. However, if we take the cylindrical limit of (4.24) the $\mathcal{Q}$ terms do not vanish, even if we transform from ψ to r as the independent variable and from $\boldsymbol{\xi}\cdot\nabla\psi$ to $\xi_r \equiv \boldsymbol{\xi}\cdot\nabla r$ (where r is the distance from the magnetic axis), as the dependent variable to obtain exact correspondence with Newcomb's usage. This suggests that (4.21) and (4.26) are not unique choices for an Euler-Lagrange equation of the form (4.24) — that, at least in the cylindrical limit, we must be able to "transform $\mathcal{Q}$ away".

Another motivation to seek various forms of the GNE is in the need to find transformations that provide a better physical insight, and we shall see in Ch. 5 that for instance the expression of Mercier's stability criterion in the two-dimensional case can be greatly simplified when applying such a transformation. Also, it is expected that other members of the class of equivalent GNEs may lead to a more accurate computation of the weak solution of Ch. 6.

To obtain the group of transformations, it is instructive to rederive the GNE from a variational principle based on the action

$$\mathcal{S} = -\int d\psi \{< [\mathcal{D}_\theta \partial_\psi + \mathcal{Q}]\xi, \mathcal{G}[\mathcal{D}_\theta \partial_\psi + \mathcal{Q}]\xi > - < \xi, \mathcal{K}\xi >\} \tag{4.28}$$

where ψ plays the role of the time-like independent variable by applying the tools of Ch. 2. We see that the action (4.28) is in fact proportional to the potential energy

$$W \equiv -\tfrac{1}{2}\int d\psi d\theta \xi^* (L\xi) \tag{4.29}$$

whose positive-definiteness (3.18) is known to ensure ideal stability towards global modes. Following the prescriptions of § 2.2, we obtain the generalized momentum

$$\delta P = \frac{\delta \mathcal{S}}{\delta \xi'^*} = \mathcal{D}_\theta \mathcal{G}\mathcal{P}\xi \tag{4.30}$$

to ξ, where $\xi' \equiv \partial_\psi \xi$. In the attempt to attach a physical interpretation to (4.30), we recognize $\mathcal{D}_\theta \mathcal{G}\mathcal{P}\xi$ as being equal to $\mathbf{B}\cdot(\mathbf{Q}+\xi_n \mathbf{j}\times\mathbf{n})$ of (4.17), which can be shown, using Eqs.(1.6) and (1.18) to yield

$$\mathbf{B}\cdot(\mathbf{Q} + \xi_n \mathbf{j}\times\mathbf{n}) = \delta p + \mathbf{B}\cdot\mathbf{Q}. \tag{4.31}$$

That is, the total of the pressure and the magnetic-pressure perturbations.

We proceed further by deriving the Hamiltonian density

$$H = \delta P^* \xi' + \xi'^* \delta P + (\mathcal{D}_\theta \xi' + \mathcal{Q}\xi)^* \mathcal{G}[\mathcal{D}_\theta \xi' + \mathcal{Q}\xi] - \xi^* \mathcal{K}\xi. \tag{4.32}$$

Since the Hamiltonian density (4.32) can be solely written in terms of the δP's and ξ's,

$$H = \delta P^* \mathcal{D}_\theta^{-1} \mathcal{G}^{-1} \mathcal{D}_\theta^{-1} \delta P - \xi^* \left(\mathcal{D}_\theta^{-1}\mathcal{Q}\right)^\dagger \delta P - \delta P^* \mathcal{D}_\theta^{-1} \mathcal{Q}\xi - \xi^* \mathcal{K}\xi \tag{4.33}$$

we can rewrite (4.24) as a set of first-order equations

$$\left.\begin{aligned} \partial_\psi \xi &= \partial H/\partial \delta P^* \\ -\partial_\psi \delta P &= \partial H/\partial \xi^* \end{aligned}\right\} \tag{4.34}$$

which is of Hamiltonian form, reducing to

$$\mathsf{J}\partial_\psi \mathsf{z} = \mathsf{H}\mathsf{z} \tag{4.35}$$

after introducing

$$\mathsf{z} \equiv \begin{pmatrix} \xi \\ \delta P \end{pmatrix}, \tag{4.36}$$

the unitary matrix, ($\mathsf{J}^2 = -\mathsf{I}$),

$$\mathsf{J} \equiv \begin{pmatrix} 0 & -1 \\ +1 & 0 \end{pmatrix} \tag{4.37}$$

and the Hermitian matrix

$$\mathsf{H} = \begin{pmatrix} -\mathcal{K} & -(\mathcal{D}_\theta^{-1}\mathcal{Q})^\dagger \\ -\mathcal{D}_\theta^{-1}\mathcal{Q} & \mathcal{D}_\theta^{-1}\mathcal{G}^{-1}\mathcal{D}_\theta^{-1} \end{pmatrix}. \tag{4.38}$$

The system of equations (4.34) bears a similar form to the set of ideal equations governing the finite-frequency motion of a cylindrical plasma [Appert *et al.* (1974)], where a similar decomposition into radial displacement-field and total pressure perturbation was used to show the existence of continuous spectra.

Consider now the canonical transformations

$$\left.\begin{aligned} \psi &\rightarrow x \\ \mathsf{z} &\rightarrow \bar{\mathsf{z}} \equiv \mathsf{U}^{-1}\mathsf{z} \end{aligned}\right\} \tag{4.39}$$

that leave the action (4.28)

$$\mathcal{S} = \int d\psi < \mathsf{z}, \mathsf{J}\mathsf{z}' - \mathsf{H}\mathsf{z} > \tag{4.40}$$

invariant,

$$\begin{aligned} \mathcal{S} \mapsto \bar{\mathcal{S}} &= \int dx\dot{\psi} < \mathsf{U}\bar{\mathsf{z}}, \mathsf{J}\mathsf{U}\bar{\mathsf{z}}' + \mathsf{J}\mathsf{U}'\bar{\mathsf{z}} - \mathsf{H}\mathsf{U}\bar{\mathsf{z}} > \\ &= \mathcal{S} \end{aligned} \tag{4.41}$$

where $\dot{\psi} \equiv d\psi/dx$. The invariance condition (4.41) requires that

$$\mathsf{U}^\dagger \mathsf{J} \mathsf{U} = C\mathsf{J}, \tag{4.42}$$

U be a *symplectic* matrix times a constant C. From (4.41) we obtain the transformation rule for

$$\mathsf{H} \mapsto \overline{\mathsf{H}} = \left[\mathsf{U}^\dagger \mathsf{H} \mathsf{U} - \mathsf{U}^\dagger \mathsf{J}(\partial_\psi \mathsf{U})\right] \dot{\psi} \tag{4.43}$$

such that

$$\mathsf{J}\partial_x \overline{\mathsf{z}} = \overline{\mathsf{H}}\overline{\mathsf{z}}. \tag{4.44}$$

As an example, we give here a very general transformation

$$\mathsf{U}^{-1} = \begin{bmatrix} 1/N(\psi) & 0 \\ -\mathcal{D}_\theta \mathcal{X}/N(\psi) & \dot{\psi}/M(\psi)N(\psi) \end{bmatrix}, \tag{4.45}$$

where the top row of U^{-1} rescales ξ

$$\xi(x,\theta) = N(x)\bar{\xi}(x,\theta) \tag{4.46}$$

and the bottom row redefines a new momentum-like variable $\delta\overline{P}$ as a linear combination of ξ and δP. The transformed GNE is

$$\left(\partial_x \mathcal{D}_\theta + \bar{\mathcal{Q}}^\dagger)\bar{\mathcal{G}}(\mathcal{D}_\theta \partial_x + \bar{\mathcal{Q}}\right)\bar{\xi} - \bar{\mathcal{K}}\bar{\xi} = 0, \tag{4.47}$$

with the transformed operators given by the transformation rule (4.38); we have

$$\mathcal{G} = M(x)\bar{\mathcal{G}}, \tag{4.48}$$

$$\mathcal{Q} = \frac{\bar{\mathcal{Q}} + \bar{\mathcal{G}}^{-1}\mathcal{X} - (\dot{N}/N)\mathcal{D}_\theta}{\dot{\psi}} \tag{4.49}$$

and

$$\bar{\mathcal{K}} \equiv (\dot{\psi}^2/M)\mathcal{K} + M\mathcal{X}^\dagger \mathcal{G}^{-1}\mathcal{X} - \dot{\psi}(\mathcal{X}^\dagger \mathcal{Q} + \mathcal{Q}^\dagger \mathcal{X}) + 2(\dot{N}/N)\mathcal{D}_\theta \mathcal{X} - \partial_x(\mathcal{D}_\theta \mathcal{X}), \tag{4.50}$$

with $\mathcal{X}$ satisfying

$$(\mathcal{D}_\theta \mathcal{X})^\dagger = \mathcal{D}_\theta \mathcal{X}. \tag{4.51}$$

It can be seen from (4.45) that the constants appearing in (4.42) and the definition (4.48) of M are identical, choosing $C = MN^2/\dot{\psi} = 1$ means that U is symplectic. Furthermore, the Hermiticity condition (4.51) of $\mathcal{D}_\theta \mathcal{X}$ is a direct consequence of the property (4.42) of U.

Note that $\mathcal{D}_\theta$ is singular at the rational surface, thus $\mathcal{D}_\theta^{-1}$ in (4.45) is not defined everywhere. This is of no consequence since the expressions for the transformed operators do not contain any $\mathcal{D}_\theta^{-1}$. We will find it, however, more convenient to use in § 5.2 a variation of the Hamiltonian form (4.35) of (4.24) which avoids the use of $\mathcal{D}_\theta$ in its inverse form. This is achieved by applying the transformation

$$\mathsf{U}^{-1} = \begin{pmatrix} 1 & 0 \\ 0 & \mathcal{D}_\theta \end{pmatrix} \tag{4.52}$$

which redefines the auxiliary variable

$$\chi \equiv \mathcal{G}\mathcal{P}\xi \equiv \mathcal{D}_\theta^{-1}\delta P. \tag{4.53}$$

Because U does not satisfy (4.42), (4.52) is not a canonical transformation and as a result the Hermiticity property (4.38) is not conserved for the transformed matrix. The transformed equation (4.35) is then equivalent to

$$(\,\mathsf{I}\,\mathcal{D}_\theta\partial_\psi - \mathsf{A})\,\mathsf{y} = 0, \tag{4.54}$$

where I is the unit 2×2 matrix,

$$\mathsf{y} \equiv \begin{pmatrix} \xi \\ \chi \end{pmatrix}, \tag{4.55}$$

and

$$\mathsf{A} \equiv \begin{pmatrix} -\mathcal{Q} & \mathcal{G}^{-1} \\ \mathcal{K} & -(\mathcal{Q} + inq')^\dagger \end{pmatrix}. \tag{4.56}$$

4.4 The GNE in the cylindrical limit

In the cylindrical limit, we take the θ variable to be the ordinary geometric angle about the axis of symmetry, the z axis. We take the periodicity length to be $2\pi R_0$ (where the constant R_0 corresponds to the major radius in a tokamak) so that $\zeta = z/R_0$ and $q = rB_z/R_0B_\theta$. Following Newcomb (1960) we take ξ to be proportional to $\exp(im\theta + ikz)$ (so that $k = -n/R_0$). We then have

$$\mathcal{D}_\theta = i(m - nq) = \frac{i(mB_\theta + krB_z)}{B_\theta}, \tag{4.57}$$

$$\mathcal{Q} = -\frac{i}{R_0 B_\theta^3}\left[\frac{(mB_\theta - krB_z)}{r}B_\theta + (mB_\theta + krB_z)\frac{dB_\theta}{dr}\right], \tag{4.58}$$

$$\mathcal{K} = \frac{1}{(R_0 B_\theta)^2}\left[\frac{2}{r}\frac{d}{dr}(rB_\theta) - \frac{(mB_\theta + krB_z)^2}{rB_\theta}\right], \tag{4.59}$$

and

$$\mathcal{G} = \frac{rB_\theta}{m^2 + k^2 r^2}. \tag{4.60}$$

To get correspondence with Newcomb (1960) we take $x = r$ and $N = \dot{\psi} = R_0 B_\theta$ so that $\bar{\xi} = \xi_r$. We also take the constant in (4.42) to be R_0, so that $\bar{\mathcal{G}}$ is just $B_\theta \mathcal{G}$. To obtain the Newcomb form of the Euler-Lagrange equation (4.24),

$$\frac{d}{dr}\left(f\frac{d\xi_r}{dr}\right) - g\xi_r = 0, \tag{4.61}$$

we seek to make $\bar{\mathcal{Q}} = 0$ so that (4.24) reduces to (4.61) with the f and g functions given by

$$f = -\mathcal{D}_\theta \bar{\mathcal{G}} \mathcal{D}_\theta, \tag{4.62}$$

and

$$g = -\bar{\mathcal{K}} \tag{4.63}$$

(not to be confused with the g of § 4.1). It can already be seen that (4.62) agrees with (16) of Newcomb (1960).

From (4.49) it is seen that we can make $\bar{\mathcal{Q}} = 0$ by choosing

$$\mathcal{X} = -i\frac{(mB_\theta - krB_z)B_\theta}{m^2 + k^2 r^2}. \tag{4.64}$$

Substitution in (4.50) leads directly to the result

$$\begin{aligned}\bar{\mathcal{K}} \;=\; & \frac{2B_\theta}{r}\frac{d}{dr}(rB_\theta) - \frac{(mB_\theta - krB_z)^2}{r(m^2 + k^2 r^2)} - \frac{(mB_\theta + krB_z)^2}{r} \\ & - \frac{d}{dr}\left[\frac{m^2 B_\theta^2 - k^2 r^2 B_z^2}{m^2 + k^2 r^2}\right],\end{aligned} \tag{4.65}$$

which, using (4.63), agrees with (17) of Newcomb (1960).

Another interesting form of the equation for ideal displacements from equilibrium was used by Furth *et al.* (1973),

$$\frac{d}{dr}\left(H\frac{d(F\xi_r)}{dr}\right) - \left[\frac{g}{F^2} + \frac{1}{F}\frac{d}{dr}\left(H\frac{dF}{dr}\right)\right]F\xi_r = 0, \tag{4.66}$$

where

$$H \equiv \frac{r^3}{m^2 + k^2 r^2}, \tag{4.67}$$

$$F \equiv kB_z + m\frac{B_\theta}{r} = \frac{(m - nq)B_\theta}{r}, \tag{4.68}$$

and g is given by (4.63) and (4.65).

Equation (4.66) follows directly from a transformed GNE of the form (4.47) with $x = r$,

$$\bar{\xi} \equiv B_\theta \xi_r / r = \xi / r R_0, \tag{4.69}$$

$\bar{\mathcal{G}} = H$,

$$\bar{\mathcal{K}} \equiv -\frac{r^2}{B_\theta^2}\left[g + F\frac{d}{dr}\left(H\frac{dF}{dr}\right)\right], \tag{4.70}$$

and $\bar{\mathcal{Q}}$ such that

$$\bar{\mathcal{Q}} + in\dot{q} = 0. \tag{4.71}$$

The choice (4.71) is equivalent to omitting $\bar{\mathcal{Q}}$ from (4.47) and commuting the $\mathcal{D}_\theta$ and ∂_x operators.

Chapter 5

Frobenius solutions

In the context of weakly resistive instabilities, the marginal stability equation (4.24) (GNE) is satisfied approximately everywhere but in the arbitrarily thin resistive-layers of §§ 1.4 and 1.5 containing the rational surfaces. The GNE can be shown to exhibit regular singularities precisely at these rational surfaces, where the solutions can be written as a power series times a fractional power, that is a *Frobenius expansion.* Two distinct singular solutions are shown in § 5.2 to occur at the rational surfaces, one presenting a non-square-integrable divergence and the other being the ideal, weak solution of the GNE which may diverge or else be asymptotically zero depending on the sign of its leading exponent. We refer to the former solution as the *big solution* whereas the square-integrable solution is termed the *small solution.* In the two-dimensional case, we also find the existence of analytic solutions, or accordingly to our terminology *regular solutions*, which are discussed in § 5.4.

Both the big and small solutions present the appropriate behaviour for matching the ideal with the resistive solutions of § 1.5, with the regular solutions arising in the form of a constant of integration in Eq.(21) of Glasser *et al.* (1975). The regular solution has no role in the matching process, its effect being only to couple the left-sided solutions to the right-sided solutions about the rational surface.

The accurate knowledge of the asymptotic behaviour of both the big and small solutions is crucial for the matching scheme of Ch. 6, by providing a set of fundamental solutions which can be superimposed to form the total solution.

5.1 Magnetic-axis singularity

We start by discussing the behaviour of ξ near the magnetic axis $\psi = 0$. This singularity arises from the vanishing of the term containing $\mathcal{G}$ in (4.24) which is the highest order derivative (in ∂_ψ). We choose, in order to derive the indicial equation, the lowest-order equation in the Frobenius expansion, to limit ourselves to the toroidal case and furthermore to assume that the magnetic-ψ surfaces are concentric circles near $\psi = 0$, thus neglecting effects of ellipticity at lowest order. We have

$$\psi \sim \frac{R_0 j_0 r^2}{4}, \tag{5.1}$$

where j_0 represents the axial current-density, R_0 the distance of the magnetic axis from the centre of the torus in Fig. 1.1 and r the radius from the magnetic axis. The assumption of circularly nested ψ-surfaces allows us to take $\zeta = \phi$, where ϕ is the toroidal angle of Fig. 1.1, so that the coordinate system is orthogonal. Since all equilibrium quantities are independent of θ, the operators of § 4.2 reduce to

$$\left.\begin{aligned} \mathcal{K} &\sim 2/R_0\psi + \mathcal{D}_\theta^2/2R_0\psi \\ \mathcal{Q} &\sim -\partial_\theta/\psi \\ \mathcal{G}^{-1} &\sim 2n^2/j_\zeta(0)R_0^2 - R_0\partial_\theta^2/2\psi \end{aligned}\right\} \tag{5.2}$$

as $\psi \to 0$. We then find that (4.24) reduces to lowest order to

$$\left[\partial_\psi \frac{2\psi/R}{m^2}\partial_\psi - \frac{1}{2R\psi}\right]\xi_m = 0, \tag{5.3}$$

the so called indicial equation, which is valid for $\xi_m \propto \exp im\theta$ being a pure Fourier mode with m positive and $\neq 0$. Equation (5.3) yields

$$\xi_m \sim \psi^{m/2} \sim r^m \tag{5.4}$$

as $\psi \to 0$, as the only admissible solution. The other solution to (5.3), $\xi_m \sim \psi^{-m/2} \sim r^{-m}$ is discarded because of its divergent behaviour. For poloidally symmetric modes $m = 0$, however, the Newcomb equation can be shown to have no singularity so that $\xi_0 \sim \psi^0$ is finite in this case.

5.2 Frobenius expansion around rational surfaces

Equation (4.24) is a second-order differential equation in ∂_ψ with the highest derivative term being $\partial_\psi \mathcal{D}_\theta \mathcal{G} \mathcal{D}_\theta \partial_\psi$, which is singular (with respect to a given n) at a mode rational surface $\psi = \psi_i$, where the safety factor q is a rational fraction,

$$q_i \equiv q(\psi_i) \equiv m_i/n, \tag{5.5}$$

with m_i an integer, the subscript i allowing to differentiate between rational surfaces arising when q has a non-monotonic behaviour. The operator $\mathcal{D}_\theta$ has, at $\psi = \psi_i$, a one-dimensional null space spanned by $\exp im_i\theta$. [$\mathcal{D}_\theta \exp im_i\theta = i(m_i - nq)\exp im_i\theta$.]

Here we treat the general two-dimensional case as given by Eqs.(4.54)–(4.56), leaving the treatment of the cylindrical case (4.61) to Appendix C. Let us expand around the rational surface $\psi = \psi_i$ defined by (5.5), assuming all equilibrium quantities are differentiable to sufficient order for their Taylor expansion

$$\mathsf{A} = \mathsf{A}_i + (\psi - \psi_i)\mathsf{A}'_i + \frac{(\psi - \psi_i)^2}{2}\mathsf{A}''_i + \cdots \tag{5.6}$$

to be carried to an order appropriate to the number of terms of the Frobenius expansion which we wish to retain. As we are setting up the present formalism to be used in a Galerkin solution of the GNE, it is natural to work within the framework of distributions or generalized functions. The generalized functions x_L^α and x_R^α [Gel'fand & Shilov (1964)] are shown in Appendix B to be equal to $|x|^\alpha$ on their respective domains of support, $(-\infty, 0)$ and $(0, +\infty)$, and are defined in such a way that they obey the usual rules of differentiation of x^α on $(-\infty, +\infty)$. Thus, in the Frobenius expansion

$$\mathsf{y}(\psi, \theta) = (\psi - \psi_i)^{\alpha_i}\left[\mathsf{y}_0(\theta) + (\psi - \psi_i)\mathsf{y}_1(\theta) + (\psi - \psi_i)^2\mathsf{y}_2(\theta) + \cdots\right] \tag{5.7}$$

$(\psi - \psi_i)^{\alpha_i}$ may be interpreted as either $(\psi - \psi_i)_L^{\alpha_i}$ or $(\psi - \psi_i)_R^{\alpha_i}$, or more generally as any linear combination of these left- and right-sided functions, each choice generating an independent solution (except for α integer, which happens to be the case for the regular solutions discussed in § 5.4). For instance, in § 6.1, we will use extensively the even $(\psi - \psi_i)_+^\alpha = (\psi - \psi_i)_R^\alpha + (\psi - \psi_i)_L^\alpha$ and odd

$(\psi-\psi_i)^\alpha_- = (\psi-\psi_i)^\alpha_R - (\psi-\psi_i)^\alpha_L$ combinations and denote by $\mathsf{y}_\pm$ the corresponding Frobenius solutions.

Substituting (5.7) in (4.54) and equating like powers of $(\psi-\psi_i)$ we find to lowest order $\mathcal{O}(|\psi-\psi_i|^{\alpha_i-1})$

$$\alpha_i \mathcal{D}_i \mathsf{y}_0 = 0, \tag{5.8}$$

where $\mathcal{D}_i \equiv (\partial_\theta - inq_i) = (\partial_\theta - im_i)$, which is solved *either* by taking $\alpha_i = 0$ and y_0 arbitrary (at this order), *or* by taking y_0 from the null space of $\mathcal{D}_i$ (i.e. proportional to $\exp im_i\theta$) and α_i arbitrary (again, at this order). For reasons which will become apparent we shall call solutions arising from the former choice the *regular* solutions, leaving their treatment to § 5.4, while those from the latter choice will be termed the *singular* solutions.

5.3 Singular solutions

Considering the singular solutions, we write

$$\mathsf{y}_0 = \mathsf{u}_i \exp im_i\theta, \tag{5.9}$$

where u_i is not determined at this order. To next order in the expansion

$$(\alpha_i+1)\mathcal{D}_i \mathsf{y}_1 = (\mathsf{A}_i + inq_i'\alpha_i\, \mathsf{I}\,)\,\mathsf{u}_i \exp im_i\theta, \tag{5.10}$$

where the subscript i denotes, as in (5.6), evaluation at ψ_i. We assume for now that $\alpha_i \neq -1$, so that the solubility condition for (5.10) is that the right-hand side have no functional component lying within the null space of $\mathcal{D}_i$. That is,

$$(< \mathsf{A}_i > + inq_i'\alpha_i\, \mathsf{I}\,)\,\mathsf{u}_i = 0, \tag{5.11}$$

where $< \cdot >$ denotes the diagonal (m_i, m_i) Fourier-matrix element of $\cdot$,

$$< \cdot > \equiv < \exp im_i\theta, \cdot \exp im_i\theta >, \tag{5.12}$$

with the inner product defined in (4.23). Normalizing the ξ component of u_i, we get

$$\mathsf{u}_i = \begin{pmatrix} 1 \\ (< \mathcal{Q}_i > - inq_i'\alpha_i)/ < \mathcal{G}_i^{-1} > \end{pmatrix}. \tag{5.13}$$

Equation (5.11) is an eigenvalue problem determining both α_i and u_i. Setting the determinant of the matrix in (5.11) to zero yields the indicial equation

$$\alpha_i(\alpha_i + 1) + D_I(\psi_i) + \tfrac{1}{4} = 0, \tag{5.14}$$

where

$$D_I(\psi_i) \equiv -\frac{1}{4} + \frac{< \mathcal{K}_i >< \mathcal{G}_i^{-1} > - < \mathcal{Q}_i + inq_i' >^* < \mathcal{Q}_i >}{n^2 q_i'^2}. \tag{5.15}$$

Since the solutions of (5.14) are

$$\alpha_i = \begin{cases} \alpha_i^{(s)} \equiv -1/2 + \mu_i \\ \alpha_i^{(b)} \equiv -1/2 - \mu_i \end{cases}, \tag{5.16}$$

where

$$\mu_i \equiv \sqrt{-D_I(\psi_i)}, \tag{5.17}$$

we recognize D_I as the Mercier function of Eqs.(1.58) and (1.65), which determines localized interchange-instability [Glasser *et al.* (1975)] at the rational surface. We assume the plasma to be interchange stable, so that $D_I < 0$, and μ_i is real. From (5.16) we see that there are two singular solutions associated with a given rational surface. One is the *big solution* generated by choosing $\alpha = \alpha_i^{(b)}$, which diverges faster than $(\psi - \psi_i)^{-1/2}$ as $\psi \to \psi_i$, and the other is the *small solution*, generated by choosing $\alpha = \alpha_i^{(s)}$, which is square integrable. The small solution may or may not diverge, depending whether $0 < \mu_i < 1/4$ or $\mu_i > 1/4$ respectively.

We denote the eigenvectors corresponding to $\alpha_i^{(t)}$ by $\mathsf{u}_i^{(t)}$, where $t \in \{s, b\}$, and the adjoint (row) eigenvectors by $\overline{\mathsf{u}}_i^{(t)}$. That is,

$$\overline{\mathsf{u}}_i^{(t)} \left(< \mathsf{A}_i > + inq_i' \alpha_i^{(t)} \, \mathsf{I} \right) = 0, \tag{5.18}$$

while adopting the normalization

$$\left.\begin{array}{rcccl} \overline{\mathsf{u}}_i^{(s)} \mathsf{u}_i^{(s)} & = & \overline{\mathsf{u}}_i^{(b)} \mathsf{u}_i^{(b)} & = & 1 \\ \overline{\mathsf{u}}_i^{(s)} \mathsf{u}_i^{(b)} & = & \overline{\mathsf{u}}_i^{(b)} \mathsf{u}_i^{(s)} & = & 0 \end{array}\right\}. \tag{5.19}$$

The operator $\mathcal{D}_i$ is invertible within the space complementary to $\exp im_i\theta$, so, given that the solubility condition (5.11) is satisfied and that $\mathcal{D}_i^{-1}\cdot$ is understood to lie within this co-space, we can write the solution of (5.10) as

$$\mathsf{y}_1^{(t)} = \left(\alpha_i^{(t)} + 1\right)^{-1} \mathcal{D}_i^{-1} \left(\mathsf{A}_i + inq_i' \alpha_i^{(t)} \, \mathsf{I} \right) \mathsf{u}_i^{(t)} \exp im_i\theta + \boldsymbol{\lambda}_1^{(t)} \exp im_i\theta, \tag{5.20}$$

where $\boldsymbol{\lambda}_1^{(t)}$ is undetermined at this order.

At next order we find, suppressing the superscript (t),

$$\begin{aligned}(\alpha_i+2)\mathcal{D}_i\mathsf{y}_2 &= [inq_i'(\alpha_i+1)\,\mathsf{I}\,+\mathsf{A}_i]\,\boldsymbol{\lambda}_1\exp im_i\theta\\ &\quad+\left\{(\alpha_i+1)^{-1}\,[\mathsf{A}_i+inq_i'(\alpha_i+1)\,\mathsf{I}\,]\,\mathcal{D}_i^{-1}\,(\mathsf{A}_i+inq_i'\alpha_i\,\mathsf{I}\,)\right.\\ &\quad\left.+\left(\mathsf{A}_i'+\tfrac{1}{2}inq_i''\alpha_i\,\mathsf{I}\,\right)\right\}\mathsf{u}_i\exp im_i\theta, \qquad (5.21)\end{aligned}$$

where A_i' arises from the Taylor expansion (5.6) of A. We can now determine $\boldsymbol{\lambda}_1^{(t)}$ from the solubility condition that the right-hand side must have zero projection on $\exp im_i\theta$:

$$\begin{aligned}\boldsymbol{\lambda}_1 &= -[<\mathsf{A}_i>+inq_i'(\alpha_i+1)\,\mathsf{I}\,]^{-1}\\ &\quad\times\left\{<[\mathsf{A}_i+inq_i'(\alpha_i+1)\,\mathsf{I}\,](\alpha_i+1)^{-1}\mathcal{D}_i^{-1}(\mathsf{A}_i+inq_i'\alpha_i\,\mathsf{I}\,)>\right.\\ &\quad\left.+<(\mathsf{A}_i'+\tfrac{1}{2}inq_i''\alpha_i\,\mathsf{I}\,)>\right\}\mathsf{u}_i. \qquad (5.22)\end{aligned}$$

This procedure can clearly be continued indefinitely, provided that no infinities are encountered and that the derivatives of the equilibrium quantities exist to all orders. The latter condition is physically reasonable, but the former problem of infinities may be encountered for special values of α_i, which we call *singular cases.* There are two potential sources of infinities — the factors $(\alpha_i^{(b)}+j)^{-1}$ and $[<\mathsf{A}_i>+inq_i'(\alpha_i^{(b)}+j)\,\mathsf{I}\,]^{-1}$ occurring in the expansion of the big solution, where j is any positive integer.

From (5.16), we see that the first factor causes the cases $\mu_i = j-1/2 = 1/2,\ 3/2,\ 5/2,\ \cdots$ to be singular. From (5.11), we see that the second factor diverges if $\alpha_i^{(b)}+j=\alpha_i^{(s)}$ which, from (5.16), occurs if $\mu_i = j/2 = 1/2,\ 1,\ 3/2,\ 2,\ \cdots$. The important case $\mu_i = 1/2$ will be treated in § 5.5.

5.4 Regular solutions

We discuss in this section the regular solutions $\mathsf{y}^{(r)}$, obtained when (5.8) is satisfied by taking $\alpha_i = 0$ and the θ dependence of y_0 arbitrary at lowest order. By examining (4.54), it is clear that $\mathsf{y}^{(r)}$ must be differentiable at $\psi=\psi_i$ in this case since $\mathcal{D}_\theta$ cannot kill the δ function arising from the action of ∂_ψ on a discontinuity at $\psi=\psi_i$.

Thus, the Frobenius expansions of the regular solutions are simple power-series in $\psi - \psi_i$, not the generalized functions $(\psi - \psi_i)^0_{L,R}$, in agreement with the remark of Appendix B concerning functions $(\psi - \psi_i)^k$ when k is integer. Assuming the Frobenius expansion to have a finite radius of convergence, we see that the regular solutions are analytic functions of ψ in the neighbourhood of $\psi = \psi_i$ — they are the generalizations of the non-resonant Fourier modes in the cylindrical case. However, in the toroidal or helical cases, they cannot be ignored in the construction of a global solution of the GNE since they will be coupled to the singular solutions by the boundary conditions, thus destroying the convenient disjointness obtained in the cylindrical case for solutions on either side of a rational surface.

Equating powers of $(\psi - \psi_i)^0$ in (4.54) we get

$$\mathcal{D}_i \mathsf{y}_1^{(r)} = \mathsf{A}_i \mathsf{y}_0^{(r)}, \tag{5.23}$$

which is soluble provided

$$< \exp im_i\theta, \mathsf{A}_i \mathsf{y}_0^{(r)} > = 0, \tag{5.24}$$

so that $\mathsf{y}_0^{(r)}$ is not quite arbitrary. The space of regular solutions is spanned by an infinite set of solutions of the form

$$\mathsf{y}_{0,m}^{(r)} = \mathsf{u}_i^{(r)} \exp im_i\theta + \boldsymbol{\lambda}_{0,m} \exp im\theta, \tag{5.25}$$

where m is an arbitrary integer $\neq m_i$ and $\boldsymbol{\lambda}_{0,m}$ can be either of the two linearly independent basis-vectors,

$$\boldsymbol{\lambda}_{0,m}^{(\pm)} \equiv \tfrac{1}{2} \begin{pmatrix} 1 \pm 1 \\ 1 \mp 1 \end{pmatrix}. \tag{5.26}$$

The two vectors $\boldsymbol{\lambda}_{0,m}^{(\pm)}$ give rise to $\mathsf{y}_+^{(r)}$ and $\mathsf{y}_-^{(r)}$, the former solution having ξ normalized to one at ψ_i and χ being asymptotically odd, whereas $\mathsf{y}_-^{(r)}$ is odd in ξ and even in χ. The 2-vector $\boldsymbol{\lambda}_{0,m}$ is determined from (5.24) to be

$$\mathsf{u}_i^{(r)} = - < \mathsf{A}_i >^{-1} < m_i|\mathsf{A}_i|m > \boldsymbol{\lambda}_{0,m}, \tag{5.27}$$

where the matrix element $< m_i|\mathsf{A}_i|m >$ is defined by

$$< m'|\mathsf{A}_i|m > \equiv < \exp im'\theta, \mathsf{A}_i \exp im\theta > . \tag{5.28}$$

This process can clearly be continued to find the higher-order terms of the Taylor expansion of $\mathsf{y}_m^{(r)}$.

5.5 Zero-pressure-gradient expansion

We consider here the situation, which is sometimes referred to as the $\beta = 0$, or pressureless case, though it is not the pressure that is required to vanish at the rational surface but the pressure gradient $p'(\psi_i)$ in (4.27). We find from Eqs.(4.9) that σ is independent of θ at ψ_i in this limit. Furthermore, the operators $\mathcal{K}$ and $\mathcal{Q}$ can be shown using Eqs.(4.27) and (4.21) to satisfy as $p' \to 0$,

$$\left.\begin{aligned} < m|\mathcal{K}_i|m_i > &= -i\sigma_i < m_i|\mathcal{Q}_i|m >^* /n \\ < m|\mathcal{Q}_i|m_i > &= -inq_i'\delta_{mm_i} - i\sigma_i < m|\mathcal{G}_i^{-1}|m_i > /n \end{aligned}\right\} \tag{5.29}$$

for all m, where m_i is, as in § 5.2, the resonant-poloidal mode. Substituting (5.29) into (5.15) we obtain

$$D_I = -\tfrac{1}{4} \tag{5.30}$$

so that the α_i of (5.7) takes the integer values,

$$\left.\begin{aligned} \alpha_i^{(s)} &= 0 \\ \alpha_i^{(b)} &= -1 \end{aligned}\right\} \tag{5.31}$$

in the $\beta = 0$ limit.

Note that the distinction between the regular solution $\mathsf{y}^{(r)}$ of § 5.4 and the continuous component of the small solution $\mathsf{y}^{(s)}$ cannot be justified in terms of the leading exponent as $\alpha_i^{(s)} \to 0$. We may recognize in this the arbitrariness involved in splitting these solutions, which will not be without consequences as we shall see in Ch. 6, where it is found that only the discontinuous part of $\mathsf{y}^{(s)}$ is uniquely defined and therefore relevant to resistive stability.

From another perspective, we find from (5.11) that

$$< \mathsf{A} > \mathsf{u}_i^{(s)} = \left[(\psi - \psi_i) < \mathsf{A}_i' > + \tfrac{1}{2}(\psi - \psi_i)^2 < \mathsf{A}_i'' > + \cdots\right] \mathsf{u}_i^{(s)} \tag{5.32}$$

is an odd function in $(\psi - \psi_i)$ as $\psi \to \psi_i$ due to the null projection of the term $\mathcal{O}(|\psi - \psi_i|^0)$ of (5.6) on $\mathsf{u}_i^{(s)}$. Provided

$$< m_i|\mathcal{D}_\theta|m_i >= -inq_i'(\psi - \psi_i) - \tfrac{1}{2}inq_i''(\psi - \psi_i)^2 + \cdots \tag{5.33}$$

remains asymptotically odd as $\psi \to \psi_i$, that is

$$\left.\begin{aligned} n &\neq 0 \\ q_i' &\neq 0 \end{aligned}\right\}, \tag{5.34}$$

the conjugate action of $\mathcal{D}_\theta$ and ∂_ψ does not alter the parity of y; it is evident that expansion (5.32) violates the parity invariance of the indicial equation of (4.24), thus removing the previously existing degeneracy between even-parity and odd-parity solutions. From the point of view of the generalized functions of Appendix B, this is of course due to the fact that x^n (n is integer) has definite parity: $x^n = x_+^n$ if n is even or $x^n = x_-^n$ if n is odd, whereas x_-^{2n} and x_+^{2n+1} are undefined. Throughout this work we will assume Eqs.(5.34) to be satisfied, thus excluding cases where the q profile may be flattened as this leads to an essential singularity which requires a different *ansatz* to that of (5.7).

Using (5.19) and (5.29), the dominant contribution $\mathsf{u}_i^{(b)}$ and $\mathsf{u}_i^{(s)}$ to y as given by (5.9) are derived from (5.11),

$$\begin{aligned} \mathsf{u}_i^{(b)} &= \begin{pmatrix} 1 \\ -i\sigma_i/n \end{pmatrix} \\ \mathsf{u}_i^{(s)} &= \begin{pmatrix} 1 \\ -i\sigma_i/n - inq_i'/ < \mathcal{G}_i^{-1} > \end{pmatrix}. \end{aligned} \tag{5.35}$$

The fact that $\mu_i = 1/2$ of (5.30) and (5.17) indicates that the limit of $\beta = 0$ corresponds to one of the "singular" cases mentioned in § 5.2; the resonant, first-order Frobenius coefficient of (5.22), and all subsequent higher-order coefficients (5.21) of the big solution turn out infinite.

To grasp the problem, let us estimate $\boldsymbol{\lambda}_1^{(b)}$ by means of (5.22); the infinities of (5.22) arising because of the singular nature of $< \mathsf{A}_i > + inq_i'(\alpha_i + 1)\,\mathsf{I}$, one may use the following formula to invert this matrix

$$[< \mathsf{A}_i > + inq_i' s\,\mathsf{I}\,]^{-1} = \frac{1}{inq_i'}\left(\frac{\mathsf{u}_i^{(b)}\overline{\mathsf{u}}_i^{(b)}}{s + \frac{1}{2} - \mu_i} + \frac{\mathsf{u}_i^{(s)}\overline{\mathsf{u}}_i^{(s)}}{s + \frac{1}{2} + \mu_i}\right) \tag{5.36}$$

with the $\overline{\mathsf{u}}_i$ and u_i obtained from (5.18) and (5.19) becoming in this limit:

$$\left.\begin{aligned} \overline{\mathsf{u}}_i^{(b)} &= < \mathcal{G}_i^{-1} > /inq_i' \quad \begin{pmatrix} i\sigma_i/n + inq_i'/ < \mathcal{G}_i^{-1} > & 1 \end{pmatrix} \\ \overline{\mathsf{u}}_i^{(s)} &= - < \mathcal{G}_i^{-1} > /inq_i' \begin{pmatrix} i\sigma_i/n & 1 \end{pmatrix} \end{aligned}\right\}, \tag{5.37}$$

so that

$$\boldsymbol{\lambda}_1^{(b)} = -\frac{\overline{\mathsf{u}}_i^{(s)} < \mathsf{A}_i' > \mathsf{u}_i^{(b)}}{inq_i'(1 - 2\mu)}\mathsf{u}_i^{(s)}$$

$$- \frac{\overline{\mathsf{u}}_i^{(b)}[< \mathsf{A}_i' > -\frac{1}{2} inq_i'' \mid]\mathsf{u}_i^{(b)}}{inq_i'} \mathsf{u}_i^{(b)}$$
$$+ \mathcal{O}\left(\tfrac{1}{2} - \mu_i\right). \tag{5.38}$$

Thus, we see from (5.38) that $\boldsymbol{\lambda}_1^{(b)} \propto \mathsf{u}_i^{(s)}$; the big solution becomes linearly dependent on the small solution in the limit of $\mu_i \to 1/2$, with all but the lowest, resonant term of $\mathcal{O}((\psi - \psi_i)^{\alpha_i^{(b)}})$ and the next non-resonant term of $\mathcal{O}((\psi - \psi_i)^{\alpha_i^{(b)}+1})$ being infinite in (5.7). This problem can arise whenever the two solutions differ by an integer order, that is $2\mu_i = n$. It is known from Ince (1956) that this problem can be overcome by seeking an independent solution which contains a power expansion times $\ln|\psi - \psi_i|$ in addition to the Frobenius expansion (5.7). A natural way of motivating this *ansatz* is given in Miller & Dewar (1986), where the infinite dependent contribution is subtracted from the big solution so as to define a *new big solution*

$$\mathsf{y}^{(b)} \mapsto \mathsf{y}^{(b)} - s(\mu_i)\mathsf{y}^{(s)}. \tag{5.39}$$

The above equation is of course valid for all μ_i since any linear combination of big and small solution is also a solution of (4.54). Thus $s(\mu_i)$ is an arbitrary function of μ_i, analytic everywhere except when μ_i takes values for which $\boldsymbol{\lambda}_n^{(b)}$ is infinite. For $2\mu_i = n$ (integer), $s(\mu_i)$ must be such that the Frobenius coefficients of the *new* $\mathsf{y}^{(b)}$ be finite at all orders, implying that

$$\lim_{\mu_i \to n/2} s(\mu_i) = \boldsymbol{\lambda}_{2\mu}^{(b)} + \mathcal{O}\left(|n - 2\mu_i|^0\right), \tag{5.40}$$

with

$$\boldsymbol{\lambda}_n^{(b)} \propto \frac{1}{n - 2\mu_i}. \tag{5.41}$$

The logarithmic terms then arise, for instance from taking

$$\begin{aligned} \lim_{\mu_i \to n/2} & \frac{(\psi - \psi_i)^{-\frac{1}{2}-\mu_i+n} - (\psi - \psi_i)^{-\frac{1}{2}+\mu_i}}{n - 2\mu_i} \\ = & \lim_{\mu_i \to n/2} (\psi - \psi_i)^{-\frac{1}{2}+\frac{n}{2}} \frac{(\psi - \psi_i)^{\frac{n}{2}-\mu_i} - (\psi - \psi_i)^{\mu_i - \frac{n}{2}}}{n - 2\mu} \\ = & (\psi - \psi_i)^{-\frac{1}{2}+\mu_i} \ln|\psi - \psi_i|. \end{aligned} \tag{5.42}$$

Choosing

$$s(\tfrac{1}{2}) = -\frac{\overline{\mathsf{u}}_i^{(s)} < \mathsf{A}_i' > \mathsf{u}_i^{(b)}}{inq_i'(1 - 2\mu_i)} \mathsf{u}_i^{(s)}, \tag{5.43}$$

we find the new big solution

$$\begin{aligned}\mathsf{y}^{(b)} \mapsto \mathsf{y}^{(b)} \;=\; & \frac{\mathsf{u}_i^{(b)}}{\psi-\psi_i}\exp im_i\theta - \frac{\overline{\mathsf{u}}_i^{(s)} < \mathsf{A}_i' > \mathsf{u}_i^{(b)}}{inq_i'}\mathsf{u}_i^{(s)} \ln|\psi-\psi_i|\exp im_i\theta \\ & - \frac{\overline{\mathsf{u}}_i^{(b)}[< \mathsf{A}_i' > - \mathsf{I}\, inq_i''/2]\mathsf{u}_i^{(b)}}{inq_i'}\mathsf{u}_i^{(b)}\exp im_i\theta \\ & + \mathcal{O}\left((\psi-\psi_i)\ln|\psi-\psi_i|\right) + \mathcal{O}(\psi-\psi_i). \end{aligned} \tag{5.44}$$

In the following chapters we shall only deal with big solutions that are properly defined for all values of μ_i (no infinite Frobenius coefficients), hence we will implicitly assume the renormalization (5.39) for half-integer values of μ_i. It has been customary to take $s(\mu_i) = 0$ in most preceding works, including Glasser *et al.* (1975); this is only appropriate for $2\mu_i \neq n$. Taking $s(\mu_i) \neq 0$ for other values of μ_i is permitted provided the inner solutions undergo the same renormalization so that the matching between outer an inner solutions remains consistent. The invariance of the matching data under renormalization, and the consequence of subtracting small solutions of even and odd parities will be discussed in § 6.6. The subtraction procedure in the zero-β case for cylindrical plasmas is expounded in Appendix C.

The Frobenius expansion derived in this section differs from the one of Dewar & Pletzer (1990) where use of the symplectic-transformation rules (4.47)–(4.51) was made in order to provide a more concise form of the Mercier function (5.15). Setting

$$\mathcal{X} = -i\frac{\sigma_i}{n} \tag{5.45}$$

of (4.49) and using (5.29), we find

$$\left.\begin{aligned} < m|\bar{\mathcal{K}}_i|m_i > &= 0 \\ < m|\bar{\mathcal{Q}}_i|m_i > &= -inq_i'\delta_{mm_i} \end{aligned}\right\}. \tag{5.46}$$

Replacing $\mathcal{K}_i$ and $\mathcal{Q}_i$ in (5.15) by $\bar{\mathcal{K}}_i$ and $\bar{\mathcal{Q}}_i$ respectively, yields (5.30) in a more obvious way. All the results of the Frobenius expansion in the $\beta = 0$ limit can be obtained by setting $\sigma_i = 0$ in Eqs.(5.29), (5.35) and (5.37).

Chapter 6

Variational principle for the matching data

Having extracted the asymptotic behaviour of the solution ξ about the rational surfaces, we concentrate in this chapter on developing a scheme for the determination of the matching data. The total solution is constructed in § 6.1 as a linear combination involving the big, small and regular solutions of Ch. 5, with various combinations of asymptotic parities (with respect to the rational surfaces) being considered in the general finite-β case.

The matching data are defined, in the usual way [that is assuming $s(\mu_i) = 0$ in (5.39)], as the ratio between small to big solution in § 6.2. The non-square integrable behaviour of the big solution leads us to extract analytically the big-solution contribution, leaving to a numerical scheme the task of computing the solution that is "left-out", the one that has the small-solution behaviour. The former solution is called the *prescribed solution* whereas the latter is treated and referred to as the *response solution*, the matching data becoming the response coefficients to driving big solution. The splitting between prescribed and small solution is at the core of the Hilbert-response formalism from which we obtain a variational principle in § 6.5 for the matching data. The variational principle provides a robust scheme for the computation of the outer-matching data.

6.1 Fundamental set of solutions

Three distinct asymptotic behaviours were found in Ch. 5; the big, small and regular solutions. We seek to construct the most general solution as a linear combination of these Frobenius solutions. Suppose the presence of N rational surfaces x_i, $i = 1, 2 \cdots N$. In this chapter, x is the independent variable, with x_i denoting either ψ_i, as in § 5.2, or $x_i = r_i$ as in Appendix C. The x_i, $i = 1, 2 \cdots N$, surfaces divide the plasma into $N + 1$ sections $x_i < x \leq x_{i+1}$ with $x_0 \equiv 0$ at the magnetic axis, and x_{N+1} the boundary of the plasma: $x_{N+1} \equiv x_a \equiv \psi_a$ or $x_{N+1} \equiv r_a$.

Because we leave as arbitrary the inner-layer physics, we must regard the solutions occurring in each section as being linearly independent of their neighbouring counterparts, this in order to allow for sufficient degrees of freedom to match the outer with the inner solutions. This is consistent with the fact that the solutions to be matched — we mean the big and small solutions since the regular solutions are trivially matched — are independent on either side of the plasma (except for some particular cases including the pressureless plasmas). Attaching to each big and small solution a magnitude coefficient which can be adjusted so as to allow proper matching with the resistive solutions of §§ 1.4 and 1.5, we find that the construction of the global solution involves $2(N + 1)$ of these coefficients, with the boundary condition at x_a and the regularity condition at x_0 reducing this number by two. Here, we adopt the convention that the $2N$ remaining coefficients measure asymptotically the big-solution amplitude on either side of the N rational surfaces. We then find that the most general, global solution can be written as

$$\xi = \sum_p \sum_{i=1}^{N} c_{ip} \left\{ \hat{\xi}_{ip} + \bar{\xi}_{(ip)} + \tilde{\xi}_{(ip)} \right\} \tag{6.1}$$

with c_{ip} representing the adjustable coefficients, and with p taking the values $+$ and $-$ in the even and odd expansion, or R and L in the right-sided and left-sided expansion. If one wishes to use the quasi-Hamiltonian formalism of § 5.2, (6.1) generalizes straightforwardly by replacing the ξ's by the y's. The big, small and regular solutions appear in (6.1) in the form of $\hat{\xi}_{ip}$, $\bar{\xi}_{(ip)}$ (not to be confused with the transformed ξ of Ch. 4) and $\tilde{\xi}_{(ip)}$ respectively, where we take the convention that

$$\hat{\xi}_{ip} \equiv \xi_{ip}^{(b)} + \mathrm{o}\left(\xi^{(s)}\right); \qquad x_i - \epsilon_i < x < x_i + \epsilon_i \tag{6.2}$$

captures the big-solution behaviour of parity p in the finite neighbourhood $\epsilon_i \neq 0$ centred around x_i, to sufficient accuracy so that the disparity between $\hat{\xi}_{ip}$ and the big solution $\xi_{ip}^{(b)}$ is of higher order than the small solution (more precise requirements of $\hat{\xi}$ will be set in § 6.6). In order that the c_{ip} represent the big solution amplitude, we must have

$$\hat{\xi}_{ip} \sim (x - x_i)_p^{\alpha_i^{(b)}} \tag{6.3}$$

as $x \to x_i$ in agreement with Eqs.(5.13) and (C.7). Requirement (6.1) can be satisfied using the Frobenius expansion derived in § 5.3 and Appendix C, thus defining $\hat{\xi}$ in the immediate vicinity of x_i but leaving otherwise its behaviour in $x < x_i - \epsilon_i$ and $x > x_i + \epsilon_i$ arbitrary. The reason for introducing $\hat{\xi}$ is merely due to the fact that $\xi^{(b)}$ is given in terms of a Frobenius expansion which applies only within the radius of convergence, that is less than or equal to the distance extending from x_i to the nearest singular surface $\min(x_{i-1}, x_{i+1})$. Outside the interval $x_i - \epsilon_i < x < x_i + \epsilon_i$, $\hat{\xi}_{ip}$ is not required to satisfy, even approximately, the GNE, thus allowing us to limit the support of $\hat{\xi}_{ip}$,

$$\hat{\xi}_{ip}(x_j) \equiv 0; \qquad \text{if } j \neq i \tag{6.4}$$

to $x_i - \delta_i < x < x_i + \delta_i$, where $\delta_i > \epsilon_i$ and $\delta_i < \min(x_i - x_{i-1}; x_{i+1} - x_i)$. We effect this by multiplying the approximate big-solution with a bell-shaped function, the *localization function* shown in Fig. 6.1. Equation (6.4) then ensures that $\hat{\xi}_{ip}$ satisfies (trivially) the GNE within finite distances of the x_j's, $j \neq i$,

$$L\left(\hat{\xi}_{ip}\right) = 0 \qquad x \approx x_j \tag{6.5}$$

and approximately satisfy the GNE

$$L\left(\hat{\xi}_{ip}\right) = o(\xi^{(s)}) \tag{6.6}$$

near $x = x_i$. This way, we avoid the dilemma of constructing the global solution using an expansion in the Frobenius solutions $\xi_{ip}^{(b)}$ and $\xi_{ip}^{(s)}$ since these are only defined within their respective radius of convergence, which extends to the nearest adjacent rational surface.

Provided (6.2) is fulfilled, we can then guarantee that, in the proximity of the surface x_j,

$$\bar{\xi}_{(ip)} \sim \sum_{q=\pm} D'_{ip,jq} \xi_{jq}^{(s)} \tag{6.7}$$

as $x \rightarrow x_j$, is a linear combination of even and odd small-solution behaviours, whereas

$$\tilde{\xi}_{(ip)} \sim \sum_{q=\pm} E'_{ip,jq} \xi^{(r)}_{jq} \tag{6.8}$$

as $x \rightarrow x_i$ extracts the regular contribution of the cumulative solution

$$\xi_{ip} \equiv \hat{\xi}_{ip} + \bar{\xi}_{(ip)} + \tilde{\xi}_{(ip)}, \tag{6.9}$$

near x_j, the latter satisfying

$$L(\xi_{ip}) = 0 \tag{6.10}$$

everywhere with ξ_{ip} subject to the appropriate boundary condition at x_a and x_0. In § 6.4, we will fix the arbitrariness involved in $\hat{\xi}_{ip}$ away from x_i, by choosing a bell-shaped function, the $\bar{\xi}_{(ip)}$ and $\tilde{\xi}_{(ip)}$ compensating so as to satisfy (6.10).

6.2 Matching to inner-solutions

Substituting Eqs.(6.7) and (6.8) into (6.1) we obtain

$$\xi = \sum_p \sum_i c_{ip} \left[\xi^{(b)}_{ip} + \sum_{q=\pm} \sum_{j=1}^{N} D'_{ip,jq} \xi^{(s)}_{jq} + \sum_{q=\pm} \sum_{j=1}^{N} E'_{ip,jq} \xi^{(r)}_{jq} \right], \tag{6.11}$$

with the matrices

$$D'_{ip,jq} \equiv \tfrac{1}{2} \begin{pmatrix} \mathrm{A}'_{ij} & \mathrm{B}'_{ij} \\ \Gamma'_{ij} & \Delta'_{ij} \end{pmatrix} \tag{6.12}$$

and $E'_{ip,jq}$ being determined by solving (6.10) for all $i, j = 1, 2 \cdots N$ and p, $q \in \{+, -\}$. The components of these matrices can be thought of as representing the response coefficients to the set of prescribed solutions $\hat{\xi}$. It turns out from Glasser *et al.* (1975), that the unreduced set of equations describing the inner layer accepts solutions which are arbitrarily constant (within the layer); these are the inner solutions which prolong the regular solutions $\xi^{(r)}$ of § 5.4 across the layer and which are not subject to any matching constraint. They can therefore not contribute in any respect to stability so that we focus here instead on the matching of the big and small solutions across the layer which depends entirely on the c_{ip}'s and the $D'_{ip,jq}$'s.

Let us consider first the problem of matching solutions across a single rational surface ($N = 1$). Using the notation of Glasser *et al.* (1984), we write the asymptotic behaviour of the general, linear solution of a symmetric layer as

$$\xi \sim C_+ \left[X_+^{\alpha^{(b)}} + \Delta_+(Q) X_+^{\alpha^{(s)}}\right] + C_- \left[X_-^{\alpha^{(b)}} + \Delta_-(Q) X_-^{\alpha^{(s)}}\right], \qquad (6.13)$$

as $X \equiv (x - x_i)/\epsilon \to \infty$, where ϵ denotes the asymptotically thin width $\epsilon \to 0$ as the resistivity vanishes (ϵ scales as η to a positive exponent). In (6.13), $\Delta_+(Q)$ and $\Delta_-(Q)$ are the growth-rate-dependent inner-matching data of § 1.5, associated to resistive modes which exhibit the interchange parity and the tearing parity respectively. As Glasser *et al.* (1984) use the simple unmodified definition of $\xi_\pm^{(b)}$, we shall do the same [i.e. we take $s(\mu) \equiv 0$ in (5.39)]. Matching the coefficients of the big solutions in (6.13) with those in (6.11) gives

$$c_\pm = C_\pm / \epsilon^{\alpha^{(b)}}. \qquad (6.14)$$

Matching the coefficients of the even and odd small-solutions gives two linear equations in C_+ and C_-. Requiring that they have a non-trivial solution yields the following determinantal dispersion relation

$$\begin{vmatrix} \epsilon^{2\mu}\Delta' - 2\Delta_+(Q) & \epsilon^{2\mu}\Gamma' \\ \epsilon^{2\mu}\Gamma' & \epsilon^{2\mu}\Delta' - 2\Delta_-(Q) \end{vmatrix} = 0. \qquad (6.15)$$

Relation (6.15) shows that either $\Delta_+(Q)$ or $\Delta_-(Q)$ or both must vanish in the $\epsilon \to 0$ limit. For example, $\Delta_+(Q) \sim \epsilon^{2\mu}$ and $\Delta_-(Q) \sim 1$ corresponds to a mode that is essentially of odd (tearing) parity, while $\Delta_-(Q) \sim \epsilon^{2\mu}$ and $\Delta_+(Q) \sim 1$ describes a resistive-interchange mode.

Equation (6.15) can be readily generalized so as to involve the full asymptotic matching problem for multiple rational surfaces, $i, j = 1, 2 \cdots N$ [Grimm *et al.* (1983), Manickam *et al.* (1983), Connor *et al.* (1988), Connor *et al.* (1991a) and Connor *et al.* (1991b)],

$$\begin{vmatrix} \epsilon^{2\mu_j} \mathrm{A}'_{ij} - 2\Delta_+^{(i)}(Q)\delta_{ij} & \epsilon^{2\mu_j} \mathrm{B}'_{ij} \\ \epsilon^{2\mu_j} \Gamma'_{ij} & \epsilon^{2\mu_j} \Delta'_{ij} - 2\Delta_-^{(i)}(Q)\delta_{ij} \end{vmatrix} = 0. \qquad (6.16)$$

This clarifies the role of the outer-matching matrix $D'_{ip,jq}$ and the inner-matching matrix $D_{ip,jq}(Q)$ given by the coefficients $\Delta_+^{(i)}(Q)$ and $\Delta_-^{(i)}(Q)$. It was assumed in

(6.16) that the inner-matching matrix is diagonal, though generalization of (6.16) to a non-diagonal matrix, corresponding to a non-symmetric layer for instance,

$$\det\left(\epsilon^{2\mu_j} D'_{ip,jq} - D_{ip,jq}(Q)\right) = 0 \tag{6.17}$$

is straightforward. In any case, the outer-matching matrix provides a sufficient set of data for matching the outer solutions to the inner solutions, independently of the inner-layer model which may even be weakly non-linear since we are still left with some degrees of freedom in choosing the c_{ip}.

It is worthwhile to add that, though we are satisfied by matching the dominant order solutions only, the proper use of the asymptotic matching-method requires the matching of high-order terms in the Frobenius expansion too. However, if the inner and outer descriptions are to be compatible, all the higher Frobenius-terms can be shown to match under the condition that (6.17) is fulfilled so that matching these terms only provides a confirmation of the correctness of the inner and outer model.

6.3 Expression for the outer-matching data

Realizing the importance of the matching data in the dispersion relation (6.16), we note that, from (6.9) and (6.11),

$$D'_{ip,j\pm} = \lim_{\epsilon\to 0+} \tfrac{1}{2}\epsilon^{-\alpha_j^{(s)}} \left\{ \left[\xi_{ip} - \hat{\xi}_{ip} - \tilde{\xi}_{(ip)}\right]_{x=x_j+\epsilon} \pm \left[\xi_{ip} - \hat{\xi}_{ip} - \tilde{\xi}_{(ip)}\right]_{x=x_j-\epsilon} \right\} \tag{6.18}$$

can be derived asymptotically from the cumulative solution. Equation (6.18) is in general not very useful to extract the matching data because of the presence of the unknown regular part $\tilde{\xi}$. Even in cylindrical geometry, where the regular solutions are absent in the formalism, (6.18) is not always satisfactory from a numerical-analysis point of view since it relies on pointwise-accurate representation of ξ_{ip}, $\hat{\xi}_{ip}$ and $\tilde{\xi}_{(ip)}$ as $x \to x_i$ — we have in particular in mind the finite-β case where the small solutions can be divergent at x_i. It is more advantageous [Miller & Dewar (1986)] to use instead an integral definition of $D'_{ip,jq}$ that is less sensitive to local inaccuracies; such a definition will be introduced in § 6.5.

A number of properties satisfied by $D'_{ip,jq}$ can immediately be derived from (6.18) in the cylindrical case, for which $\tilde{\xi}_{(ip)} \equiv 0$. Considering first the simpler case of a unique rational surface x_1 we find that, as a consequence of the disjointness of the left-hand and right-hand solutions,

$$\lim_{\epsilon \to 0} \left[\xi_\pm - \hat{\xi}_\pm\right]_{x_1+\epsilon} = \pm \lim_{\epsilon \to 0+} \left[\xi_\pm - \hat{\xi}_\pm\right]_{x_1-\epsilon}, \tag{6.19}$$

there can be only two independent matching data so that

$$\left.\begin{aligned} D'_{++} &= (\Delta_R + \Delta_L), \quad D'_{+-} = (\Delta_R - \Delta_L) \\ D'_{-+} &= (\Delta_R - \Delta_L), \quad D'_{--} = (\Delta_R + \Delta_L) \end{aligned}\right\}, \tag{6.20}$$

where $\Delta_{L,R}$ are the matching data in the left- and right-sided representation. Equation (6.20) yields the symmetry relation

$$\left.\begin{aligned} \mathrm{A}' &= \Delta' \\ \Gamma' &= \mathrm{B}' \end{aligned}\right\}, \tag{6.21}$$

with the last expression being an example of the reciprocity relation following from the variational principle of § 6.5.

Other properties of (6.18) include

$$D'_{ip,jq} = 0 \qquad \text{for } |j - i| > 1 \tag{6.22}$$

in cylindrical geometry. In toroidal geometry, however, (6.22) is not expected to hold because of the presence of the regular contribution $\tilde{\xi}_{(ip)}$ which "leaks" into all sections (x_i, x_{i+1}), $i = 0, 1, \cdots N$. The inclusion of $\tilde{\xi}_{(ip)}$ is also responsible for the breakdown of (6.19) so that $\mathrm{A}' = \Delta'$ does not hold in general, whereas the symmetry relation $\Gamma' = \mathrm{B}'$ will be shown in § 6.7 to remain satisfied in toroidal geometry as a result of the Hermiticity of the GNE.

6.4 Response formalism in Hilbert space

In the previous section we have defined the matching data and shown how to obtain a dispersion relation by matching the outer with the inner solutions. We have also given a geometrical interpretation to these data in the form of (6.18), a relation which expresses the ratio between the big and the small solution on either side of

the rational surface ψ_i. There are various reasons why we shall not expect (6.18) to provide an accurate estimate of $D'_{ip,jq}$; first, (6.18) is given by the difference of two asymptotically large terms whose difference scales as the small solution and second, because (6.18) is based on a pointwise representation of the solution near singularity. This will provide the main motivation for seeking a variational principle from which the matching data can be derived.

As the concept of variational principle is intimately related to the property of Hermiticity of the GNE, it is natural to cast the problem into the Hilbert formalism. We use here the definition of inner product given by (2.33), $(u,v) \equiv 4\pi^2 \int_{x_0}^{x_a} dx < u, v >$, which also defines the square of the norm $\| u \|^2 = (u,u)$ in the Hilbert space $\mathcal{H}$. The operator L of (4.24) is said to be Hermitian if

$$\tfrac{1}{2}(u, Lv) = \tfrac{1}{2}(Lu, v) = -W[u; v], \tag{6.23}$$

for sufficiently well-behaved u and v; that is $u, v \in \mathcal{H}$ and u and v satisfying the boundary conditions

$$\mathcal{D}_\theta \mathcal{G}(\mathcal{Q} + \mathcal{D}_\theta \partial_x) v(x_a, \theta) = \frac{1}{4\pi^2} \sigma_a(\theta) v(x_a, \theta), \tag{6.24}$$

where $W[u;v]$ is the bilinear functional

$$\begin{aligned} W[u;v] \equiv\ & \tfrac{1}{2} \int_{x_0}^{x_a} dx \int_0^{2\pi} d\theta \, \{ [(\mathcal{Q} + \mathcal{D}_\theta \partial_x) u]^* \, \mathcal{G} (\mathcal{Q} + \mathcal{D}_\theta \partial_x) v - u^* \mathcal{K} v \} \\ & + < u(x_a), \sigma_a v(x_a) > . \end{aligned} \tag{6.25}$$

The boundary conditions (6.24) are the most general boundary conditions compatible with the Hermiticity of $W[u;v]$, including as a special case the presence of an infinitely conducting wall at x_a when choosing $\sigma_a \to \infty$, and more generally any non-dissipative interface such as a plasma-vacuum contact at x_a which follows from taking σ_a finite. The quadratic form $W[u;u]$ is immediately recognized as being the ideal (potential) plasma energy [Newcomb (1960), Freidberg (1987)] of § 2.6 for a perturbation $\xi = u$, and the result (6.23) as a proof of the well-known Hermiticity of L (i.e. $L^\dagger = L$).

Since we assume the plasma to be ideally stable, $W[u;u]$ must be positive for all non-zero u satisfying the admissible boundary-conditions (6.24) and so we can adopt

$$\|u\|_w \equiv W[u;u]^{\frac{1}{2}} > 0 \tag{6.26}$$

as the *energy norm* in the Hilbert space $\mathcal{H}_w$ of functions satisfying the boundary conditions (6.24) with $W[u;v]$ as inner product [Miller & Dewar (1986)]. We shall show in § 6.5 that a sufficient condition for u and v to be "sufficiently well-behaved", used in deriving (6.23) is in fact the assumption that $u, v \in \mathcal{H}_w$.

If we could find a solution ξ to (4.24) such that $\xi \in \mathcal{H}_w$, then (6.23) shows that $W[\xi;\xi]$ would be zero. That is the plasma would be only marginally stable, violating the assumption in (6.26). Thus we are led to conclude that the ξ we seek cannot lie in $\mathcal{H}$. Indeed it is easy to see that $\|\xi^{(b)}\|_w = \infty$ — the big solutions have *infinite energy-norm* (6.26).

Nevertheless we seek a variational principle for the ξ's and the matching data. The critical step performed in § 6.1 is [Dewar & Grimm (1984), Miller & Dewar (1986)] to split the cumulative ξ_{ip} into the *prescribed* $\hat{\xi}_{ip}$ of infinite energy-norm, and the *response solution*

$$\begin{aligned} \check{\xi}_{(ip)} &\equiv \xi_{ip} - \hat{\xi}_{(ip)} \\ &= \bar{\xi}_{(ip)} + \tilde{\xi}_{(ip)} \end{aligned} \tag{6.27}$$

which belongs to $\mathcal{H}_w$ and which we can vary, using integration by parts in the usual way. The parentheses around ip are a reminder that according to Eqs.(6.7) and (6.8), $\check{\xi}_{(ip)}$ *does not in general have a well-defined asymptotic parity* p, nor is it localized near x_i as indicated by Fig. 6.2.

To be specific, we take first

$$\hat{\xi}_{ip} = H_i(x)\xi^{(b)}_{ip} \tag{6.28}$$

where H_i is illustrated in Fig. 6.1, so that $\hat{\xi}_{ip}$ extracts the behaviour of the big solution to arbitrary high order within the interval $(x_i - \epsilon_i, x_i + \epsilon_i)$. (We shall give in § 6.6 the precise minimum number of Frobenius terms that is required in $\hat{\xi}$, which, of course, must be for practical reasons defined as a finite sum, and one may also relax the requirement that H_i be flat in the neighbouring region.) As the support of H_i does not extend to the next surfaces $x_{i\pm1}$, this guarantees that a similar relation to (6.23)

$$\left(\hat{\xi}_{ip}, L\hat{\xi}_{jq}\right) = \left(L\hat{\xi}_{ip}, \hat{\xi}_{jq}\right) \qquad \forall\ i,j \in \{1,2,\cdots N\} \text{ and } \forall\ p,q \in \{+,-\} \tag{6.29}$$

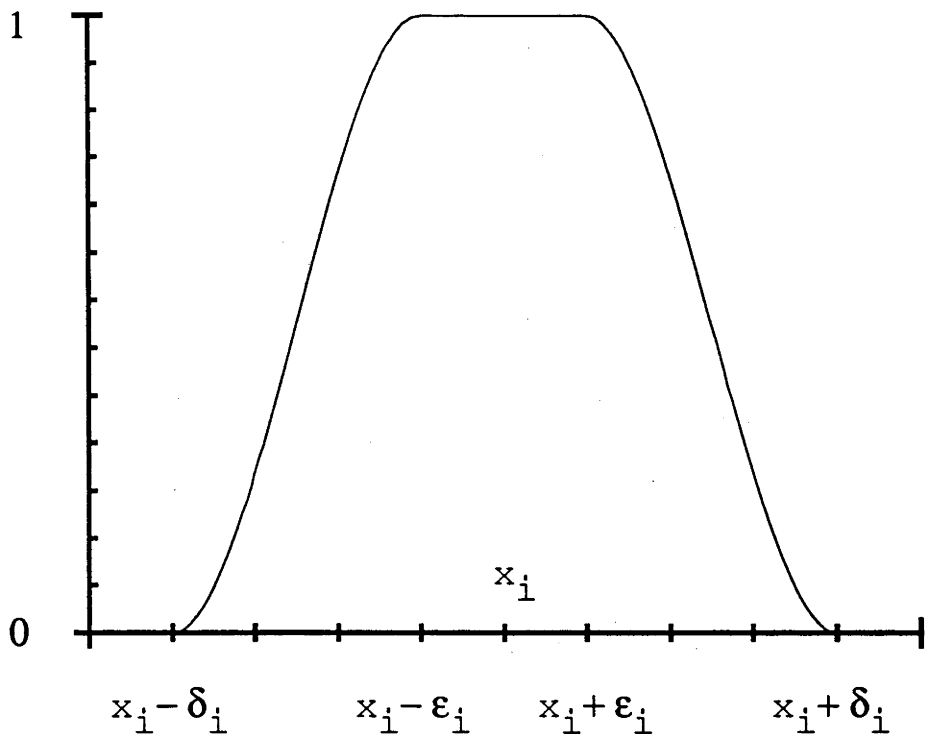

Figure 6.1: Bell-shaped localization function $H_i(x)$, which is flat for $x_i-\epsilon_i < x < x_i+\epsilon_i$ and vanishes for $x > x_i+\delta_i$ and $x < x_i-\delta_i$.

also holds for the $\hat{\xi}$ despite the fact that $W[\hat{\xi};\hat{\xi}]$ does not exist ($\hat{\xi} \notin \mathcal{H}_w$) . Equation (6.29) is readily proven for $p,q = L,R$, and can be proven with the same ease for $p,q = +,-$ by writing $\hat{\xi}_\pm = \hat{\xi}_R \pm \hat{\xi}_L$.

It should be added that the choice of (6.28) with the appropriate H_i ensures that $(\hat{\xi}, L\hat{\xi})$ be finite, as

$$L\hat{\xi}_{ip} \equiv 0, \; x_i - \epsilon_i < x < x_i + \epsilon_i, \tag{6.30}$$

and (trivially) outside the support of $H_i(x)$. Elsewhere $\hat{\xi}_{ip}$ does not satisfy (4.24) but since this occurs where there are no singularities, we have $L\hat{\xi}_{ip} \in \mathcal{H}$. Substituting (6.27) in (4.24) we find the inhomogeneous equation

$$L\check{\xi}_{(ip)} = -L\hat{\xi}_{ip}. \tag{6.31}$$

By the assumption of ideal stability, L is a nonsingular Hermitian operator within $\mathcal{H}_w$. Since, by construction, $\check{\xi}_{(ip)}$ and $L\hat{\xi}_{ip}$ lie within $\mathcal{H}$, we can solve (6.31) to give $\check{\xi}_{(ip)}$ as the *linear response* $-L^{-1}(L\hat{\xi}_{ip})$ driven by an imposed big solution $\hat{\xi}_{ip}$. The finite-element method developed in § 7.4 can be thought of as a constructive proof of the existence of L^{-1}.

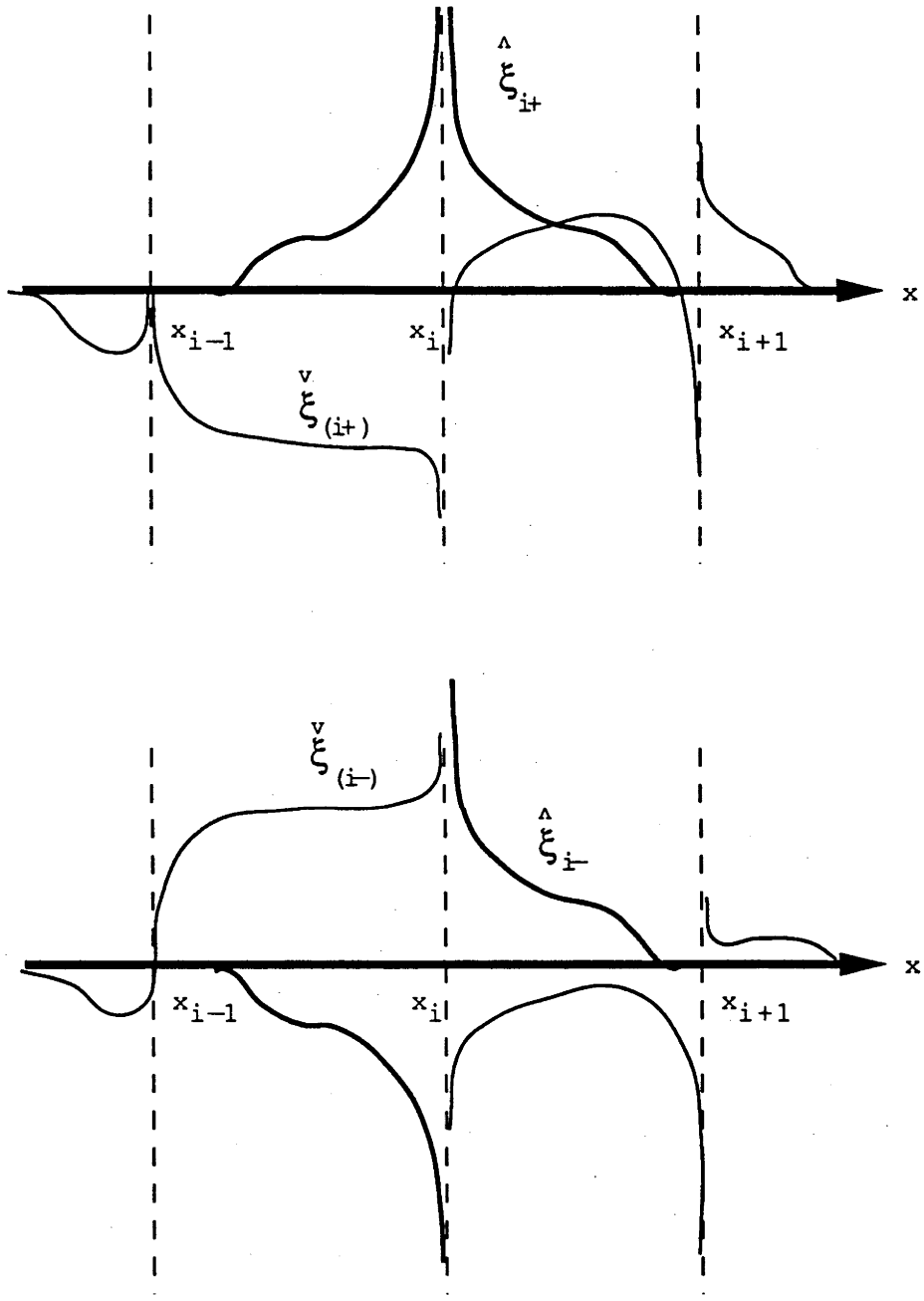

Figure 6.2: Schematic representation of the response $\check{\xi}_{(ip)}$ to localized big forcing term $\hat{\xi}_{ip}$, $p = \pm$, around x_i. In a cylindrical plasma, we would have $\check{\xi}$ vanishing in the sections where $\hat{\xi}$ is zero, and furthermore have $\check{\xi}_{(i-)} = \check{\xi}_{(i+)}\mathrm{sgn}(x - x_i)$.

From (6.31) it is seen that $L\check{\xi}_{(ip)}$ also vanishes around $x = x_i$, and near the other rational surfaces, $x = x_j$ say, it satisfies $L\check{\xi}_{(ip)} = 0$ since, by construction, $\hat{\xi}_{ip}$ vanishes near $x = x_j$, $i \neq j$, and thus $\check{\xi}_{(ip)} \equiv \xi_{ip}$ there. Hence, near all rational surfaces $\check{\xi}_{(ip)}$ exhibits the behaviour of the small solutions.

The coefficients of the leading terms are just the matching data of (6.12) so that according to (6.31),

$$\begin{aligned} \check{\xi}_{(i+)}(x_j + x) &= \tfrac{1}{2}\left[\mathrm{A}'_{ij}\xi^{(s)}_{j+} + \mathrm{B}'_{ij}\xi^{(s)}_{j-}\right] + \mathcal{O}(\xi^{(r)}), \\ \check{\xi}_{(i-)}(x_j + x) &= \tfrac{1}{2}\left[\Gamma'_{ij}\xi^{(s)}_{j+} + \Delta'_{ij}\xi^{(s)}_{j-}\right] + \mathcal{O}(\xi^{(r)}) \end{aligned} \tag{6.32}$$

for $-\epsilon_j < x < \epsilon_j$, where $\mathcal{O}(\xi^{(r)})$ denotes the contribution from the regular solution. In this representation, the coefficients A'_{ij}, B'_{ij}, Γ'_{ij} and Δ'_{ij} are the asymptotic response-coefficients corresponding to the excitation of small-solution behaviour at rational surface x_j by a big solution at surface x_i.

It is perhaps the facility with which (6.32) generalizes the matching data to multiple rational surfaces that the power of the Hilbert-space response-formalism is most apparent since we do not have to exhibit an explicit construction for the solution [c.f. Connor *et al.* (1988)] given that L^{-1} exists on quite general grounds.

6.5 Variational principle

Multiplying (4.24) for the fundamental solution ξ_{ip} by ξ^*_{jq} and integrating over the plasma, we have

$$(\xi_{jq}, L\xi_{ip}) = 0, \tag{6.33}$$

where $p, q \in \{+, -\}$. Because ξ_{ip} does not lie in the Hilbert space $\mathcal{H}_w$ we must proceed cautiously when integrating by parts. Introducing the decomposition (6.27) into (6.33) we have an equation involving four terms

$$\left(\check{\xi}_{(jq)}, L\check{\xi}_{(ip)}\right) + \left(\check{\xi}_{(jq)}, L\hat{\xi}_{ip}\right) + \left(\hat{\xi}_{jq}, L\check{\xi}_{(ip)}\right) + \left(\hat{\xi}_{jq}, L\hat{\xi}_{ip}\right) = 0. \tag{6.34}$$

Recalling that we wish to vary the $\check{\xi}$ component we see that it is only the third term which presents a problem. If we effect its integration by parts we find the concomitant identity (2.27) of Ch. 2 recurring here,

$$4\pi^2\left[< u, Lv > - < Lu, v >\right] \equiv \partial_x P[u; v|x), \; x \neq x_i, \tag{6.35}$$

which is pointwise true (except at the rational surfaces if u and v are "badly behaved"), with the bilinear concomitant of (4.24) given by

$$P[u;v|x) = 4\pi^2 [< u, \mathcal{D}_\theta \mathcal{G} (\mathcal{Q} + \mathcal{D}_\theta \partial_x) v > - < \mathcal{D}_\theta \mathcal{G} (\mathcal{Q} + \mathcal{D}_\theta \partial_x) u, v >], \quad (6.36)$$

an expression involving u and v as well as their conjugate momenta $\mathcal{D}_\theta \mathcal{G} (\mathcal{Q} + \mathcal{D}_\theta \partial_x) u$ and $\mathcal{D}_\theta \mathcal{G} (\mathcal{Q} + \mathcal{D}_\theta \partial_x) v$ respectively. These were encountered in (4.30), giving rise to the total-pressure perturbation for $u = v = \xi$.

The importance of P derives from the fact, immediately apparent from (6.35), that $P(x)$ is *constant* in any region where u and v satisfy (4.24) (except at the surfaces x_i). If $u = \mathcal{O}(|x - x_i|_i^\alpha)$ and $v = \mathcal{O}(|x - x_i|_i^\beta)$ in the neighbourhood of x_i, then $P = \mathcal{O}(|x - x_i|^{\alpha_i + \beta_i + 1})$. Thus if $\alpha_i + \beta_i > -1$ then $P \to 0$ as $x \to 0\pm$ and P is continuous at $x = x_i$, but if $\alpha_i + \beta_i = -1$ then $P = \mathcal{O}(\text{const})$ on either side of x_i, which, as noted above, is consistent with u and v locally being solutions of the Newcomb equation (4.24). However the constant is typically different on either side of x_i so that P is *discontinuous* at x_i, and $\partial_x P = [\![P]\!]_i \delta(x - x_i)$ in the neighbourhood of x_i, where

$$[\![P]\!]_i \equiv P(x_i + 0) - P(x_i - 0) \quad (6.37)$$

is the *jump* in P at x_i. On the other hand, the left-hand side of (6.35) has at most an integrable singularity at $x = x_i$, with no δ function. Thus, to make (6.35) true in a generalized-function sense on the whole interval $0 < x \leq x_a$ we must subtract off the δ function contributions at the rational surfaces, yielding an equation reminiscent of that defining a Green's function

$$4\pi^2 [< u, Lv > - < Lu, v >] = \partial_x P[u;v|x) - \sum_{i=1}^{N} [\![P]\!]_i \delta(x - x_i). \quad (6.38)$$

We now see that the condition for the integration by parts leading to the Hermiticity condition (6.23) for u and v satisfying the physical boundary conditions (so that $P = 0$ at $x = 0$ and x_a) to be valid is that $[\![P]\!]_i$ *vanishes* at all rational surfaces, since the right-hand side of (6.38) is then a complete derivative. If $u, v \in \mathcal{H}$ then $\alpha_i > -\frac{1}{2}$ and $\beta_i > -\frac{1}{2}$ for $\|u\|$ and $\|v\|$ to converge, hence $\alpha_i + \beta_i > -1$ and P is continuous, as noted above, and the $[\![P]\!]_i$ vanish. Thus a sufficient condition for Hermiticity is $u, v \in \mathcal{H}$. It is readily verified that $u, v \in \mathcal{H}$ is also sufficient for $u, v \in \mathcal{H}_w$ since $W[u;v]$ is also finite in this case.

This is not the only circumstance in which $[\![P]\!]_i$ vanishes, however. In particular, the concomitant between odd and even powers is continuous

$$[\![P[(x-x_i)_+^{\alpha_i};(x-x_i)_-^{\beta_i}]]\!]_i = 0, \tag{6.39}$$

even if $\alpha_i + \beta_i = -1$. Also, if $\alpha = \alpha_i^{(b)}$ then we can have $\alpha_i + \beta_i > -1$ simply by requiring $\beta_i > \alpha_i^{(s)}$. That is, if $u = \mathcal{O}(\xi_{ip}^{(b)})$ then we can still freely integrate by parts if we require v to be $o(\xi_{ip}^{(s)})$. As an example, we illustrate in Fig. 6.3 the concomitant taken between the normalized big and small solution which is shown to be constant for opposite parities.

Using (6.38) in the third term of (6.34) we find an integral expression for the jump in the concomitant

$$[\![P[\hat{\xi}_{jq};\check{\xi}_{(ip)}]]\!]_j = (\xi_{jq}, L\xi_{ip})', \tag{6.40}$$

where we have defined the *symmetrized matrix-element*

$$\begin{aligned}(\xi_{jq}, L\xi_{ip})' \equiv\ & \left(\check{\xi}_{(jq)}, L\check{\xi}_{(ip)}\right) + \left(\check{\xi}_{(jq)}, L\hat{\xi}_{ip}\right) \\ & + \left(\check{\xi}_{(ip)}, L\hat{\xi}_{jq}\right)^* + \left(\hat{\xi}_{jq}, L\hat{\xi}_{ip}\right),\end{aligned} \tag{6.41}$$

differing from that corresponding to (6.34) only in the third term of the right-hand side.

We give now a simple argument why $P[\hat{\xi};\xi^{(r)}|x)$ cannot contribute in (6.41) to $[\![P]\!]_i$; from the above discussion we find that

$$P[\hat{\xi}_{jq};\xi^{(r)}|x) = \mathcal{O}\left(|x-x_j|^{\alpha_j^{(b)}+1}\right), \tag{6.42}$$

which cannot give rise to a δ function under the action of ∂_x on the concomitant, unless $\alpha_j^{(b)} + 1 = -1$, or by using (5.14) $\mu_j = \frac{1}{2}$ which is the zero-β case discussed in § 5.5. But we know that in the latter case, the continuous part of the small solution is degenerate with the regular solution allowing us to discard the regular solution. It is verified explicitly in Appendix D that each term of the Frobenius expansion of $P[\hat{\xi}_{jq};\xi^{(r)}|x)$ vanishes provided $\mu_i \neq 1/2,\ 3/2\cdots$.

Equation (6.40) is the fundamental result on which the Generalized Green's Function Method expounded in Ch. 7 will be based.

From (6.28) and (6.12) we see that the jump shown in Fig. 6.3 is,

$$[\![P[\hat{\xi}_{jq};\check{\xi}_{(ip)}]]\!]_j = 4f_0^{(j)}\mu_j D'_{ip,jq} \tag{6.43}$$

to within a factor, the matching data we seek, so that (6.40) gives

$$\left.\begin{aligned} \mathrm{A}'_{ij} &= (\xi_{j+}, L\xi_{i+})'/2f_0^{(j)}\mu_j, \quad \mathrm{B}'_{ij} = (\xi_{j-}, L\xi_{i+})'/2f_0^{(j)}\mu_j, \\ \Gamma'_{ij} &= (\xi_{j+}, L\xi_{i-})'/2f_0^{(j)}\mu_j, \quad \Delta'_{ij} = (\xi_{j-}, L\xi_{i-})'/2f_0^{(j)}\mu_j \end{aligned}\right\} \tag{6.44}$$

with

$$f_0^{(j)} = 4\pi^2 \frac{n^2 q_j'^2}{< \mathcal{G}_j^{-1} >} \tag{6.45}$$

in the toroidal case [a rigorous derivation of (6.45) will be performed in § 7.2], and $f_0^{(j)}$ representing the leading term of the Taylor expansion (C.2).

Varying the $\check{\xi}$ component we have

$$\delta\,(\xi_{jq}, L\xi_{ip})' = \left(\delta\check{\xi}_{(jq)}, L(\check{\xi}_{(ip)} + \hat{\xi}_{ip})\right) + \left(\delta\check{\xi}_{(ip)}, L(\check{\xi}_{(jq)} + \hat{\xi}_{jq})\right)^*, \tag{6.46}$$

which vanishes for arbitrary $\check{\xi}$ variations if and only if (6.31) is satisfied. Thus we have a *variational principle*: A'_{ij}, B'_{ij}, Γ'_{ij} and Δ'_{ij} are stationary with respect to variations in the $\check{\xi}$ component if and only if the response equation (6.31) is satisfied[1].

6.6 Uniqueness and related questions

In this section we consider the question of the behaviour of the matching data, as given now by the symmetrized matrix-element expressions (6.44), under transformations of the form

$$\begin{aligned} \hat{\xi}_{ip} &\mapsto \hat{\xi}_{ip} + \eta_{ip}, \\ \check{\xi}_{(ip)} &\mapsto \check{\xi}_{(ip)} - \eta_{ip}, \end{aligned} \tag{6.47}$$

where η is an arbitrary function in $\mathcal{H}_w$. These transformations leave the fundamental solution ξ_{ip} unchanged. Substituting (6.47) into (6.41) we find that all but two of the terms containing η immediately cancel. Using (6.38) gives

$$(\xi_{jq}, L\xi_{ip})' \mapsto (\xi_{jq}, L\xi_{ip})' - [\![P[\hat{\xi}_{jq};\eta_{ip}]]\!]_j. \tag{6.48}$$

[1]This variational principle has been found independently by Chu *et al.* (1990b)

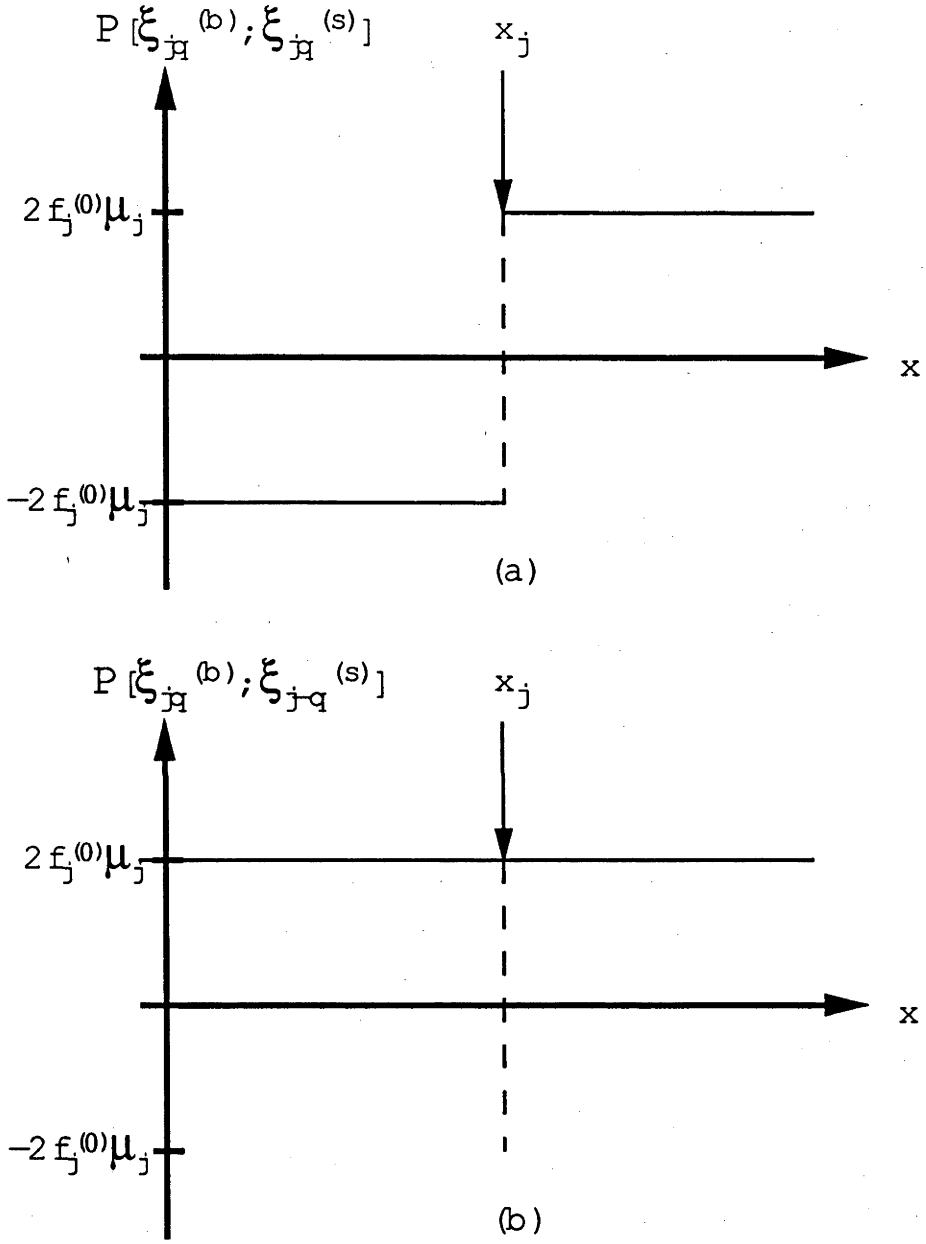

Figure 6.3: The jump in concomitant of normalized big and small solution. If the big and small solution have same parity [case (a)] $P[\xi^{(b)};\xi^{(s)}] = 2\mu_j f_0^{(j)}\mathrm{sgn}(x-x_j)$ whereas $P[\xi^{(b)};\xi^{(s)}] = \text{const}$ when the big and small solution have opposite parity [case (b)].

First consider the case $\eta_{ip} = o(\check{\xi})$. From the discussion after (6.39) we know that the jumps $[\![P[\hat{\xi}_{jq}; \eta_{ip}]]\!]_j$ vanish in this case. Thus we have the result: *The symmetrized matrix-element is invariant under arbitrary redefinitions of the part of infinite energy-norm, provided that the difference between the old and new definitions vanishes faster than the small solutions near the rational surfaces.* This is consistent with (6.44) in that a change which was of the same order as the small solutions would "pollute" the small solution component of $\check{\xi}$ and thus affect the matching data, which are response coefficients measuring this component.

A useful corollary of this invariance is the fact that we can truncate the series (5.7) and (C.4) defining the big solution at a finite number of terms, provided that the truncation error η_{ip} is of lower order than the leading term of the small solution. This is essential for practical purposes since high-order coefficients a_k in the series (C.4), respectively the y_k in (5.7), defining the big solution, as used in (6.28), involve high-order derivatives of equilibrium quantities which are difficult to compute accurately. Summing from $k = 0$ to $k = k_i$ such that the first term omitted from (6.28), which is $\mathcal{O}(|x - x_i|^{\alpha_i^{(b)}+1+k_i})$ for the resonant part (i.e. the Fourier component $m = m_i$) and $\mathcal{O}(|x - x_i|^{\alpha_i^{(b)}+2+k_i})$ for the non-resonant part, be of higher order than $\mathcal{O}(|x - x_i|^{\alpha_i^{(s)}})$ for the resonant part and of higher order than $\mathcal{O}(|x - x_i|^{\alpha_i^{(s)}+1})$ for the non-resonant part respectively, we find that the condition that the response solution be dominated by the small solution is

$$k_i > 2\mu_i - 1. \tag{6.49}$$

As noted by Chu *et al.* (1990b) we can do even better than this for $\frac{1}{2} < \mu_j < 1$ if we seek only to evaluate the matching data A'_{ij} and Δ'_{ij}, which, by (6.44) involve matrix elements of L between fundamental solutions with the *same* dominant parity. In these cases the second term in the Frobenius expansion of the big solution contained in ξ_{ip} is of opposite parity to the leading term of the big solution contained in $\hat{\xi}_{jp}$, so that if it is regarded as the error η_{ip} its contribution to the jump $[\![P[\hat{\xi}_{jp}; \eta_{ip}]]\!]_j$ vanishes identically by (6.39). Thus we can truncate at $k_i = 0$, keeping only one term in the Frobenius expansion in this case.

A similar argument allows us to extend the class of the $H_i(x)$, by taking $H_i(x) = 1 + \mathcal{O}((x - x_i)^{k_i+1})$ as $x \to x_i$ instead of $H_i(x) = 1$ in $(x_i - \epsilon_i, x_i + \epsilon_i)$. With this

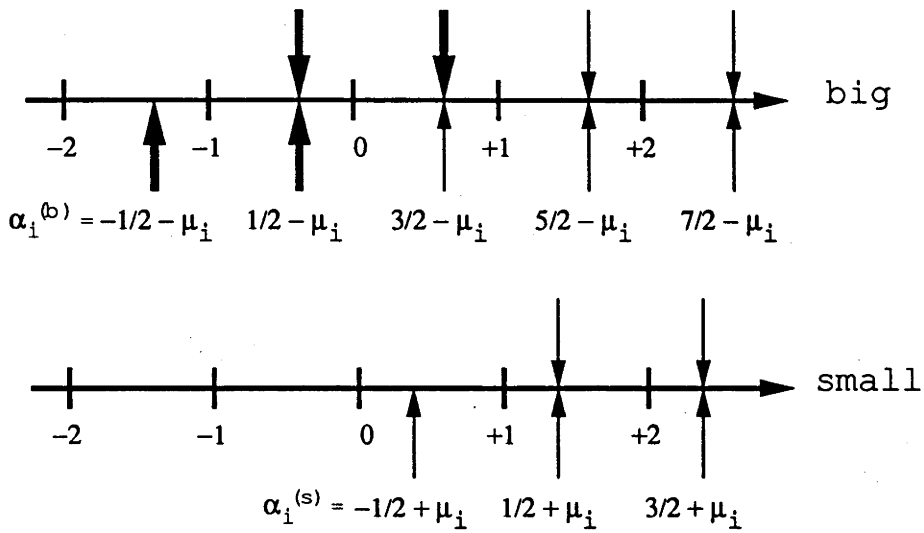

Figure 6.4: Powers of $x - x_i$ occurring in the Frobenius expansion of the big (top) and small (bottom) solutions marked on the real line. The prescribed solution $\hat{\xi}_{ip}$ must be truncated at order $\alpha_i^{(b)} + k_i + 1 > \alpha_i^{(s)}$ for the resonant poloidal mode $m = m_i$ and at order $\alpha_i^{(b)} + k_i + 2 > \alpha_i^{(s)} + 1$ for the non-resonant modes $m \neq m_i$ in order that $\check{\xi}_{(ip)}$ extract the small-solution behaviour at leading resonant and non-resonant order. The top scale shows the resonant ($\uparrow$) and the non-resonant ($\downarrow$) exponents with the bold arrows emphasizing the Frobenius terms that are mandatory in the prescribed solution. In this example $k_i \geq 1$.

choice of $\hat{\xi}_{ip}$ and $H_i(x)$, $L\hat{\xi}_{ip} \in \mathcal{H}$ but vanishes only asymptotically, and (6.32) remains true at lowest order.

The result (6.48) can also be used to investigate the consequences of making different choices for the functions $s_{i\pm}(\mu)$ used in the modified big solution defined by (5.39) and (C.12). In this case we take

$$\eta_{ip} = -\left[\delta s_{i+}(\mu) + \mathrm{sgn}(x - x_i)\,\delta s_{i-}(\mu)\right] H_i(x)\xi_{ip}^{(s)}(x) \tag{6.50}$$

where $\delta s_{i\pm}$ represent the changes in the choices of $s_{i\pm}$. Then (6.39) and (6.48) give

$$(\xi_{jq}, L\xi_{ip})' \mapsto (\xi_{jq}, L\xi_{ip})' + 4\delta_{i,j}\delta_{p,q} f_0^{(j)} \mu_j \delta s_{i+}(\mu) + 4\delta_{i,j}\delta_{p,-q} f_0^{(j)} \mu_j \delta s_{i-}(\mu). \tag{6.51}$$

Since $\delta s_{i+}(\frac{1}{2}) \equiv s_{i+}(\frac{1}{2}) \equiv 0$ it follows that A'_{ij} and Δ'_{ij} are *unaffected* by the redefinition (5.39) in the low-β limit $\mu_i \to \frac{1}{2}$.

The uniqueness of A'_{ij} and Δ'_{ij} as $\mu_i \to \frac{1}{2}$ is a strong indication that these are the only relevant outer-matching data to stability, in agreement with the constant-Ψ approximation used in § 1.4. Because fusion plasmas are characterized by small β values of the order of 0.01 to 0.1, it is observed (see Ch. 8) and expected that the A''s and the Δ''s are at least of one order of magnitude smaller than the corresponding values of the B''s and Γ''s; for that reason, the A''s and Δ''s play a more crucial role in resistive stability.

6.7 Reciprocity relations and other symmetries

Note that, although we chose in (6.23) to use the Hermitian inner product because this is more appropriate in the general, toroidal case (provided the plasma is asymmetric with respect to reflections in the plane $Z = 0$ shown in Fig. 1.1), in the cylindrical case ξ_{ip} is manifestly real and the complex conjugate can be dispensed with.

As well as providing the basis for efficient finite-element computation of the matching data, as will be shown in § 7.4, the explicit integral expressions for the matching data provided by (6.44) allow easy demonstration of fundamental symmetries between the coefficients.

The first type of symmetry, which, maintaining the linear response viewpoint, we call *reciprocity relations*, follows from the (Hermitian) symmetry of $(\xi_{jq}, L\xi_{ip})'$ under interchange of (j,q) and (i,p). This is apparent in the first term of (6.41) from Hermiticity of L within $\mathcal{H}$, manifestly for the sum of the next two terms, and by explicit consideration of the form of $\hat{\xi}_{ip}$, given by (6.28), for the last term. In the case $i = j \pm 1$ it is simplest for purpose of proof to assume that the supports of the shape functions $H_i(x)$ and $H_j(x)$ do not overlap, so that the last term of (6.41) vanishes identically, though invariance under (6.47) shows that it is not necessary to assume this.

The reciprocity relations are

$$\left.\begin{aligned} \mu_j f_0^{(j)} \mathrm{A}'_{ij} &= \mu_i f_0^{(i)} \mathrm{A}'_{ji} \\ \mu_j f_0^{(j)} \mathrm{B}'_{ij} &= \mu_i f_0^{(i)} \Gamma'_{ji} \\ \mu_j f_0^{(j)} \Gamma'_{ij} &= \mu_i f_0^{(i)} \mathrm{B}'_{ji} \\ \mu_j f_0^{(j)} \Delta'_{ij} &= \mu_i f_0^{(i)} \Delta'_{ji} \end{aligned}\right\}. \tag{6.52}$$

The relation $\mathrm{B}' = \Gamma'$ (6.21) derived in § 6.3 is an instance of a reciprocity relation: it expresses the fact that the even response (the amplitude of the even small-solution) to an odd imposed big solution is equal to the odd response to an imposed even big-solution. These reciprocity relations are valid for both the cylindrical and toroidal case.

The second type of symmetry, which is peculiar to the cylindrical problem, is a consequence of the disjointness of the solution on either side of a rational surface. First note that, as a consequence of this, the support of ξ_{ip} is limited to the region on either side of $x = x_i$ bounded by $x_{i\pm1}$ (or a boundary). Thus in the unlikely event that there were more than two rational surfaces in the cylindrical plasma, there would be no overlap for $|i-j| > 1$ and the matching coefficients A'_{ij} etc. would vanish for $|i-j| > 1$.

Also, since we can change the sign of ξ_{ip} in the interval $x_i < x < x_{i+1}$ and still have a valid solution of (4.24), there is a simple relation between the basis functions corresponding to big solutions of opposite parities

$$\xi_{ip}(x_i + x) = \mathrm{sgn}x\, \xi_{i,-p}(x_i + x). \tag{6.53}$$

Consider first the case $i = j + 1$. Using (6.53) in (6.41) we find

$$(\xi_{jq}, L\xi_{j+1,p})' = (\xi_{j,-q}, L\xi_{j+1,p})' = -(\xi_{jq}, L\xi_{j+1,-p})', \tag{6.54}$$

whence

$$A'_{j+1,j} = B'_{j+1,j} = -\Gamma'_{j+1,j} = -\Delta'_{j+1,j}. \tag{6.55}$$

Now consider the case $i = j$. In this case we get

$$A'_{ii} = \Delta'_{ii} \tag{6.56}$$

as well as the reciprocity relation $B'_{ii} = \Gamma'_{ii}$ which we had from (6.52). As mentioned in § 6.3, (6.56) does not remain valid in the toroidal case.

Chapter 7

Finite-element solution

It is our intention to discuss the implementation of the variational scheme derived in Ch. 6 into the resistive-stability code PEST3.4. The structure of PEST3.4 is based on a spectral decomposition (Fourier expansion) in the poloidal direction and uses a radial finite-element expansion which takes full advantage of the variational principle, as will be shown in § 7.4.

In spite of the robustness of the finite-element method, it is anticipated that a major source of inaccuracies can still persist in the process of evaluating the source term in the response equation. This becomes increasingly a matter of concern when the small-solution exponent differs from the big-solution exponent by a large amount representing the number of Frobenius terms to be incorporated in the prescribed solution in order that the response solution have the small behaviour. Computing high-order Frobenius terms requires extremely smooth equilibrium-data so as to allow accurate estimates of radial derivatives at the rational surfaces. In PEST3.4, the equilibrium data are loaded from input files and then remapped onto the mesh using cubic splines which guarantee continuity of the data up to their first derivatives, thus permitting the calculation of only two Frobenius terms in the prescribed solution.

The problem of sensitivity towards higher Frobenius terms can be reduced by using the quasi-Hamiltonian form of the GNE, which already proved efficient in deriving the Frobenius expansion in § 5.2. Recall that the prescribed solution is rather arbitrary away from the rational surfaces; similarly we introduce a "quasi-

momentum" variable $\hat{\chi}$ with localized support, which converges to the "true" quasi-momentum $\mathcal{GP}\hat{\xi}$ near the rational surfaces while being allowed to depart significantly from it elsewhere. By doing so, the source term of the weak form splits into two components which are recessive with respect to the small solution, each of these involves first-order radial derivatives acting on $\hat{\xi}$ and $\hat{\chi}$ only. Therefore, no radial derivatives of equilibrium quantities are required except at the rational surfaces; for this reason we find the quasi-Hamiltonian form of the GNE more attractive.

Section 7.1 is devoted to deriving the weak form. The quasi-Hamiltonian weak-form differs only slightly from the GNE weak-form by the presence of an additional source term. The concomitant jump of § 6.5 is rederived in § 7.2 in terms of the finite-element solution where the matching data are shown to derive from an extremum principle which minimizes the potential energy over the class of functions belonging to the Hilbert space. In § 7.3 we focus on a subset of the Hilbert space: the Sobolev space, spanned by the square-integrable functions which are continuous in value and from which the solution is drawn to *maximize* the matching data. In that sense, the numerical determination of the matching data will systematically tend to overestimate stability. The matching-data error and their convergence are analyzed in § 7.4. Due to the presence of singular surfaces, we are led to rescale the mesh in the vicinity by increasing the mesh-node density in order to retain the maximum convergence rate of the finite-element scheme. As an example, the mesh generating algorithm of PEST3.4 is discussed in § 7.5.

7.1 Two weak forms

Recall that we seek solutions to the set of linear response-equations $L\check{\xi}_{(ip)} = -L\hat{\xi}_{ip}$ [see (6.31)] for $i = 1, 2, \cdots N$ and $p \in \{+, -\}$, with the solutions $\check{\xi}_{(ip)}$ being subject to the boundary conditions (6.24) [assuming the $\hat{\xi}$'s are localized (6.28) as in Fig. 6.1 and vanish at $x = 0$ and $x = x_a$]. If we multiply the response equations by an arbitrary, well-behaved function u and integrate over the plasma, we find

$$W[u; \check{\xi}_{(ip)}] = \tfrac{1}{2}(u, L\hat{\xi}_{ip}) \tag{7.1}$$

$\forall\ u \in \mathcal{H}$ with $W[u;v]$ being the energy inner-product (6.25). Equation (7.1) is called the weak form of (6.31), the terminology being justified by the fact that only first-order derivatives are applied on $\check{\xi}_{(ip)}$.

The focus of the second part of this section is the extension of (7.1) to accommodate the quasi-Hamiltonian formalism developed in § 4.3. Let us rewrite the response equation as

$$(\ \mathsf{I}\ \mathcal{D}_\theta \partial_x - \mathsf{A})\check{\mathsf{y}}_{(ip)} = -(\ \mathsf{I}\ \mathcal{D}_\theta \partial_x - \mathsf{A})\hat{\mathsf{y}}_{ip}, \tag{7.2}$$

where A is defined by (4.56),

$$\check{\mathsf{y}}_{(ip)} \equiv \begin{pmatrix} \check{\xi}_{(ip)} \\ \check{\chi}_{(ip)} \end{pmatrix} \tag{7.3}$$

and

$$\hat{\mathsf{y}}_{ip} \equiv \begin{pmatrix} \hat{\xi}_{ip} \\ \hat{\chi}_{ip} \end{pmatrix}. \tag{7.4}$$

The following prescription is adopted

$$\hat{\mathsf{y}}_{ip} = H_i(x)\,(x - x_i)_p^{\alpha_i^{(b)}} \sum_{k=0}^{k_i+(1)} (x - x_i)^k \mathsf{y}_k^{(ib)}(\theta) \tag{7.5}$$

with k_i satisfying (6.49) and representing the value at which the big solution is truncated. Since the non-resonant terms $m \neq m_i$ are, according to Fig. 6.4, truncated at one order higher in the Frobenius expansion, we introduce the notation $k_i + (1)$ in (7.5) to denote k_i for $m = m_i$, $k_i + 1$ for $m \neq m_i$, so that

$$< m_i, [\ \mathsf{I}\ \mathcal{D}_\theta \partial_x - \mathsf{A}]\hat{\mathsf{y}}_{ip} > \sim \mathcal{O}\left(|x - x_i|^{\alpha_i^{(b)}+k_i+1}\right) \qquad \text{for all } m, \tag{7.6}$$

as $x \to x_i$. Equation (7.6) shows that the GNE is satisfied to same order for both the resonant and non-resonant terms. Note that because of the presence of $H_i(x)$ in (7.5), $\hat{\chi}_{ip}$ violates (4.53) in general in the region where H_i is neither zero nor one. In the vicinity of x_i, $\hat{\chi}_{ip}$ is required by (7.6) to merge asymptotically with $\mathcal{G}\mathcal{P}\hat{\xi}_{ip}$,

$$\mathcal{G}\mathcal{P}\hat{\xi}_{ip} - \hat{\chi}_{ip} \sim \mathrm{o}\left(\xi^{(s)}\right) \in \mathcal{H}_w \tag{7.7}$$

as $x \to x_i$, where $\mathcal{G}$ is the surface operator (4.22) involving no ∂_x and where $\mathcal{P} \equiv \mathcal{D}_\theta \partial_x + \mathcal{Q}$ is defined in (4.19). The discrepancy (7.7) is of the same order as the correction between $\hat{\xi}$ and $\xi^{(b)}$.

Solving the top equation of (7.2) for $\check{\chi}_{(ip)}$, we find

$$\check{\chi}_{(ip)} = \mathcal{G}\mathcal{P}\check{\xi}_{(ip)} + \mathcal{G}\mathcal{P}\hat{\xi}_{ip} - \hat{\chi}_{ip}. \tag{7.8}$$

Equation (7.8) is substituted into the bottom equation (7.2) to yield

$$\mathcal{P}^\dagger\mathcal{G}\mathcal{P}\check{\xi}_{(ip)} - \mathcal{K}\check{\xi}_{(ip)} = -\mathcal{P}^\dagger\hat{\chi}_{ip} + \mathcal{K}\hat{\xi}_{ip} - \mathcal{P}^\dagger\left(\mathcal{G}\mathcal{P}\hat{\xi}_{ip} - \hat{\chi}_{ip}\right) \tag{7.9}$$

with each of the two terms in brackets vanishing faster than the small solution ($k_i > 2\mu_i - 1$). Multiplying (7.9) by $\frac{1}{2}u^*$, integrating over the plasma volume and performing integration by parts of the terms $u^*\mathcal{P}^\dagger(\cdot)$, we then find the *quasi-Hamiltonian weak-form*

$$W[u;\check{\xi}_{(ip)}] = -\tfrac{1}{2}\left(u, \mathcal{P}^\dagger\hat{\chi}_{ip} - \mathcal{K}\hat{\xi}_{ip}\right) - \tfrac{1}{2}\left(\mathcal{P}u, \mathcal{G}\mathcal{P}\hat{\xi}_{ip} - \hat{\chi}_{ip}\right), \tag{7.10}$$

which is true for all well-behaved u, since $\mathcal{D}_\theta\mathcal{G}\mathcal{P}\check{\xi}_{(ip)} \sim \mathcal{D}_\theta(\mathcal{G}\mathcal{P}\hat{\xi}_{ip} - \hat{\chi}_{ip}) \sim o(\xi^{(s)})$ vanish as $x \to x_i$.

Setting $\hat{\chi}_{ip} \equiv \mathcal{G}\mathcal{P}\hat{\xi}_{ip}$, we then immediately recover (7.1) from (7.10). The advantages of using (7.10) compared to (7.1) are similar to those which lead us to use the weak form instead of the response equation; because only first-order derivatives are applied on the prescribed solution in (7.10), it is clear that a rugged behaviour of the prescribed solution is better tolerated in the latter form. Equations (7.10) and (7.1) are otherwise equivalent, the former possessing the virtue of easier numerical implementation, (7.1) is analytically more tractable and will thus be preferentially used in § 7.4.

7.2 Concomitant jump

Alternatively, we can also multiply (7.9) by $\frac{1}{2}\hat{\xi}^*_{jq} \notin \mathcal{H}$ and integrate over the plasma, giving

$$\begin{aligned}\tfrac{1}{2}\left(\hat{\xi}_{jq}, \mathcal{P}^\dagger\mathcal{G}\mathcal{P}\check{\xi}_{(ip)} - \mathcal{K}\check{\xi}_{(ip)}\right) \;=\; & -\tfrac{1}{2}\left(\hat{\xi}_{jq}, \mathcal{P}^\dagger\hat{\chi}_{ip} - \mathcal{K}\hat{\xi}_{ip}\right) \\ & - \tfrac{1}{2}\left(\mathcal{P}\hat{\xi}_{jq}, \mathcal{G}\mathcal{P}\hat{\xi}_{ip} - \hat{\chi}_{ip}\right).\end{aligned} \tag{7.11}$$

We wish to have the operator $\mathcal{P}^\dagger\mathcal{G}\mathcal{P} - \mathcal{K}$ applying on the prescribed solution only, to do so we apply the rules set in § 6.5 to integrate by parts $\hat{\xi}^*_{jq}\mathcal{P}^\dagger\mathcal{G}\mathcal{P}\check{\xi}_{(ip)}$,

$$\left(\hat{\xi}_{jq}, L\check{\xi}_{(ip)}\right) \;=\; -\left(\hat{\xi}_{jq}, \mathcal{P}^\dagger\mathcal{G}\mathcal{P}\check{\xi}_{(ip)} - \mathcal{K}\check{\xi}_{(ip)}\right)$$

$$= -\left(\mathcal{P}^{\dagger}\mathcal{G}\mathcal{P}\hat{\xi}_{jq} - \mathcal{K}\hat{\xi}_{jq}, \check{\xi}_{(ip)}\right) - [\![P[\hat{\xi}_{jq}; \check{\xi}_{(ip)}]]\!]_j. \tag{7.12}$$

Notice that $P[\hat{\xi}_{jq}; \check{\xi}_{(ip)}]$ of (6.36) may be written as

$$P[\hat{\xi}_{jq}; \check{\xi}_{(ip)}] = -4\pi^2 < \hat{\mathsf{y}}_{jq}, \boldsymbol{\sigma}\mathcal{D}_{\theta}\check{\mathsf{y}}_{(ip)} >, \tag{7.13}$$

where

$$\boldsymbol{\sigma} \equiv \begin{pmatrix} 0 & 1 \\ 1 & 0 \end{pmatrix}. \tag{7.14}$$

Using the representation

$$\left.\begin{aligned} \hat{\mathsf{y}}_{jq} &\sim \mathsf{u}_j^{(b)}(x - x_j)_q^{-\frac{1}{2}-\mu_j} \exp im_j\theta + \mathcal{O}\left(|x - x_j|^{\frac{1}{2}-\mu_j}\right) \\ \check{\mathsf{y}}_{(ip)} &\sim \mathsf{u}_j^{(s)}(x - x_j)_p^{-\frac{1}{2}+\mu_j} \exp im_j\theta + \mathcal{O}\left(|x - x_j|^{\frac{1}{2}+\mu_j}\right) \end{aligned}\right\} \tag{7.15}$$

where the u_j are defined in § 5.3, it is clear from (7.15) that $P \sim (x - x_j)^0$ as $x \to x_j$. Substituting expressions (5.13) into (7.15) and using the property $< \mathcal{Q}_j >^* = - < \mathcal{Q}_j >$; the jump in (7.13) at x_j becomes

$$[\![P[\hat{\xi}_{jq}; \check{\xi}_{(ip)}]]\!]_j = \frac{16\pi^2 n^2 {q_j'}^2 \mu_j}{< \mathcal{G}_j^{-1} >} D'_{ip,jq}. \tag{7.16}$$

To express the matching data in terms of the potential energy, we replace the left-hand side of (7.11) by the right-hand side of (7.12). Using (7.1), we obtain

$$\begin{aligned} \frac{8\pi^2 n^2 {q_j'}^2 \mu_j}{< \mathcal{G}_j^{-1} >} D'_{ip,jq} &= W[\check{\xi}_{(jq)}; \check{\xi}_{(ip)}] \\ &\quad - \tfrac{1}{2}\left(\hat{\xi}_{jq}, \mathcal{P}^{\dagger}\hat{\chi}_{ip} - \mathcal{K}\hat{\xi}_{ip}\right) \\ &\quad - \tfrac{1}{2}\left(\mathcal{P}\hat{\xi}_{jq}, \mathcal{G}\mathcal{P}\hat{\xi}_{ip} - \hat{\chi}_{ip}\right). \end{aligned} \tag{7.17}$$

An equivalent expression to (7.17) can be derived from Eqs.(6.44) and (6.41),

$$4\mu_j f_j^{(0)} D'_{ip,jq} = \left(L\hat{\xi}_{jq}, \check{\xi}_{(ip)}\right) + \left(\hat{\xi}_{jq}, L\hat{\xi}_{ip}\right) \tag{7.18}$$

with the first two terms defining the symmetrized-matrix element (6.41) vanishing in virtue of (6.31).

7.3 Ritz approximation

Let the solution $\check{\xi}_{(ip)}$, $i = 1, 2, \cdots N$ and $p = +, -$, be approximated by the finite expansion

$$\check{\xi}_{(ip)}^{(M,l,L)} = \sum_{\nu=1}^{M} \sum_{m=l}^{L} \Xi_{ip}^{(\nu,m)} e_{\nu}^{(m)}(x, \theta) \tag{7.19}$$

in the basis functions

$$e_\nu^{(m)}(x,\theta) \equiv e_\nu(x) \exp im\theta \tag{7.20}$$

with $e_\nu(x)$ belonging to the Sobolev space $\mathcal{H}_M$ and $\exp im\theta$ spanning the finite-dimensional Fourier space $\mathcal{H}_{l,L}$. A typical choice of finite elements $e_\nu(x)$ is shown in Fig. 7.1: these are the linear tent-functions which vanish outside their respective support extending from $x^{(\nu-1)}$ to $x^{(\nu+1)}$ (except for e_1 and e_M which have supports extending from $x^{(1)}$ to $x^{(2)}$, and $x^{(M-1)}$ to $x^{(M)}$ respectively). Equation (7.19) is called the Ritz approximation of $\check{\xi}_{(ip)} \in \mathcal{H}$ with $\mathcal{H}_M \otimes \mathcal{H}_{l,L} \subseteq \mathcal{H}$.

Replacing $\check{\xi}_{(ip)}$ by $\check{\xi}_{(ip)}^{(M,l,L)}$ in (7.10), we find the set of $M(L-l+1)$ *Galerkin equations*

$$W[u;\check{\xi}_{(ip)}^{(M,l,L)}] = -\tfrac{1}{2}\left(u, \mathcal{P}^\dagger\hat{\chi}_{ip} - \mathcal{K}\hat{\xi}_{ip}\right) - \tfrac{1}{2}\left(\mathcal{P}u, \mathcal{G}\mathcal{P}\hat{\xi}_{ip} - \hat{\chi}_{ip}\right), \tag{7.21}$$

which leads after substituting (7.19) into (7.21) and setting $u = e_{\nu'}^{(m')}$, to the system of linear equations

$$\begin{aligned}\sum_{\nu=1}^{M}\sum_{m=l}^{L} W[e_{\nu'}^{(m')}; e_\nu^{(m)}]\Xi_{ip}^{(\nu,m)} &= -\tfrac{1}{2}\left(e_{\nu'}^{(m')}, \mathcal{P}^\dagger\hat{\chi}_{ip} - \mathcal{K}\hat{\xi}_{ip}\right) \\ &\quad - \tfrac{1}{2}\left(\mathcal{P}e_{\nu'}^{(m')}, \mathcal{G}\mathcal{P}\hat{\xi}_{ip} - \hat{\chi}_{ip}\right),\end{aligned} \tag{7.22}$$

for the coefficients $\Xi_{ip}^{(\nu,m)}$. Equations (7.22) admit a unique solution, provided the integral on the right-hand side converges. The condition that this is the case is given by (7.6).

Similarly, one obtains an estimate $D'^{(M,l,L)}_{ip,jq}$ for the matching data $D'_{ip,jq}$ by replacing the $\check{\xi}$ by their respective finite-element expansions $\check{\xi}^{(M,l,L)}$, giving

$$\begin{aligned}2\mu_j f_j^{(0)} D'^{(M,l,L)}_{ip,jq} &= \sum_{\nu,\nu'}\sum_{m,m'} \Xi_{jq}^{(\nu',m')*} W[e_{\nu'}^{(m')}; e_\nu^{(m)}]\Xi_{ip}^{(\nu,m)} \\ &\quad - \tfrac{1}{2}\left(\hat{\xi}_{jq}, \mathcal{P}^\dagger\hat{\chi}_{ip} - \mathcal{K}\hat{\xi}_{ip}\right) \\ &\quad - \tfrac{1}{2}\left(\mathcal{P}\hat{\xi}_{jq}, \mathcal{G}\mathcal{P}\hat{\xi}_{ip} - \hat{\chi}_{ip}\right).\end{aligned} \tag{7.23}$$

Expression (7.23) is used in § 7.4 as the starting point of the error analysis.

7.4 Finite-element convergence

The purpose of this section is to derive the convergence of the matching-data computation as the number of finite elements M increases. We may for that purpose

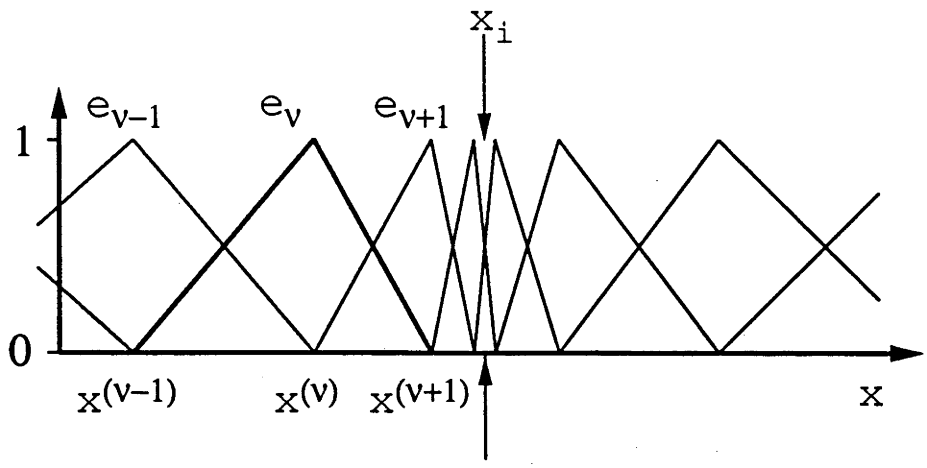

Figure 7.1: Basis functions e_ν. Each element e_ν extends from node $x^{(\nu-1)}$ to node $x^{(\nu+1)}$. The distribution of nodes can be nonuniform about the singularity x_i. Note that no singular shaped element is used.

discard the spectral part of (7.19) and (7.20) without loss of generality, since the singularities of the GNE are x surfaces and hence the convergence is only expected to be affected in the radial direction.

We start by choosing $u \equiv u_M \in \mathcal{H}_M$ in the weak form (7.10), and subtracting (7.21) from it,

$$W[u_M; \check{\xi}_{(ip)} - \check{\xi}^{(M)}_{(ip)}] = 0, \tag{7.24}$$

it is seen that the error $\check{\xi}_{(ip)} - \check{\xi}^{(M)}_{(ip)}$ is *orthogonal* in the sense of the energy inner-product to any function belonging to $\mathcal{H}_M$. We shall estimate, in the following, the error resulting from the Ritz approximation (7.19) in the calculation of the matching data, using (7.18),

$$\begin{aligned} 2\mu_j f_0^{(j)} \left[D'_{ip,jq} - D'^{(M)}_{ip,jq}\right] &= \tfrac{1}{2}\left(L\hat{\xi}_{jq}, \check{\xi}_{(ip)} - \check{\xi}^{(M)}_{(ip)}\right) \\ &= W[\check{\xi}_{(jq)}; \check{\xi}_{(ip)}] - W[\check{\xi}_{(jq)}; \check{\xi}^{(M)}_{(ip)}] \\ &= W[\check{\xi}_{(jq)} - \check{\xi}^{(M)}_{(jq)}; \check{\xi}_{(ip)} - \check{\xi}^{(M)}_{(ip)}], \end{aligned} \tag{7.25}$$

since, from (7.24), $W[\check{\xi}^{(M)}_{(jq)}; \check{\xi}_{(ip)} - \check{\xi}^{(M)}_{(ip)}] = 0$. Equation (7.25) can be further bounded using the inequality

$$W[\check{\xi}_{(jq)} - \check{\xi}^{(M)}_{(jq)}; \check{\xi}_{(ip)} - \check{\xi}^{(M)}_{(ip)}] \leq \|\check{\xi}_{(jq)} - \check{\xi}^{(M)}_{(jq)}\|_w \, \|\check{\xi}_{(ip)} - \check{\xi}^{(M)}_{(ip)}\|_w \tag{7.26}$$

and the ideal-stability assumption that $W[\check{\xi}_{(jq)} - \check{\xi}^{(M)}_{(jq)}; \check{\xi}_{(ip)} - \check{\xi}^{(M)}_{(ip)}]$ is positive and

real. Define the convergence rate r by

$$\|\check{\xi}_{(ip)} - \check{\xi}^{(M)}_{(ip)}\|_w \equiv \mathcal{O}(M^r) \tag{7.27}$$

as $M \to \infty$. Note that r is the convergence rate for the solution $\check{\xi}$, (7.26) shows that the convergence rate $2r$ of the matching data

$$2\mu_j f_0^{(j)} \left[D'_{ip,jq} - D'^{(M)}_{ip,jq}\right] = \mathcal{O}\left(M^{2r}\right) \tag{7.28}$$

as $M \to \infty$ is *twice as fast* as that of the solution itself, a characteristic property of a variational principle.

From (7.27) it is seen that $\check{\xi}^{(M)}_{(ip)}$ can be made arbitrarily close to $\check{\xi}_{(ip)}$ by increasing M *if* $r < 0$. To estimate r we first show that, using (7.24),

$$\begin{aligned} \|\check{\xi}_{(ip)} - u_M\|_w &= \|\check{\xi}_{(ip)} - \check{\xi}^{(M)}_{(ip)} + \check{\xi}^{(M)}_{(ip)} - u_M\|_w \\ &= \left\{\|\check{\xi}_{(ip)} - \check{\xi}^{(M)}_{(ip)}\|_w^2 + \|\check{\xi}^{(M)}_{(ip)} - u_M\|_w^2\right\}^{\frac{1}{2}} \end{aligned} \tag{7.29}$$

$\forall\ u_M \in \mathcal{H}_M$. Hence $\|\check{\xi}_{(ip)} - u_M\|_w \geq \|\check{\xi}_{(ip)} - \check{\xi}^{(M)}_{(ip)}\|_w$, that is the finite-element method provides the best approximation of $\check{\xi}_{(ip)}$ by minimizing

$$\|\check{\xi}_{(ip)} - \check{\xi}^{(M)}_{(ip)}\|_w = \inf_{u_M \in \mathcal{H}_M} \|\check{\xi}_{(ip)} - u\|_w. \tag{7.30}$$

In particular, we have

$$\|\check{\xi}_{(ip)} - \check{\xi}^{(M)}_{(ip)}\|_w \leq \|\check{\xi}_{(ip)} - \check{\xi}^{(I)}_{(ip)}\|_w \tag{7.31}$$

where $\check{\xi}^{(I)}_{(ip)} \in \mathcal{H}_M$ interpolates $\check{\xi}_{(ip)}$ linearly (for tent functions),

$$\check{\xi}_{(ip)}(x^{(\nu)}) = \check{\xi}^{(I)}_{(ip)}(x^{(\nu)}) \tag{7.32}$$

between the nodes $\nu = 1, 2 \cdots M$.

To evaluate the right-hand side of (7.31), we introduce

$$\epsilon_\nu(x) \equiv \check{\xi}_{(ip)}(x) - \check{\xi}^{(I)}_{(ip)}(x) \tag{7.33}$$

and $\epsilon_\nu' \equiv d\epsilon_\nu(x)/dx$ defined for $x^{(\nu)} \leq x \leq x^{(\nu+1)}$, which can be shown [Morton (1987)] to be bounded by

$$\left.\begin{aligned} \epsilon_\nu &\leq \tfrac{1}{2}\check{\xi}''_\nu[x^{(\nu+1)} - x^{(\nu)}]^2 \\ \epsilon_\nu' &\leq \check{\xi}''_\nu[x^{(\nu+1)} - x^{(\nu)}] \end{aligned}\right\}, \tag{7.34}$$

where $\check{\xi}''_\nu$ represents the maximum value

$$\check{\xi}''_\nu \equiv \max_{x\in(x^{(\nu)},x^{(\nu+1)})} \frac{d^2\check{\xi}_{(ip)}}{dx^2} \tag{7.35}$$

within the interval $(x^{(\nu)}, x^{(\nu+1)})$. From (7.31) and (7.34), we then obtain

$$\begin{aligned} \|\check{\xi}_{(ip)} - \check{\xi}^{(M)}_{(ip)}\|_w \;\leq\; & \left\{ \sum_{\nu=1}^{M-1} \check{\xi}''^2_\nu \left(x^{(\nu+1)} - x^{(\nu)}\right)^2 \right. \\ & \left. \times \int_{x^{(\nu)}}^{x^{(\nu+1)}} dx \left[f + \tfrac{1}{2} g \left(x^{(\nu+1)} - x^{(\nu)}\right)^2 \right] \right\}^{\frac{1}{2}} \end{aligned} \tag{7.36}$$

(where f and g are defined in § 4.4).

Assuming $\check{\xi}_{(ip)}$ sufficiently regular in $(0, x_a)$ so that $|\check{\xi}''_\nu| < \infty$, then (7.36) reduces to

$$\|\check{\xi}_{(ip)} - \check{\xi}^{(M)}_{(ip)}\|_w \leq \text{const}\ \ \check{\xi}'' h \tag{7.37}$$

where $h \equiv \max_{\nu=1,2\ldots M-1}(x^{(\nu+1)} - x^{(\nu)})$ and $\check{\xi}'' \equiv \max_{\nu=1,2\ldots M-1} \check{\xi}''_\nu$. Thus a linear mesh gives a convergence rate of $r = -1$, and often provides the best accuracy since $h \propto M^{-1}$ is minimal.

The situation is quite different for $|\check{\xi}''_\nu| \to \infty$ in $(0, x_a)$. We expect in this case that increasing the density of nodes around the singularity improves accuracy, and is even necessary to recover the convergence rate of $r = -1$. We can pack the nodes by taking a node-distribution function

$$F : x^{(\nu)} = F(t^{(\nu)}), \tag{7.38}$$

where

$$t^{(\nu)} \equiv \frac{\nu - 1}{M - 1} \tag{7.39}$$

$(\nu = 1, 2 \ldots M)$, such that

$$x^{(\nu)} = x_i - \text{const}\ \left(t_i - t^{(\nu)}\right)^{\gamma_i} \tag{7.40}$$

for $t^{(\nu)} < t_i$ with $t_i = F^{-1}(x_i)$,

$$x^{(\nu)} = x_i + \text{const}\ \left(t^{(\nu)} - t_i\right)^{\gamma_i} \tag{7.41}$$

for $t^{(\nu)} > t_i$ near x_i and with

$$\gamma_i \geq 1. \tag{7.42}$$

(see Fig. 7.2).

We are confronted with singular surfaces (points) located at x_i, $i = 0, 1, \cdots N$, which are characterized by the vanishing of the function $f(x)$ in (7.36). We distinguish between singularities occurring at the magnetic axis (see § 5.1) and those at the rational surfaces by letting

$$f \sim f_0^{(i)}(x - x_i)^{\beta_i} \tag{7.43}$$

as $x \to x_i$: with the exponent taking the values $\beta_0 = 1$ ($m \neq 0$) at the magnetic axis, and $\beta_i = 2$ for $i = 1, 2 \cdots N$ at the rational surfaces. Similarly,

$$\check{\xi}_{(ip)} \sim a_0(x - x_i)^{\alpha_i} \tag{7.44}$$

as $x \to x_i$: we have $\alpha_0 = m/2$ ($m \neq 0$) and $\alpha_i = -\frac{1}{2} + \mu_i$ for $i = 1, 2, \cdots N$ respectively.

Taking the limits

$$\left.\begin{aligned} M &\to \infty \\ t^{(\nu)} &\to t = \nu/M \\ 1/M &\to dt \\ x^{(\nu+1)} - x^{(\nu)} &\to dx \end{aligned}\right\} \tag{7.45}$$

while assuming

$$\frac{dx}{dt} \propto t^{\gamma_i - 1} \tag{7.46}$$

to be continuous, yields

$$\|\check{\xi}_{(ip)} - \check{\xi}_{(ip)}^{(M)}\|_w \leq \text{const } \alpha(\alpha - 1) \left\{ M \int_0^T dt\, t^{2\gamma_i(\alpha_i - 2)} \frac{t^{3(\gamma_i - 1)}}{M^3} t^{\gamma_i \beta_i} \right\}^{\frac{1}{2}} \tag{7.47}$$

for arbitrary $T \neq 0$. We see that the error converges as M^{-1} — the matching data converge as M^{-2} — provided integral (7.47) converges, that is

$$\gamma_i > \frac{2}{2\alpha_i + \beta_i - 1}. \tag{7.48}$$

This gives the following minimal scaling of the mesh:

$$\left.\begin{aligned} \gamma_0 &> 2/m \quad \text{for} \quad m \neq 0 \\ \gamma_0 &= 1 \quad\;\; \text{for} \quad m = 0 \end{aligned}\right\} \tag{7.49}$$

near $x = 0$, and

$$\left.\begin{array}{lll} \gamma_i \geq 1/\mu_i & \text{for} & \mu_i \neq 1/2,\ 3/2 \\ \gamma_i = 1 & \text{for} & \mu_i = 1/2,\ 3/2 \end{array}\right\} \tag{7.50}$$

about x_i, $i = 1, 2, \cdots N$. In the case of $\beta = 0$, it is appropriate to take a linear mesh.

7.5 Node-distribution function in PEST3.4

In order to illustrate the mesh requirements (7.40), (7.41) and (7.46), which are essential if the results of § 7.4 are to apply, it is instructive to explain the construction of the mesh as performed in PEST3.4. It is always desirable from an accuracy viewpoint to adopt a linear mesh whenever possible. We therefore restrict the use of a graded mesh to the immediate vicinities of the singular surfaces x_i. Consider a plasma with N rational surfaces and focus on a particular section (x_i, x_{i+1}); we start with a graded zone

$$F(t) = x_i + \frac{bw_i}{\gamma_i}\left(\frac{t - t_i}{w_i}\right)^{\gamma_i} \qquad t_i \geq t \geq t_i + w_i, \tag{7.51}$$

which is prolonged to a zone where the distribution function is linear,

$$F(t) = b\left\{t - \frac{w_0(\gamma_0 - 1)}{\gamma_0} - 2\sum_{j+1}^{i}\frac{w_j(\gamma_j - 1)}{\gamma_j}\right\} \qquad t_i + w_i \geq t \geq t_{i+1} - w_{i+1} \tag{7.52}$$

and ends with a zone of packed nodes,

$$F(t) = x_{i+1} - \frac{bw_{i+1}}{\gamma_{i+1}}\left(\frac{t_{i+1} - t}{w_{i+1}}\right)^{\gamma_{i+1}} \qquad t_{i+1} - w_{i+1} \geq t \geq t_{i+1} + w_{i+1}. \tag{7.53}$$

In Eqs.(7.51)–(7.53), w_i, $i = 0, 1, \cdots N$, represents the graded-zone width on the t axis (see Fig. 7.2). It is easy to check that the mesh so constructed satisfies all the continuity requirements of § 7.4, with the slope

$$b = x_a\left\{1 - \frac{w_0(\gamma_0 - 1)}{\gamma_0} - 2\sum_{i=1}^{N}\frac{w_i(\gamma_i - 1)}{\gamma_i}\right\}^{-1} \tag{7.54}$$

and

$$t_i = \frac{x_i}{b} + \frac{w_0(\gamma_0 - 1)}{\gamma_0} + 2\sum_{j=1,}^{i-1}\frac{w_j(\gamma_j - 1)}{\gamma_j} + \frac{w_i(\gamma_i - 1)}{\gamma_i} \tag{7.55}$$

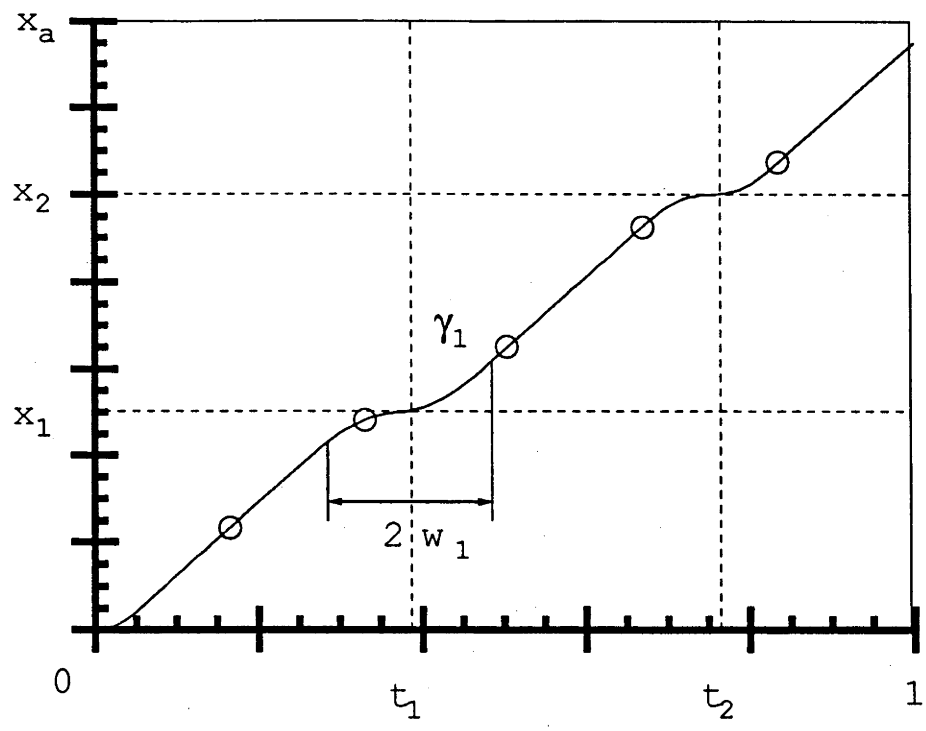

Figure 7.2: Typical node-distribution function $x = F(t)$ for two rational surfaces x_1 and x_2. A linear mesh is adopted in most regions with the mesh nodes being packed near x_i, $i = 0, 1, 2$. The slopes in all linear zones are equal.

ensuring that the spacing between nodes in each linear zone remains constant across the $N + 1$ sections. The condition that $b > 0$ requires in addition

$$\frac{w_0(\gamma_0 - 1)}{\gamma_0} + 2\sum_{i=1}^{N} \frac{w_i(\gamma_i 1)}{\gamma_i} < 1 \tag{7.56}$$

which imposes some constraint on the maximum value of the w_i.

Chapter 8

Numerical test-cases

The variational method of Ch. 6 is applied to various one- and two-dimensional plasmas. We start in § 8.1 by treating first cylindrical plasmas. There are several reasons to do so; clearly cylindrical plasmas contain most of the physics that also characterizes two-dimensional plasmas, as far as the splitting between big and small solutions is concerned. Furthermore, the ease with which accurate equilibria can be generated in cylindrical geometry also is appropriate for convergence studies, for one has more flexibility to explore different regimes of Mercier parameter. In that sense, the three cylindrical equilibria of § 8.1 provide a good test of the robustness of the variational matching-data method, which will be illustrated by convergence studies. The validity of the error analysis derived in § 7.4 will be confirmed in § 8.1.

We choose a zero-β equilibrium of large aspect-ratio in § 8.2, which possesses one rational surface, to compare the matching-data computation as carried out with the resistive stability code PEST3.3 [Manickam *et al.* (1983)], with the data computed by the version PEST3.4, which embodies the variational scheme of Ch. 6. The code PEST3.3 uses singular elements near the rational surface to mimic the big and small solutions behaviour. The two versions converge to the same matching data Δ' (except that the definition of Δ' in PEST3.3 differs by a factor two). The reason for good agreement between PEST3.3 and PEST3.4 is due to the "regular" nature of the small solution in the zero-β case (with exception of the jump at the rational surface), which allows us to use a linear mesh (equally distributed nodes). In the zero-β case, it can be shown that the solution converges pointwise at the *same rate*

as the energy norm so that Δ' can be estimated accurately from its geometrical intepretation [see § 6.3] of a small-solution discontinuity.

A major outcome of the variational principle of Ch. 6 is the reciprocity relation, or symmetry relation prevailing between the off-diagonal elements of the matching matrix. In the case of a unique rational surface, these relations are quite trivial. In the double-tearing case treated in § 8.3, however, we find that the variational method is superior because it makes explicit use of the reciprocity relations in the matching-data computation.

The case of a finite-β toroidal plasma with two rational surfaces is considered in § 8.4. This is the regime where the regular solutions intervene; there is in general no reliable geometrical estimate of the matching data from the pointwise representation of the solution near rational surfaces. The variational matching-data approach offers in this case the only alternative. Provided the mesh nodes are packed near the rational surfaces, according to the prescriptions of § 7.4, convergence in M^{-2} is achieved yielding an accurate matching matrix.

8.1 Cylindrical equilibria

In order to access the regime $\mu_1 > \frac{1}{2}$, we are led to consider hollow pressure profiles

$$p(\psi) = p_0(1+\rho)\frac{1-(\psi/\psi_a)^2}{1+\rho[1-(\psi/\psi_a)^2]^2} \tag{8.1}$$

in cylindrical geometry, where ρ is a parameter which determines the pressure profile. For $0 \leq \rho \leq 1$, the pressure decreases monotonically from $\psi = 0$ to $\psi = \psi_a$. But for $\rho > 1$, the pressure profile is hollow with positive pressure gradient at the rational surface.

We take the safety factor to be a monotonically growing function of the radius r,

$$q(r) = 1 + 3(r/r_a)^2, \tag{8.2}$$

with $r_a \equiv r(\psi_a)$, so that there always exists one and only one rational surface at r_1, $0 < r_1 < r_a$, for $m = 2$ and $n = 1$. The following profiles denoted by a, b and c,

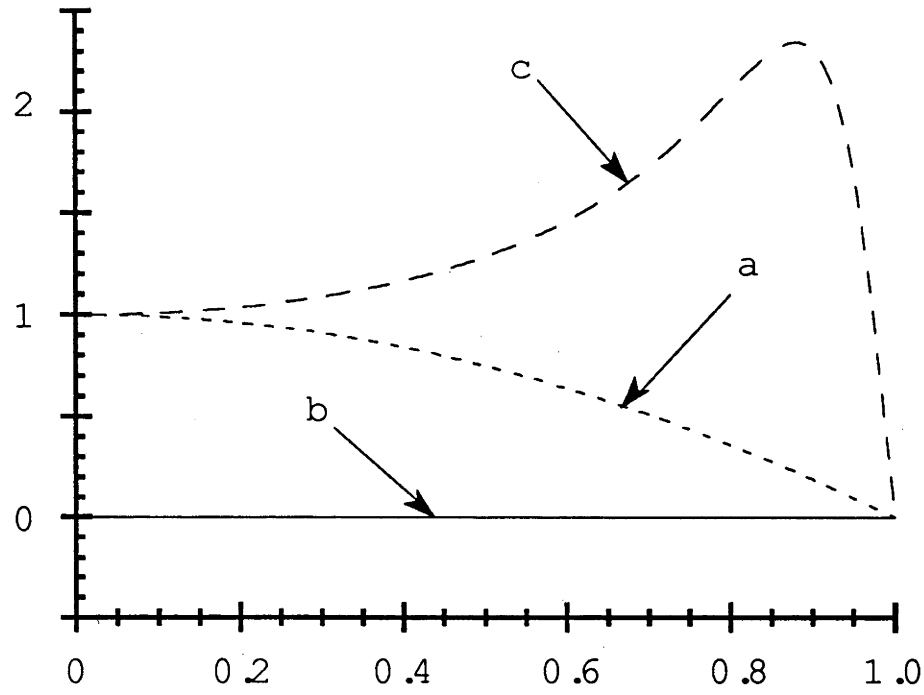

Figure 8.1: Three pressure profiles a, b and c are considered. To the normal profile a corresponds a negative pressure gradient at ψ_1. The pressure is identically zero ($\beta = 0$) in case b. The pressure gradient is positive at ψ_1 in the hollow pressure case c.

and illustrated in Fig. 8.1, are considered:

p profile	p_0	ρ	μ_1
a	1	0	0.41673
b	0		0.5
c	1	20	0.60305

(8.3)

where $\mu_1 \equiv \sqrt{-D_I(r_1)}$. Because in cylindrical geometry the left- and right-hand side problems decouple, it is advantageous to use the left-sided and right-sided functions for the calculation of the matching data,

$$\begin{aligned} \mu_1 f_1^{(0)} \Delta_L &= 2W[\check{\xi}_{(iL)}; \check{\xi}_{(iL)}] + \left(\hat{\xi}_{iL}, L\hat{\xi}_{iL}\right) \\ \mu_1 f_1^{(0)} \Delta_R &= 2W(\check{\xi}_{(iR)}, \check{\xi}_{(iR)}) + \left(\hat{\xi}_{iR}, L\hat{\xi}_{iR}\right). \end{aligned} \tag{8.4}$$

We set $s_1(\mu_1) = 0$ in (6.28) except for case b where s_1 is given by (C.11).

The convergence of algorithm (6.44) and (8.4) is tested by varying the number of nodes (10–200), as well as γ_1, the exponent of the scaled zone shown in Fig. 7.2. Each mesh is characterized by M_L, the number of mesh nodes on the left-hand

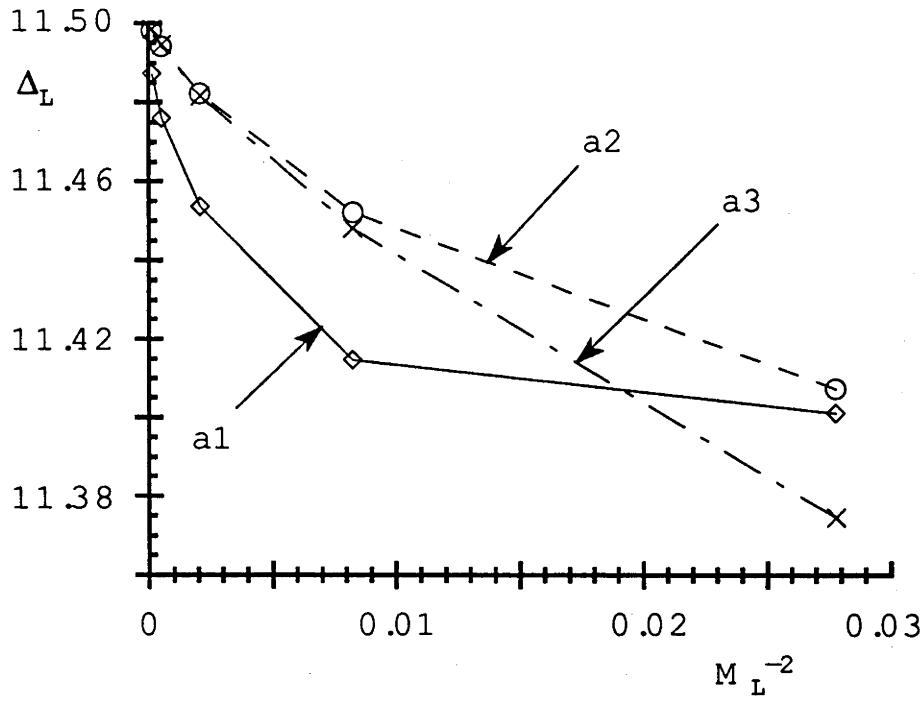

Figure 8.2: Convergence of Δ_L versus the inverse square of the number of mesh nodes M_L on the left-hand side of ψ_1 for the pressure profile a. Three meshes $a1$, $a2$ and $a3$ are considered with mesh scaling exponents $\gamma_1 = 1$, $\gamma_1 = 2.4$ and $\gamma_1 = 4.0$ respectively.

side of ψ_1 and M_R, the number of mesh nodes on the right-hand side of ψ_1 with $M = M_L + M_R$. We choose the width $w_0 = w_1 \equiv w$ of the scaled zone to be identical about $\psi = 0$ and $\psi = \psi_1$. The different meshes are summarized in the following table

p profile	Mesh	w	γ_0	γ_1
	$a1$			1.0
a	$a2$	0.2	1.1	2.4
	$a3$			4.0
b	b	0.2	1.1	1.0
c	$c1$	0.2	1.1	1.0
	$c2$			1.7

(8.5)

The pressure profile a is the numerically most constraining case, for μ_1 is small so that a high density of nodes is required according to (7.48). This is exhibited by Figs. 8.2 and 8.3. For a linear mesh, Δ_L and Δ_R converge (negative r) but, as

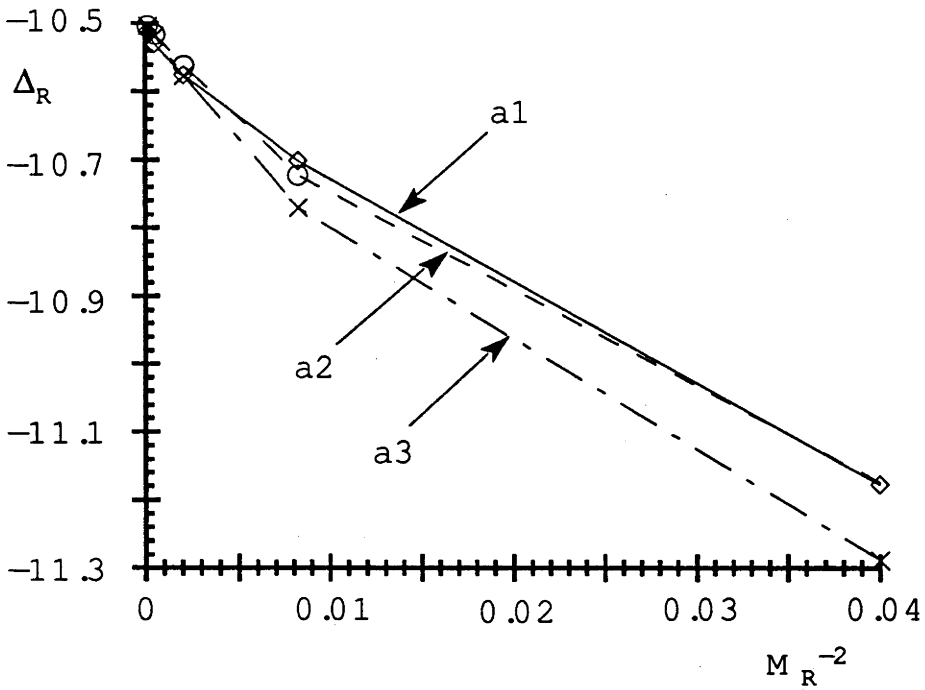

Figure 8.3: Convergence of Δ_R versus the inverse square of the number of mesh nodes M_R on the right-hand side of ψ_1 for the pressure profile a. Three meshes $a1$, $a2$ and $a3$ are considered with mesh scaling exponents $\gamma_1 = 1$, $\gamma_1 = 2.4$ and $\gamma_1 = 4.0$ respectively.

expected, without reaching the maximal convergence rate of $2r = -2$. Increasing γ_1 to $\gamma_1 = 2.4 \approx 1/\mu_1$ is sufficient to recover $r = -1$ so that Δ_L and Δ_R converge as M^{-2} for $M > 40$. The convergence is further improved at smaller M for $\gamma_1 = 4.0$ at the expense of a deteriorated accuracy. A characteristic feature of μ_1 approaching $\frac{1}{2}$ when $s_1(\mu_1)$ is set to zero, is $|\Delta'| \ll |\Gamma'|$, already noticeable at $\mu_1 = 0.41673$ (case a) in that the sum of Δ_L and Δ_R is an order of magnitude smaller than the difference.

In the pressureless case b, the dominant behaviour of $L\hat{\xi}_{ip} = \mathcal{O}(\psi - \psi_1)$ is less localized, leading to a convergence in M^{-2} at low $M \approx 10$ for a linear mesh, as illustrated in Figs. 8.4 and 8.5. For higher values of μ_1 (see case c in Figs. 8.6 and 8.7), the mesh scaling becomes less crucial as often linear meshes turn out to be sufficiently accurate and convergent.

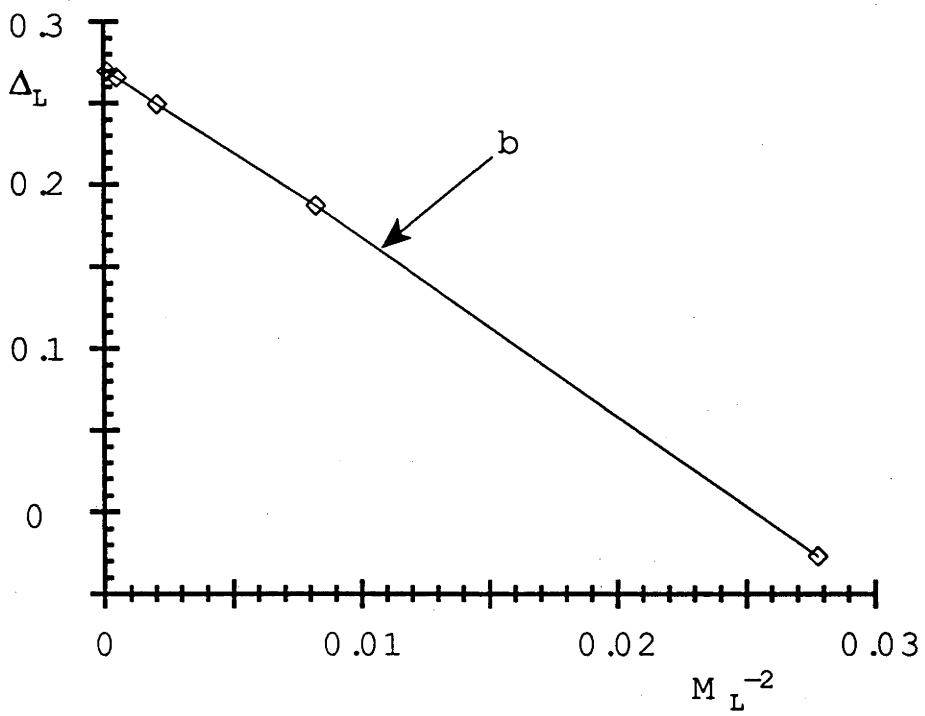

Figure 8.4: Convergence of Δ_L versus the inverse square of the number of mesh nodes M_L on the left-hand side of ψ_1 for the $\beta = 0$ case b and for linear mesh ($\gamma_1 = 1$).

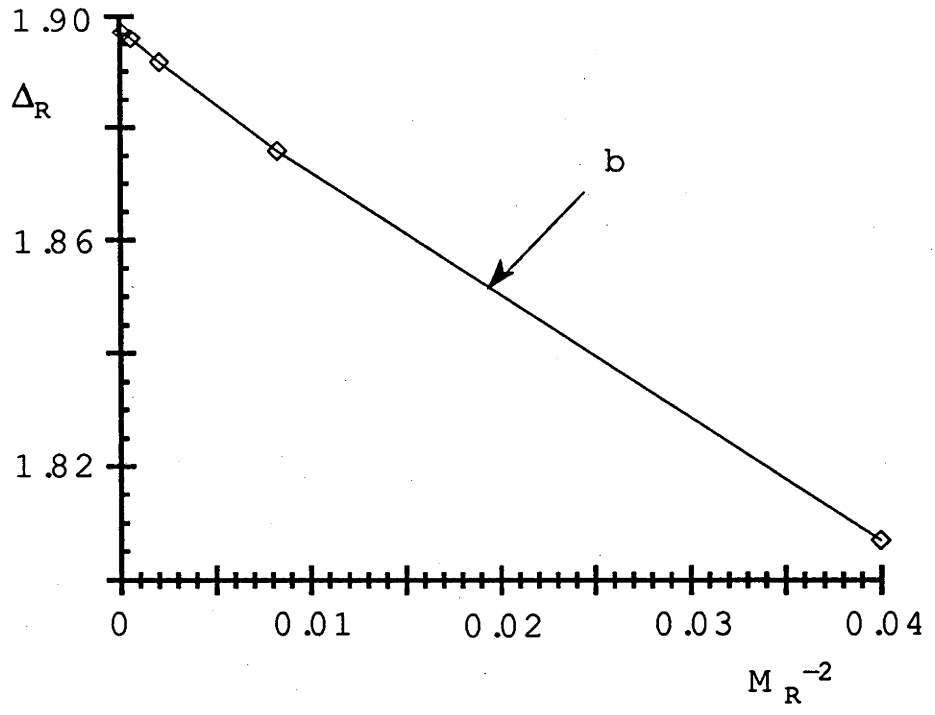

Figure 8.5: Convergence of Δ_L versus the inverse square of the number of mesh nodes M_L on the left-hand side of ψ_1 for the $\beta = 0$ case b and for linear mesh ($\gamma_1 = 1$).

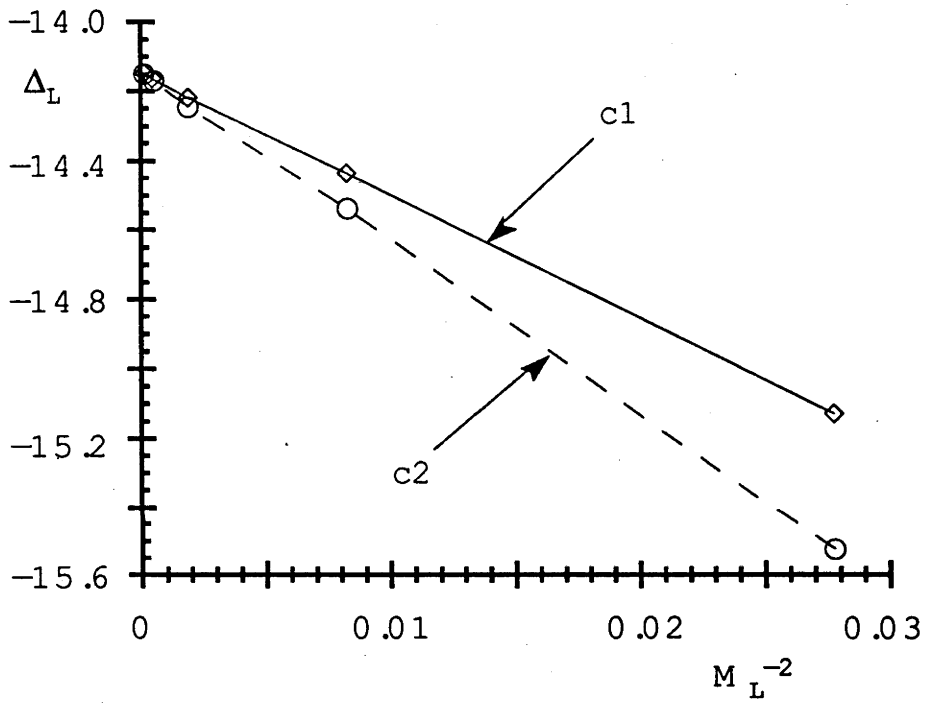

Figure 8.6: Convergence of Δ_L versus the inverse square of the number of mesh nodes M_L on the left-hand side of ψ_1 for the hollow pressure profile c. Two meshes $c1$ and $c2$ are considered with mesh scaling exponents $\gamma_1 = 1$ and $\gamma_1 = 1.7$ respectively.

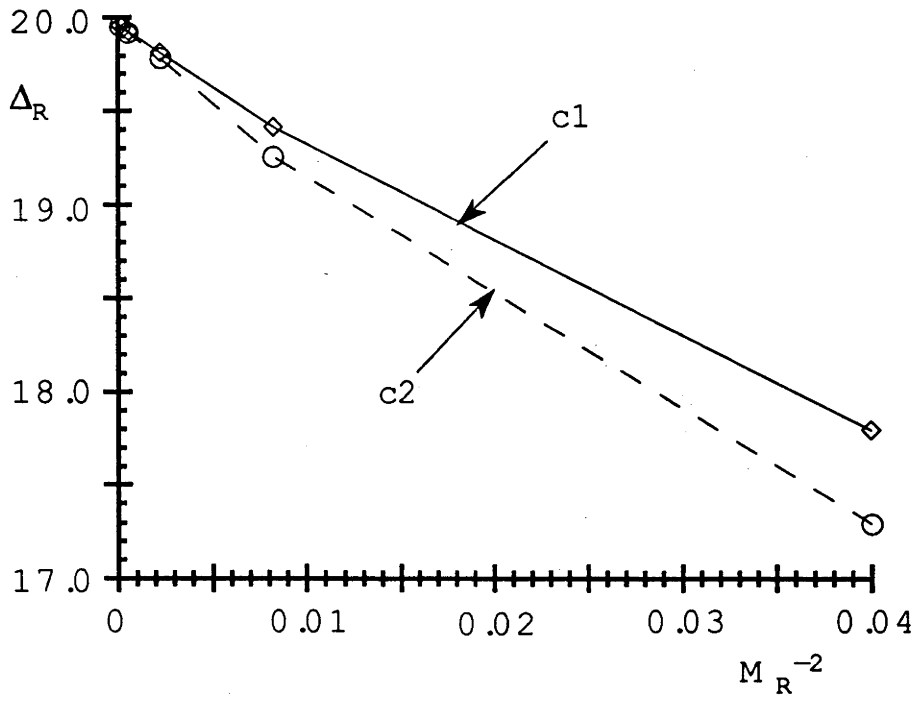

Figure 8.7: Convergence of Δ_L versus the inverse square of the number of mesh nodes M_L on the left-hand side of ψ_1 for the hollow pressure profile c. Two meshes $c1$ and $c2$ are considered with mesh scaling exponents $\gamma_1 = 1$ and $\gamma_1 = 1.7$ respectively.

8.2 Zero-β toroidal plasma

We consider in this section the large aspect-ratio equilibrium of Fig. 8.8, characterized by the safety-factor profile shown in Fig. 8.9. The safety factor varying between $1 < q < 3$, there is only one rational surface located at approximately 2/3 of ψ_a.

Before expounding the results of the equilibrium of Fig. 8.8, we take first the opportunity to discuss the conceptual differences arising between the resistive-stability code PEST3.3 and the version PEST3.4 that replaces it and from which all the results of the remaining part of this chapter derive from. The latter incorporating the variational matching-data method. The accuracy of PEST3.3 relies on the small singular-elements $s_{i\pm}$ and the big elements $b_{i\pm}$ shown in Fig. 8.10 to capture the Frobenius solutions near ψ_i. The shape of these elements and the unit amplitude of the big driving element being prescribed, the matching data are then simply given in PEST3.3 by the ratio of the amplitude of the s's. it is crucial, in this approach, to keep the support of the $s_{i\pm}$ and $b_{i\pm}$ as localized as possible since these elements

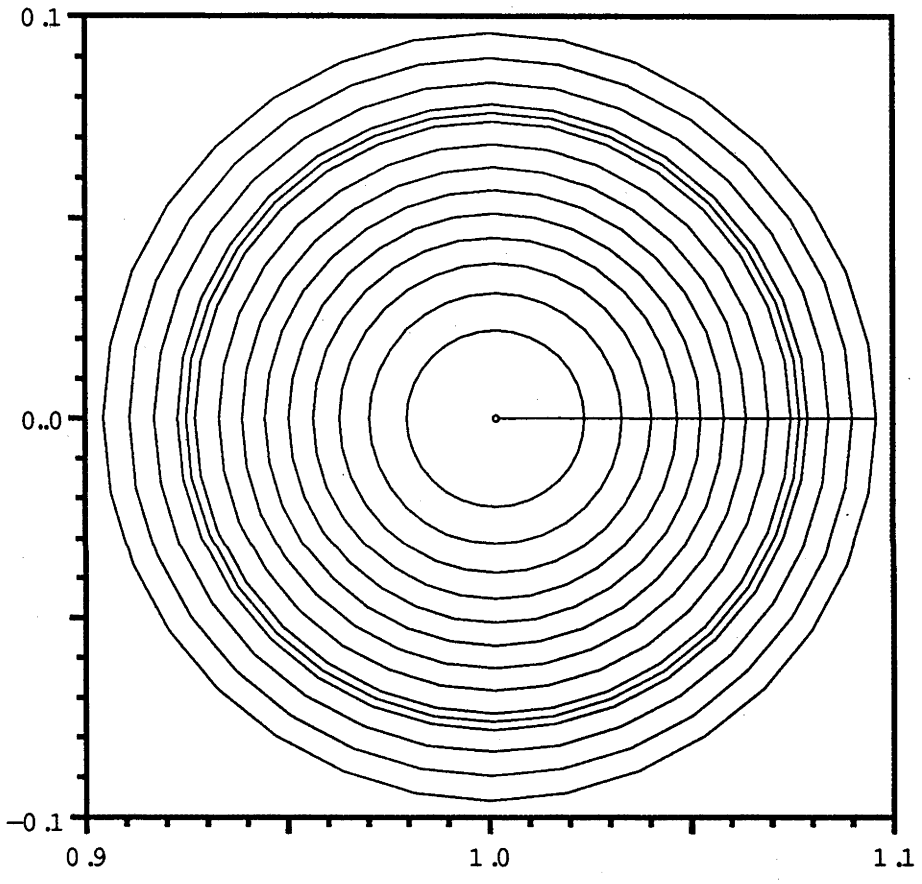

Figure 8.8: Flux surfaces of the zero-β toroidal equilibrium.

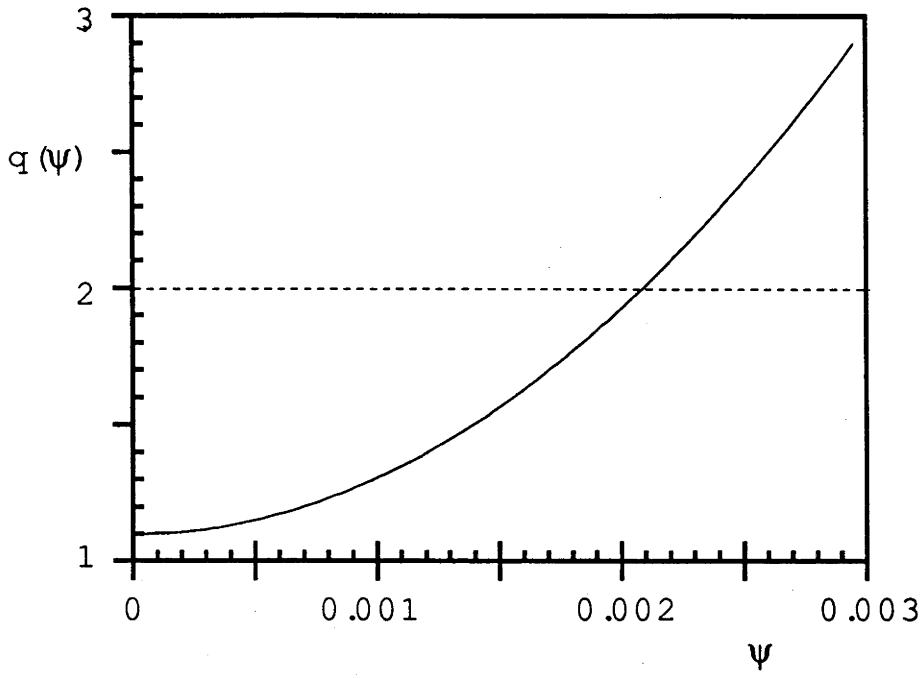

Figure 8.9: Equilibrium profiles of the safety factor q versus the poloidal flux coordinate ψ. The dashed line at $\psi = 0.0020856$ indicates the location of the unique rational-surface.

approximate the infinite Frobenius series of the normalized small and big solution, respectively. Therefore, the extraction procedure follows in general two convergence studies, one in the number of mesh nodes while keeping the support of these singular elements constant (see Fig. 8.11), and the other by varying the support the singular elements [Manickam *et al.* (1983)].

In PEST3.4, on the other hand, no singular elements are needed, as a result of the convergence studies in Pletzer & Dewar (1991) and Miller & Dewar (1986); the matching data converge as M^{-2} provided the mesh is scaled according to Eqs.(7.40) and (7.40). In this case where $\beta = 0$, for which $\alpha^{(s)} = 0$, the response solution behaves locally on either side of the rational surface as a regular solution. Therefore, a linear mesh is sufficient to ensure proper convergence (in M^{-2} for tent functions) as indicated in § 7.4, and by Figures 8.4 and 8.5. It is also known from Morton (1987) that the solution converges pointwise at a rate equal or exceeding the convergence rate in the energy norm for $\alpha = 0$.

Therefore, this zero-β equilibrium constitutes a good test-case; for both PEST3.3 and PEST3.4 converge in M^{-2}, allowing thus direct comparisons between Δ' ob-

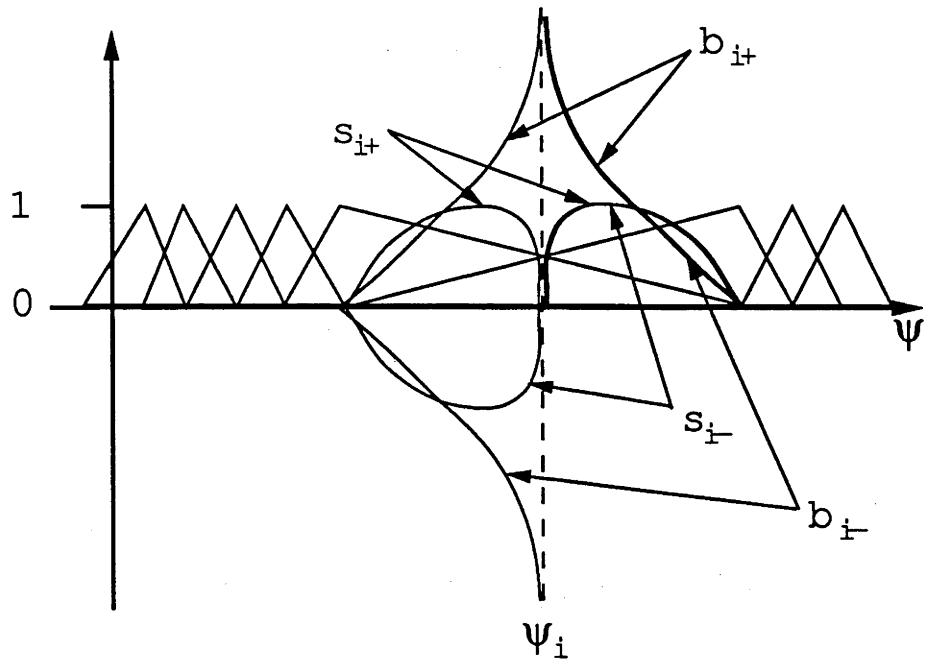

Figure 8.10: Mesh structure in the old version PEST3.3. In the vicinity of the rational surfaces ψ_i, singular elements (s_{i-} and s_{i+}) are used for the extraction of the small solution. The prescribed big solutions b_{i-} and b_{i+} only extend up to the nearest, adjacent finite-elements.

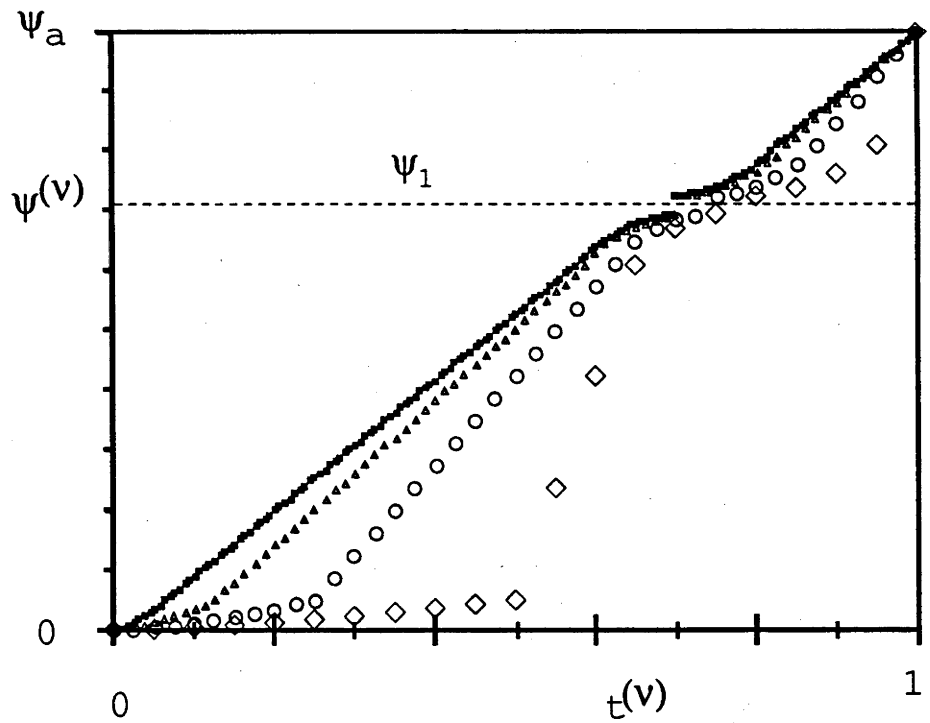

Figure 8.11: Mesh as generated in PEST3.3 for $M = 20, 40, 80$ and 160 mesh nodes respectively. The support of the singular elements is kept constant.

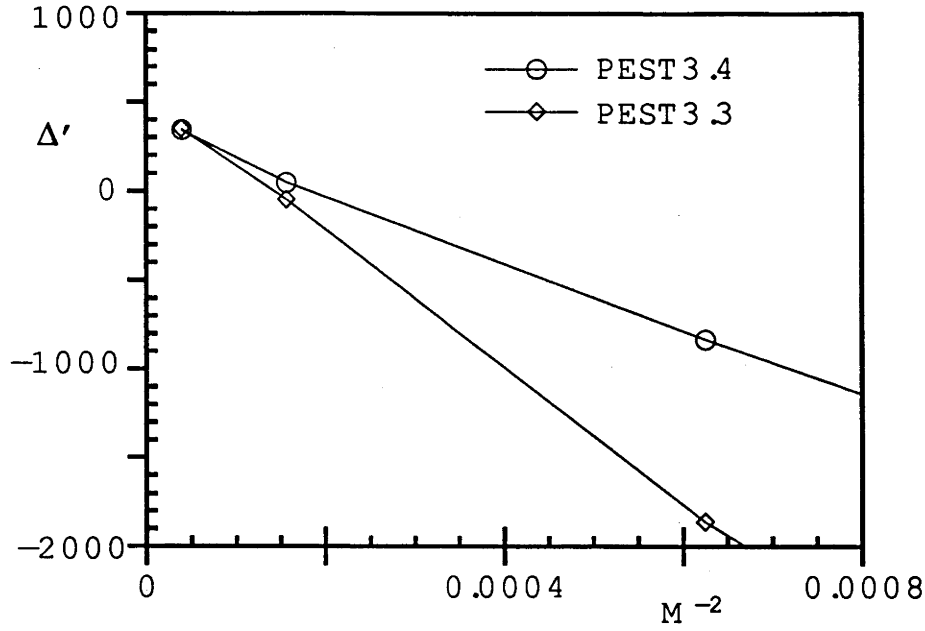

Figure 8.12: Comparative study of the convergence properties of Δ' versus the inverse square of the number of mesh nodes M^{-2}.

tained by employing either code (the Γ' do not correspond which is an example of the non-unique definition of the big solution in the zero-β case). In the comparative convergence study, a linear mesh is chosen for PEST3.4, whereas the two adjacent elements in PEST3.3 are kept constant as the number mesh-nodes M (Fig. 8.11). The convergence study by varying the support of the singular elements turns out unnecessary in this particular case.

To prevent inaccuracies in the multi-tearing studies of §§ 8.3 and 8.4, where smaller supports for the localization-function H_i are required, we vary the parameter δ_i of Fig. 6.1 and analyze the resulting effect on the convergence in Figures 8.13 and 8.14. It is immediately seen that a small δ is less accurate. This can be understood in different ways. Note that the resonant $m = 2$ response-solution of Fig. 8.15 exhibits a dramatic change of amplitude in the regions $0.0014 < \psi < 0.0018$ and $0.0024 < \psi < 0.0028$ with discontinous slopes at these endpoints. This has no physical significance, being merely due to the variation of the localization function H_i from the flat plateau $H_i \equiv 1$ to the region where H_i is zero. These are therefore also the regions where the source-term is dominant in the weak form (7.10). In PEST, all quadratures are performed by taking the values of the integrand at the

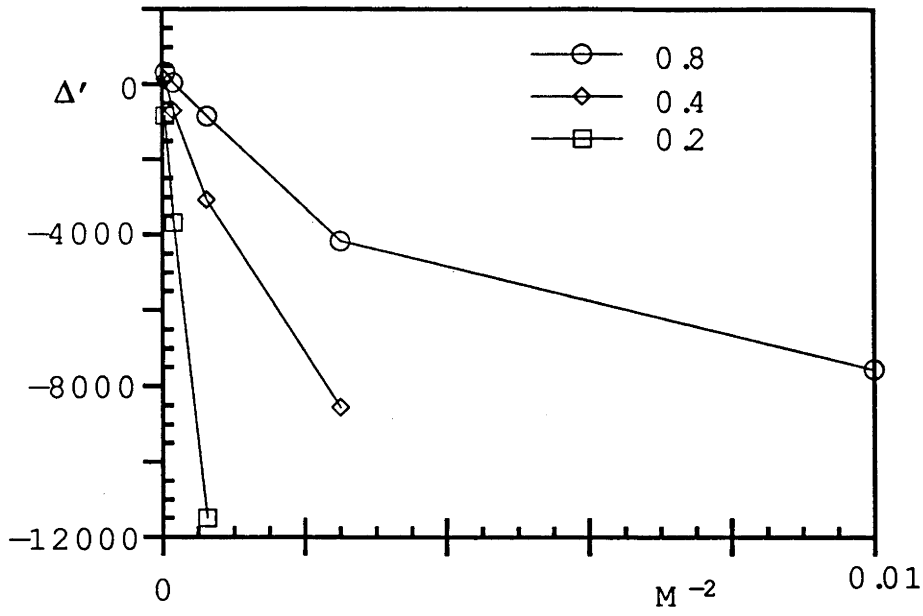

Figure 8.13: Convergence properties of Δ' versus the inverse square of the number of mesh nodes M^{-2}. This case is tearing unstable.

mesh nodes and at mid-distance inbetween (Simpson's rule), it is thus not surprising that a prescribed solution that embraces a large number of nodes (large δ) is more accurate.

The result of the convergence studies in δ, however, also shows that both the extrapolated matching-data as ($M \to \infty$) and the overall convergence rate remains intact as δ shrinks from 80 % to 20 % of the distance separating the rational surface from the plasma edge.

Since PEST3.3 performs well in this case, we may naturally ask why. The geometric interpretation of the matching data as given by

$$\left.\begin{aligned} \Delta' &= \lim_{x\to 0+} x_+^{-\alpha(s)} \left[\check{\xi}_{(-)}(\psi_i + x) - \check{\xi}_{(-)}(\psi_i + x)\right] \\ \Gamma' &= \lim_{x\to 0+} x_+^{-\alpha(s)} \left[\check{\xi}_{(-)}(\psi_i + x) + \check{\xi}_{(-)}(\psi_i + x)\right] \end{aligned}\right\}, \tag{8.6}$$

which is a variant of (6.18), valid in the zero-β case only, yields matching data in accordance with those given from Figures 8.13 and 8.14.

Magnifying the region in Fig. 8.15 near ψ_i where $H_i \equiv 1$, we see in Fig. 8.16 that $\Delta' \approx 450$ and $\Gamma' \approx 6200$, values which are confirmed by Figures 8.12–8.14. One can also discern a moderate discontinuity in Fig. 8.16 (the magnitude of which being tempered in the present case by the smallness of Δ'/Γ'), of the non-resonant

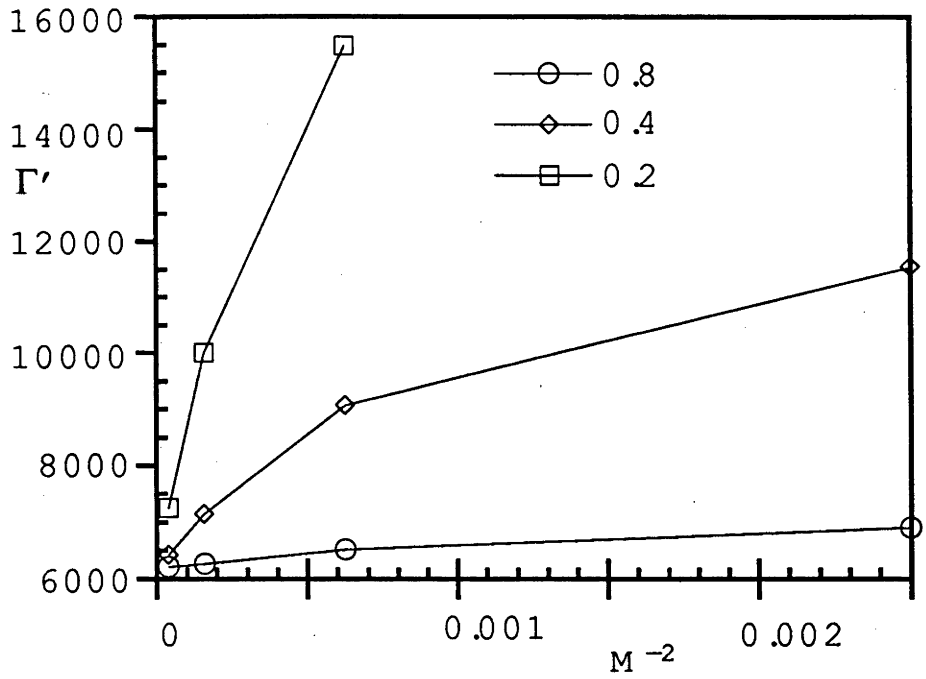

Figure 8.14: Convergence properties of Γ' versus the inverse square of the number of mesh nodes M^{-2} (irrelevant for tearing stability).

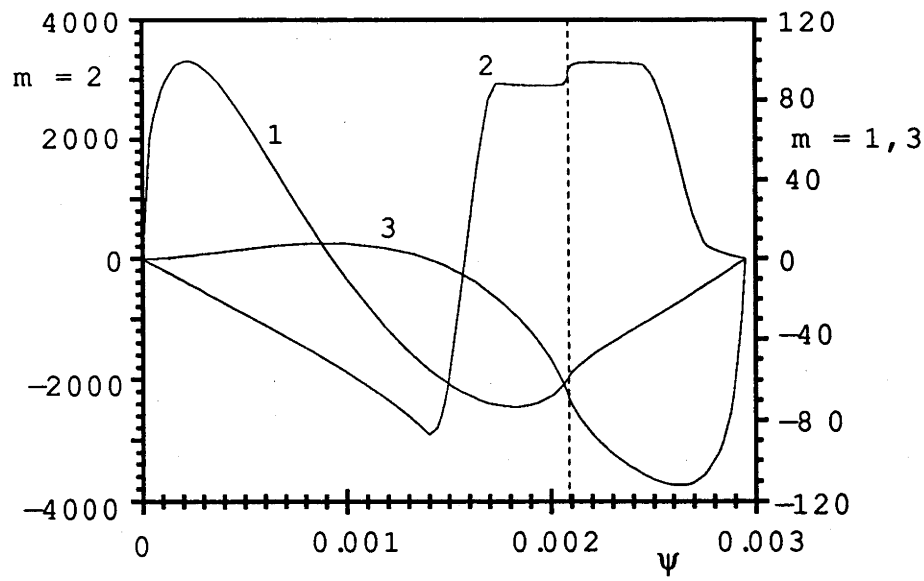

Figure 8.15: Small solution response to big driving solution of asymptotic odd parity for the zero-β toroidal plasma. The calculation was carried out with $M = 160$, $L = 6$, $l = -2$. The amplitudes of the higher $m > 3$ and lower $m < 1$ modes are negligible, and are thus not represented. The vertical dashed line represents the position of the rational surface.

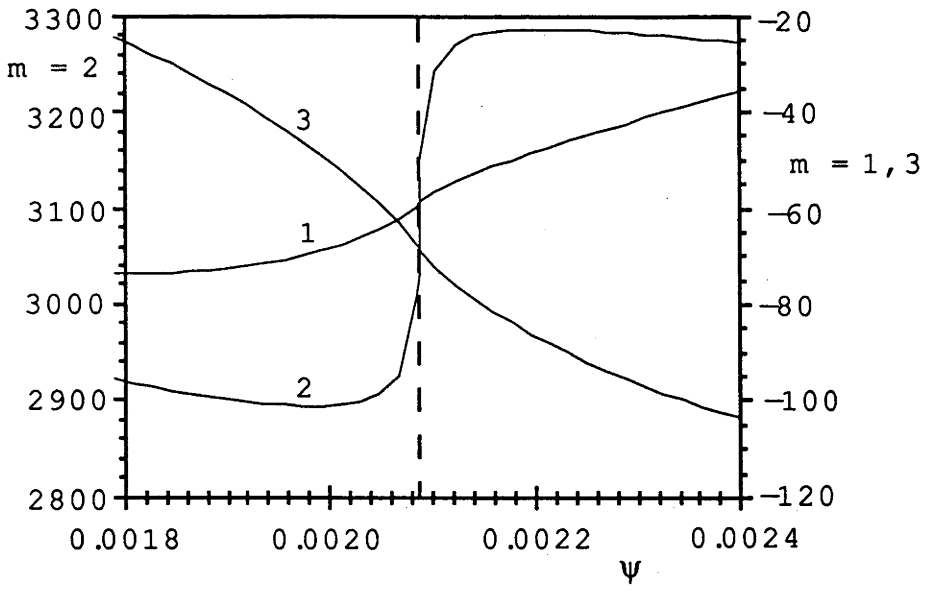

Figure 8.16: Resonant, $m = 2$, and non-resonant, $m = 1$ and $m = 3$, poloidal modes of $\tilde{\xi}_{(-)}$ versus ψ in the vicinity of the rational surface $\psi = 0.0020856$, for the zero-β case.

modes $m \neq 2$ which must be, according to § 5.5, of order $(\psi - \psi_i)\ln|\psi - \psi_i|)$ and $\psi - \psi_i$.

8.3 Double-tearing mode equilibrium

Following the path of increasing difficulty, we next turn our attention to the zero-β equilibrium of Figures 8.17 and 8.18, which is characterized by the presence of two rational surfaces at $\psi_1 = 0.02055$ and $\psi_2 = 0.03108$ respectively, where the safety factor takes the values $q_1 = 2$ and $q_2 = 3$ respectively.

The reciprocity relation existing between the off-diagonal elements of the matching matrix are most apparent in this case. The ratio of $\mu_1 f_0^{(1)}/\mu_2 f_0^{(2)} = 0.9753$ being approximately one, we must have $\Delta'_{1,2} \approx \Delta'_{2,1}$. A closer look at Figures 8.19 and 8.20 shows that $\Delta'_{1,2} \approx 29$ and $\Delta'_{2,1} \approx 32$, thus confirming this result. The variational method of PEST3.4 uses this symmetry explicitely in the construction of the matching matrix Δ'_{ij}, whereas the off-diagonal data can be shown to differ by 10 % (data not shown) in PEST3.3, and we may see in this a definite advantage of the variational formalism which becomes increasingly crucial as the size of the matching matrix increases.

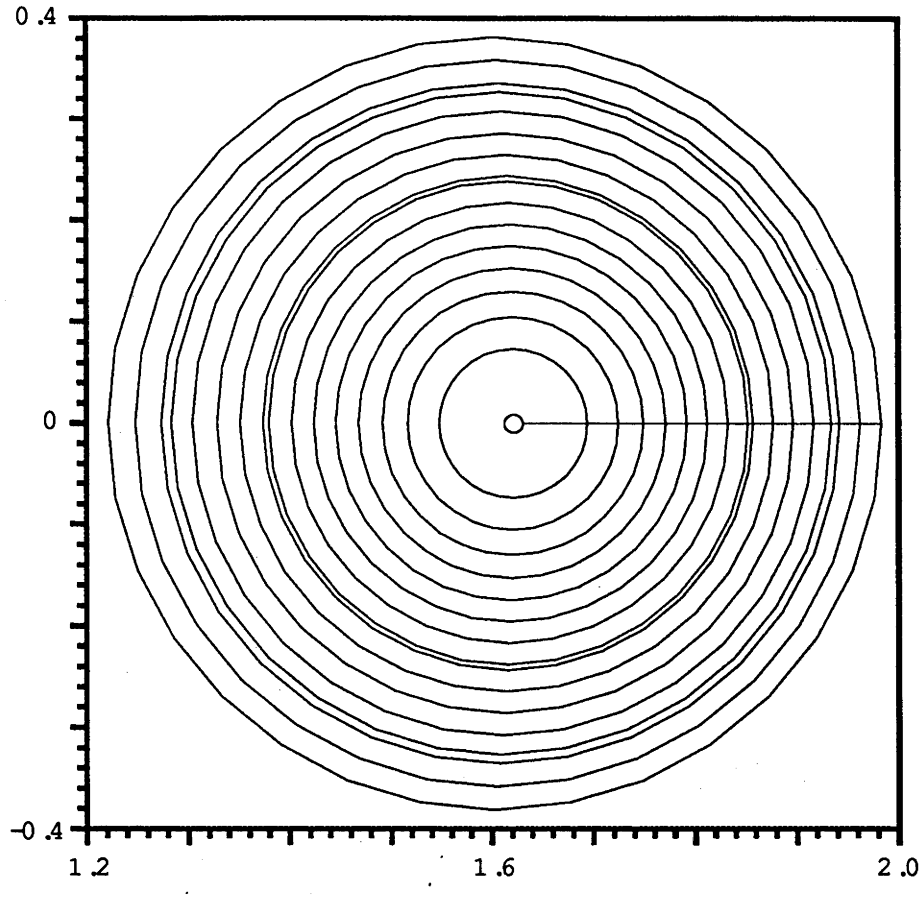

Figure 8.17: Flux surfaces of the double-tearing equilibrium.

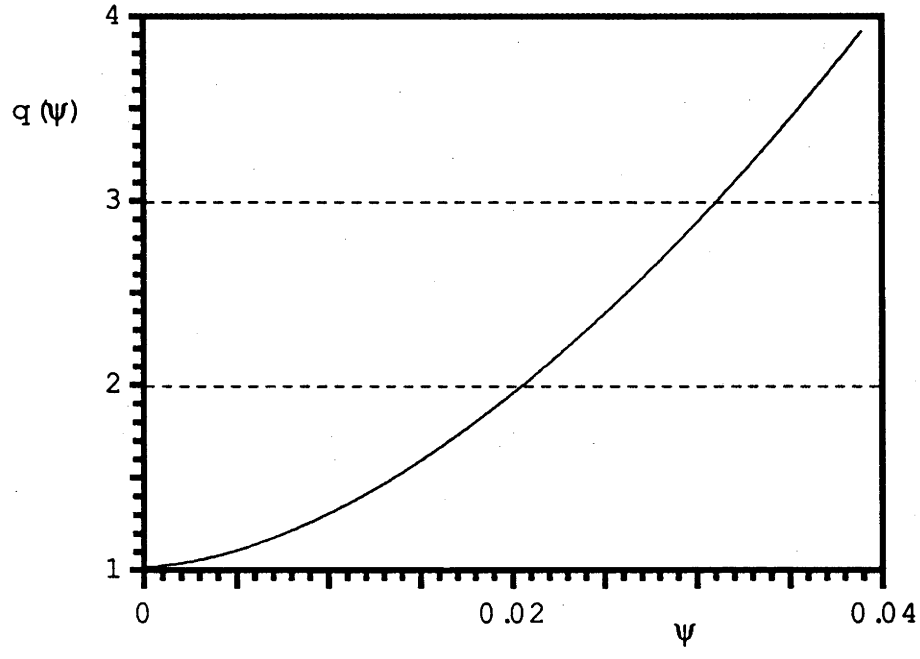

Figure 8.18: Safety-factor profile for the double-tearing equilibrium.

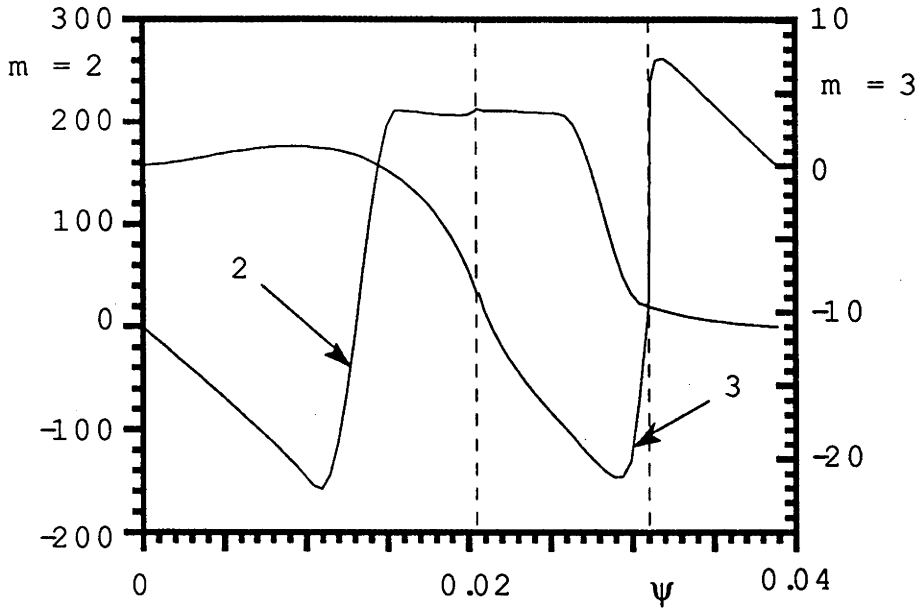

Figure 8.19: The two resonant Fourier-modes of the response solution $\check{\xi}_{(1,-)}$ driven at the rational surface ψ_1.

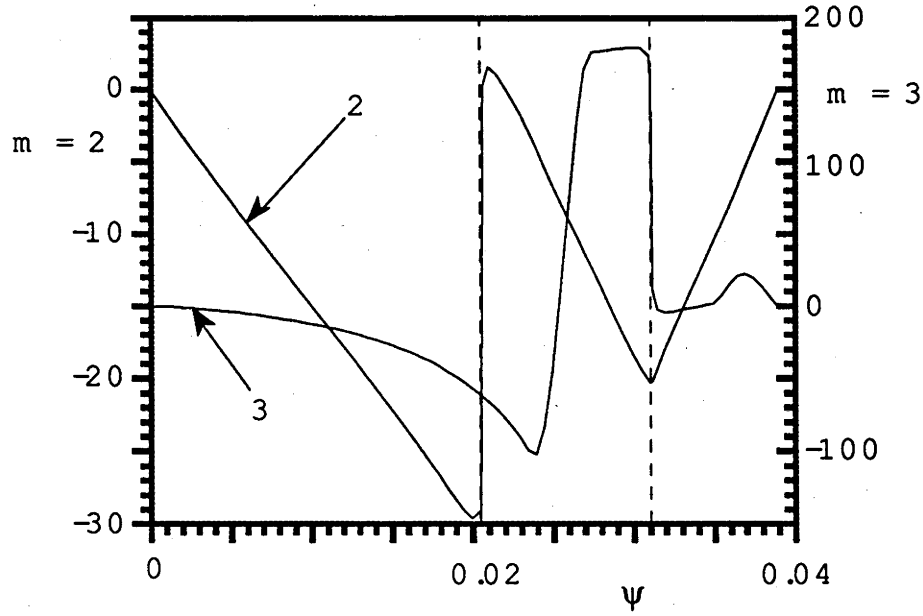

Figure 8.20: The two resonant Fourier-modes of the response solution $\check{\xi}_{(2,-)}$ driven at the rational surface ψ_2.

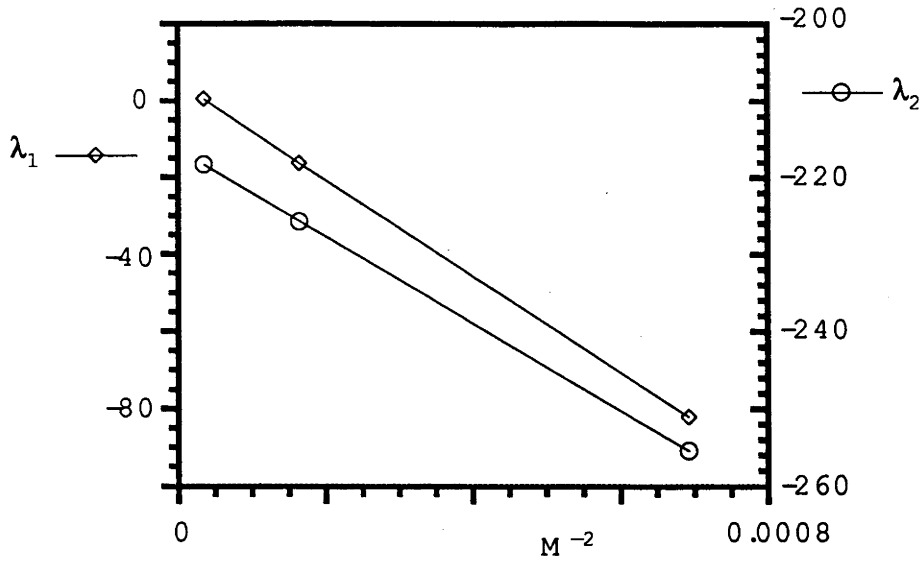

Figure 8.21: Convergence of the eigenvalues of the matching matrix for $M = 40$, 80 and 160. Rational surface ψ_1 is tearing unstable.

As a result of the error analysis of § 7.4, it was found, in particular, that the variational caculation of the matching data systematically underestimates Δ' (the difference between the the exact and the approximated value being a positive-definite functional). This was illustrated in the previous examples, and remains true in this case also, as shown by Fig. 8.21 which represents the convergence of the eigenvalues of Δ'_{ij}, $i, j = 1, 2$ as $M \to \infty$. In this particular example, the plasma is tearing stable for moderate values of M and becomes unstable as $M \to \infty$.

8.4 Double-resistive mode in a finite-β plasma

Finally we treat the finite-β case of Fig. 8.22, whose equilibrium profiles are given in Figures 8.23 and 8.24. This plasma possesses two rational surfaces, $\psi_1 = 0.09663$ and $\psi_2 = 0.13844$, where the Fourier modes $m_1 = 2$ and $m_2 = 3$ are resonant. The low value of β means that both $\alpha_1^{(s)} = 0.0626$ and $\alpha_2^{(s)} = 0.0598$ remain near the zero-β limit of $\alpha = 0$. From an error-analysis viewpoint, however, a linear mesh is not sufficient to guarantee, as in the two previous examples, proper convergence. The mesh is thus rescaled according to $\psi^{(\nu)} \sim \pm|t^{(\nu)} - t_i|^{\gamma_i}$ about ψ_i $[t^{(\nu)} \equiv (\nu - 1)/(M - 1)]$, $i = 1, 2$, with γ_i given by (7.49). In this particular case we adopted $\gamma_1 = \gamma_2 = 1.8$ to recover the M^{-2} convergence for all elements of the

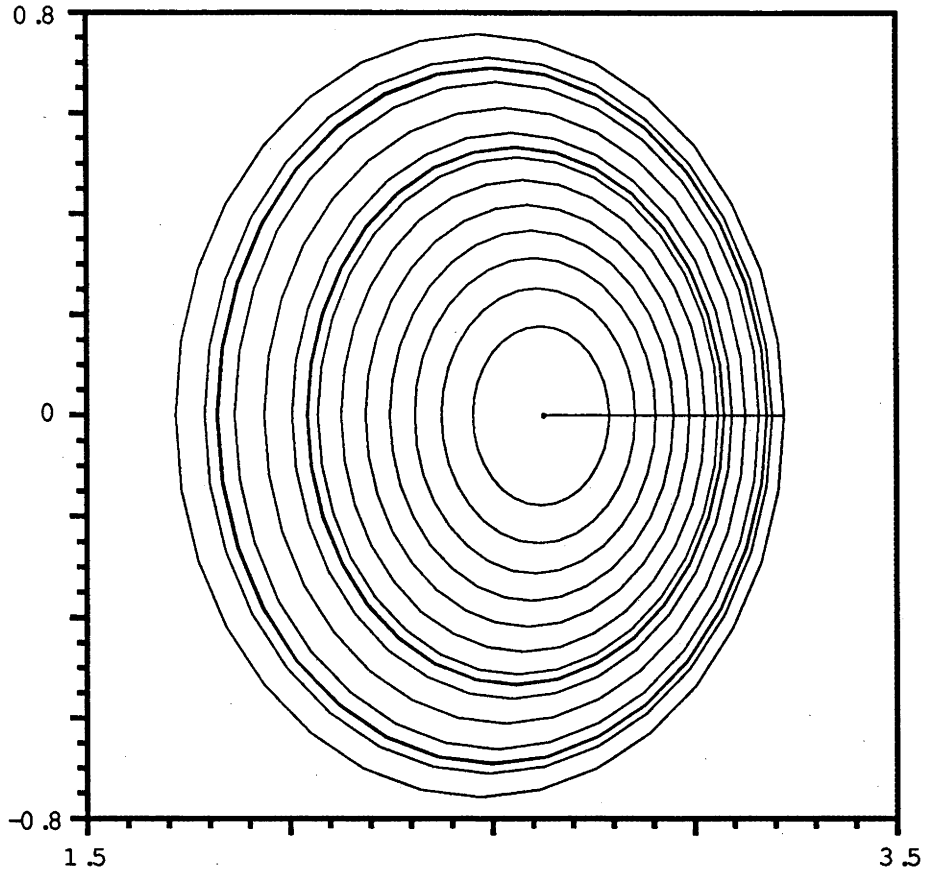

Figure 8.22: Flux surfaces of the double-tearing, finite-β equilibrium.

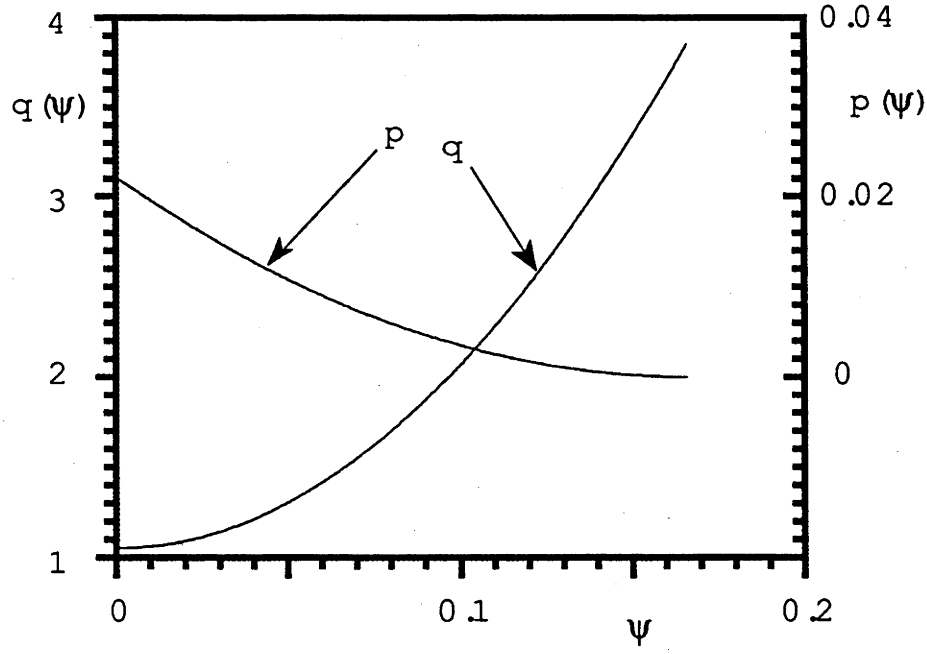

Figure 8.23: Safety-factor and pressure profiles of the double-tearing, finite-β equilibrium.

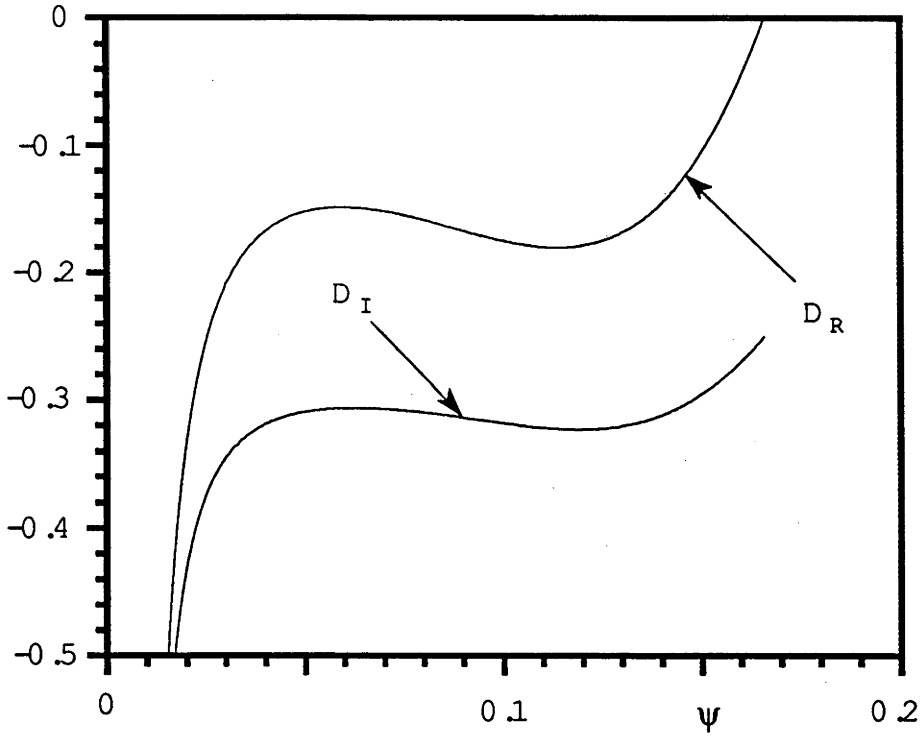

Figure 8.24: Mercier D_I and and resistive D_R profiles of the double-tearing, finite-β equilibrium.

matching matrix. The asymptotic matching data, as $M \to \infty$, are summarized as follows:

$$\left(D'_{ip,jq}\right) \approx \tfrac{1}{2} \begin{pmatrix} -548.1 & 25.7 & 50.4 & 10.4 \\ 26.9 & 656.5 & -26.2 & -80.90 \\ 50.4 & -25.07 & -47.3 & -11.3 \\ 10.9 & -80.90 & -11.8 & -135.2 \end{pmatrix} \tag{8.7}$$

with the first two rows yielding the response coefficients A''s and B''s to even prescribed solution, and the bottom rows given by the Γ''s and Δ''s [see (6.12)].

Another major distinction arising between this case and the zero-β equilibria treated in §§ 8.2 and § 8.3, is due to the regular solutions which were previously absorbed in the small solutions. The regular solutions affect more radically the continuous part of the response than the discontinuous part. That is where the limit of Δ'_{ij}, for instance, is well-defined as $\beta \to 0$ whereas Γ'_{ij} blows up in the same limit [Wilson (1990)], thus calling for the renormalization of the big solution in § 5.5. This effect is noticeable in Fig. 8.25 with the values $\Delta'_{1,1}$ and $\Delta'_{2,2}$ coinciding with those of (8.7). In the same way, $B'_{1,1}$ and $B'_{2,2}$ of Fig. 8.26 are in agreement

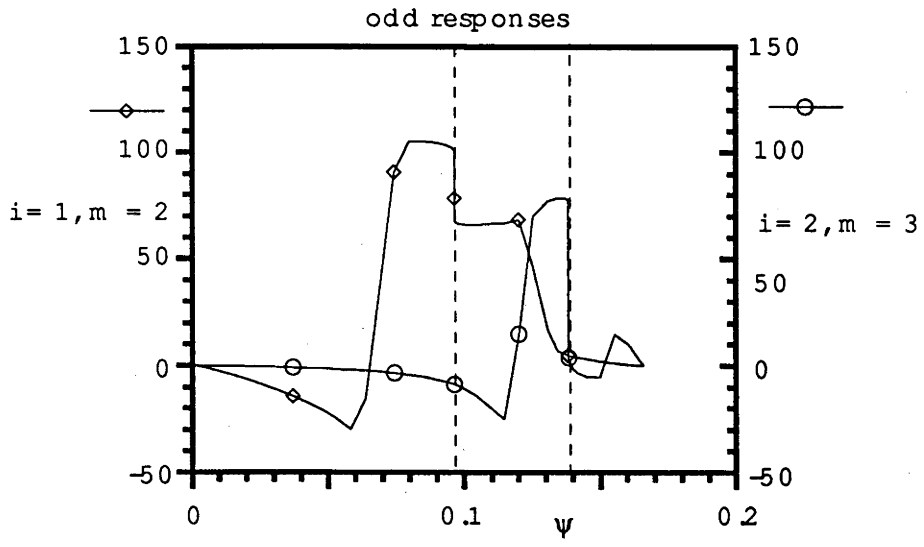

Figure 8.25: Resonant Fourier-modes of the odd-parity responses $\check{\xi}_{(1,-)}$ and $\check{\xi}_{(2,-)}$ for the double-tearing, finite-β equilibrium.

with the corresponding values shown in (8.7).

The violation of the reciprocity relation prevailing between the A''s and Δ''s [see (6.56)] in the cylindrical case, can also be observed in (8.7). One consequence of this, is the removal of the degeneracy previously existing between two eigenvalues of the dispersion relation (6.17). From (8.7), one finds the following set of eigenvalues

$$\left.\begin{aligned} \lambda_{1+} &\approx -554 \\ \lambda_{2+} &\approx 666 \\ \lambda_{1-} &\approx -37.5 \\ \lambda_{2-} &\approx -144 \end{aligned}\right\} \tag{8.8}$$

indicating the equilibrium is tearing stable whereas the positive eigenvalue indicates resistive-interchange instability at ψ_2. Note furthermore that, since we chose $s_\pm = 0$ in the definition of the big solution (see § 6.6), the interchange eigenvalues λ_{i+}, $i = 1$, 2, are roughly one order of magnitude smaller than their tearing counterparts λ_{i-}, this is characteristic of $\mu_i \approx 1/2$.

With the exception of the rescaling of the mesh near ψ_1 and ψ_2, finite-β cases are treated with the same ease as the zero-β case of the preceding sections. Maximum convergence should be achieved for all equilibria, but those for which the (ideal) energy norm is not positive-definite (global ideal instability). In such a situation, the convergence study in § 7.4 does not apply. It is nevertheless indicative of the close

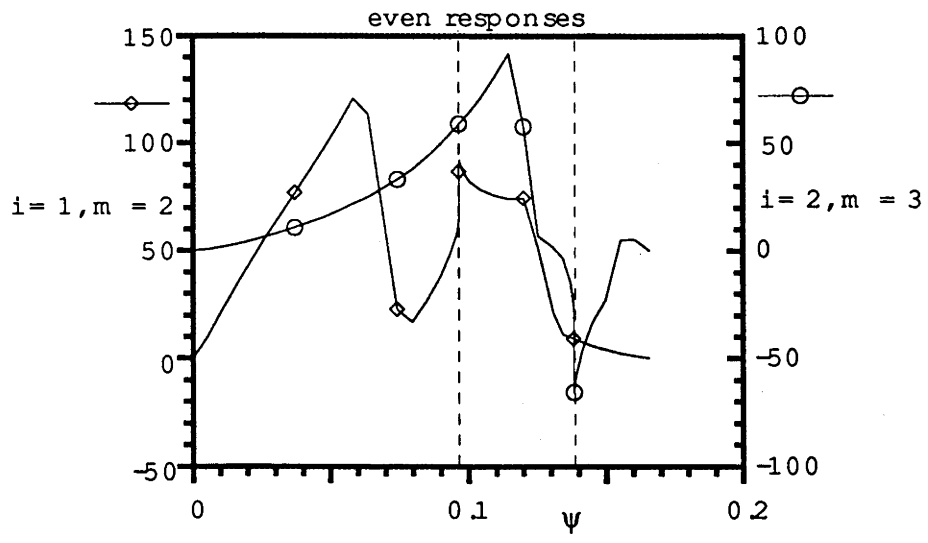

Figure 8.26: Resonant Fourier-modes of the even-parity responses $\tilde{\xi}_{(1,+)}$ and $\tilde{\xi}_{(2,+)}$ for the double-tearing, finite-β equilibrium.

connection existing between the numerical scheme and the ideal stability criterion. In that respect we may regard the symmetrized expression for the concomitant jump (6.41) as a generalization of the ideal potential energy [Chu *et al.* (1992)].

Summary

We have adopteded two approaches to investigate the stability of resistive modes in fusion plasmas. In the first part of this thesis, we are concerned with the symmetries of the equations governing the linear motion of a plasma from equilibrium, which are best exhibited by using the Lagrangian formalism. For all systems, dissipative and non-dissipative, one can define a Hamiltonian which is a bilinear functional involving the solutions and the adjoint solutions. Provided the Lagrangian depends only on time through the variables and their adjoint (time invariance), the Hamiltonian is conserved for dissipative and non-dissipative systems alike. The energy functional derives from a symmetric form of the Hamiltonian. The condition of existence of an energy principle is that the time derivative of the energy integral be a Lyapunov functional, that is a definite functional. If this is the case, we obtain a necessary and sufficient stability criterion based on the definiteness of the energy integral. For the subclass of dissipative systems for which the time derivative of the energy integral is negative-definite, the criterion for stability is that the energy be positive-definite.

The difficulty of applying the enounciated energy principle lies in the fact that most systems do not exhibit explicitly the definiteness of the time derivative of the energy, except under restricted conditions. These include considering purely growing modes only. Provided this assumption is satisfied, Tasso's [Tasso (1990)] criterion can be shown, by applying Lyapunov's stability theorem on the resistive energy integral, to be necessary in addition to sufficient. The formalism also allows straightforward derivation of the resistive interchange stability criterion in cylindrical geometry, while being unable to extract a simple criterion in the toroidal equations of Glasser *et al.* (1975) because of the lack of symmetry exhibited by these equations.

The energy intergal is, however, not the only choice of Lyapunov functional. We show in Ch. 3 how to recover the monotonic dependence in the (real) growth rate of the jump in Δ' occurring in the constant-Ψ approximation, by using a functional which possesses the units of an action density. The generalization of this expression to the finite-β case remains at present unclear.

The coefficient Δ', can be thought of as a particular element forming the matching-data matrix which contains all the information required to match the resistive solutions with the corresponding solution in the outer region. In the zero-β case, the sign of Δ' yields a sufficient criterion ensuring stability in the toroidal case [Chu *et al.* (1992)], and a necessary and sufficient criterion in the cylindrical case. Therefore, the task of computing stability reduces to the one of determining the outer matching-data in this case.

Next, the concept of matching data is generalized in Ch. 6 to finite-β plasmas, defining these as the the ratio of the small-solution coefficients to the big-solution amplitude [Manickam *et al.* (1983)]. The outer matching-data form a complete set allowing for the matching of resistive with outer solutions [Connor *et al.* (1988)]. The big solutions arise at the rational surfaces where they present a non-square integrable singularity. The small solutions, on the other hand exhibit only a weakly, square-integrable singular behaviour, being therefore suitable for extraction by means of a finite-element scheme, for instance. For sake of generality, we do not assume the big and small solutions to have a given parity. In the finite-β case, asymptotic solutions may present in general a combination of the tearing [Connor *et al.* (1991a)] and the ballooning (interchange) parity [Connor & Hastie (1991b)].

The crucial step for the accurate determination of the outer-matching data consists in capturing analytically the big solution to appropriate accuracy, and then compute the left-out contribution whose behaviour is dominated by the small solution. The outer matching data, then play the role of response coefficients to normalized, prescribed big solution. The determinant factor permitting accurate outer matching-data is the variational principle derived in Ch. 6, which guarantees good convergence as the number of mesh nodes increases for both the zero-β and

the finite-β cases.

The variational method, as presented, applies to cylindrical and toroidal geometry only. It is interesting to specule about extending the scheme to three-dimensional plasmas, where the rational surfaces densely fill the plasma volume. However, numerical truncation in Fourier space will still give a finite number of rational surfaces. We do therefore expect the present algorithm to apply for the three-dimensional case, provided also a similar equation to the GNE is available.

Bibliography

Adler, A. E., Kulsrud, R. M., and White, R. B. (1980). *Phys. Fluids* **23**, 1375–1379.

Appert, K., Gruber, R., and Vaclavik, J. (1974). *Phys. Fluids* **17**, 1471–1472.

Bateman, G. (1978). 'MHD Instabilities' The MIT Press.

Bernstein, I. B., Frieman, E. A., Kruskal, M. D., and Kulsrud, R. M. (1958). *Proc. Roy. Soc.* **A244**, 17–44.

Bineau, M. (1962). *Nucl. Fusion* **2**, 130–147.

Bondeson, A. and Sobel, J. R. (1984). *Phys. Fluids* **27**, 2028–2034.

Chu, M. S., Chance, M. S., Greene, J. M., and Jensen, T. H. (1990a). *Phys. Fluids B* **2**, 97–105.

Chu, M. S., Dewar, R. L., Greene, J. M., and Pletzer, A. (1992). Submitted to *Phys. Fluids B* GA-A20622 General Atomics San Diego CA 92186-9784 USA.

Chu, M. S., Greene, J. M., Klasky, M., and Chance, M. S. (1990b) *Report* GA-A20135 General Atomics.

Connor, J. W., Cowley, S. C., Hastie, R. J., Hender, T. C., Hood, A., and Martin, T. J. (1988). *Phys. Fluids* **31**, 577–590.

Connor, J. W., Hastie, R. J., and Taylor, J. B. (1991a). *Phys. Fluids B* **3**, 1532–1537.

Connor, J. W., Hastie, R. J., and Taylor, J. B. (1991b). *Phys. Fluids B* **3**, 1539–1545.

Coppi, B., Greene, J. M., and Johnson, J. L. (1966). *Nucl. Fusion* **6**, 101–117.

Dewar, R. L. and Glasser, A. H. (1983). *Phys. Fluids* **26**, 3038–3052.

Dewar, R. L. and Grimm, R. C. (1984). *In* 'Computational Techniques and Applications: CTAC-83' (Eds. Noye, B. and Fletcher, C.), p. 730.

Dewar, R. L., Monticello, D. A., and Sy, W. N.-C. (1984). *Phys. Fluids* **27**, 1723–1732.

Dewar, R. L. and Pletzer, A. (1990). *J. Plasma Phys.* **43**, 291–310.

Dobrott, D., Prager, S. C., and Taylor, J. B. (1977). *Phys. Fluids* **20**, 1850–1854.

Fonda, L. and Ghirardi, G. C. (1970). 'Symmetry Principles in Quantum Physics' Marcel Dekker Inc.

Freidberg, J. P. (1987). 'Ideal Magnetohydrodynamics' Plenum.

Furth, H. P., Killeen, J., and Rosenbluth, M. N. (1963). *Phys. Fluids* **6**, 459–484.

Furth, H. P., Rutherford, P. H., and Selberg, H. (1973). *Phys. Fluids* **16**, 1054–1063.

Gel'fand, I. M. and Shilov, G. E. (1964). 'Generalized Functions' Academic.

Glasser, A. H., Greene, J. M., and Johnson, J. L. (1975). *Phys. Fluids* **18**, 875–888.

Glasser, A. H., Jardin, C. C., and Tesauro, G. (1984). *Phys. Fluids* **27**, 1225–1242.

Gradshteyn, I. S. and Ryzhik, I. M. (1980). 'Table of Integrals, Series and Products' Academic Press.

Greene, J. M. (1976). *Set of lectures presented at the EPFL* LRP 114/76.

Greene, J. M. (1992). Private communication.

Grimm, R. C., Dewar, R. L., and Manickam, J. (1983). *J. Comp. Phys.* **49**, 94–117.

Iacono, R. and Bhattacharjee, A. (1992). Private communication.

Ince, E. (1956). 'Ordinary Differential Equations' Dover.

Itzykson, C. and Zuber, J.-P. (1980). 'Quantum Field Theory' McGraw-Hill.

Johnson, J., Greene, J., and Coppi, B. (1963). *Phys. Fluids* **6**, 1169–1184.

Kerkovian, J. and Cole, J. (1981). 'Perturbations Methods in Applied Mathematics' Springer.

Kull, H., Berk, H., and Morrison, P. (1989). *Phys. Fluids B* **1**, 55–61.

Manickam, J., Grimm, R. C., and Dewar, R. (1983). *In* 'Energy Modelling and Simulation' (Eds. A. S. Kydes et al.) North-Holland, pp. 355–359.

Miller, A. and Dewar, R. (1986). *J. Comput. Phys.* **66**, 356–390.

Morse, P. and Feshbach, H. (1953). 'Methods of Theoretical Physics' International Series in Pure and Applied Physics.

Morton, K. W. (1987). 'Finite Elements in Physics'. Ed. R. Gruber.

Newcomb, W. A. (1960). *Ann. Phys.* **10**, 232–267.

Parker, R. D., Bondeson, A., and Hugon, M. (1990). *In* 'Papers contributed to the 17th EPS Conference on Controlled Fusion and Plasma Heating'.

Parker, R. D., Dewar, R. L., and Johnson, J. L. (1989). *Phys. Fluids B* **2**, 508–515.

Pletzer, A. and Dewar, R. L. (1991). *J. Plasma Phys.* **45**, 427–451.

Rosenau, P. (1983). *Phys. Fluids* **26**, 2578–2589.

Saaty, T. L and Bram, J. (1964). 'Nonlinear Mathematics' Dover.

Spitzer, L. (1962). 'Physics of Fully Ionized Gases' John Wiley (Interscience).

Strauss, H. R. (1976). *Phys. Fluids* **19**, 134-140.

Suydam, B. R. (1958). *In* 'IAEA Geneva Conf.' pp. 157–159.

Tasso, H. (1983). *Phys. Lett.* **94 A**, 217–218.

Tasso, H. (1990). *Physics Letters* **147**, 28-30.

Wesson, J. A. (1991). *Report* JET-P(91)39.

White, R. B. (1986). *Rev. Modern Physics* **58**, 183-207.

Wilson, H. R. (1990). *Plasma Phys. and Controlled Fusion* **32**, 443-458.

Appendix A

Euler-Lagrange equations

In this appendix, intermediate steps for the derivation of (2.39) are presented. To do so the Lagrangian density (3.1) must be rewritten in a form including only inner products of $\boldsymbol{\xi}^+$, $\mathbf{a}^+$, $\nabla\boldsymbol{\xi}^+$ and $\nabla\mathbf{a}^+$ [or inner products of $\boldsymbol{\xi}$, $\mathbf{a}$, $\nabla\boldsymbol{\xi}$ and $\nabla\mathbf{a}$ to derive (2.40)]. For instance, we write $\mathbf{Q} = \nabla\times(\boldsymbol{\xi}\times\mathbf{B})$ as $\mathbf{B}\cdot(\nabla\boldsymbol{\xi}) - \mathsf{I}:(\nabla\boldsymbol{\xi})\mathbf{B} - \boldsymbol{\xi}\cdot(\nabla\mathbf{B})$, where I is the identity tensor: $\mathsf{I}\cdot\mathbf{f} = \mathbf{f}$. Using the standard Gibb's notation, we write

$$\nabla\times\mathbf{f} = \sum_i \nabla\times\mathbf{e}_i\mathbf{e}_i\cdot\mathbf{f} \equiv \nabla\times\mathsf{I}\cdot\mathbf{f}, \tag{A.1}$$

where $\mathbf{f}$ is any vector and $\{\mathbf{e}_i\}$ is an orthonormal basis so that $\mathsf{I} = \sum_i \mathbf{e}_i\mathbf{e}_i$. To express $\nabla\times\mathbf{f}$ in terms of $\nabla\mathbf{f}$, we introduce the triadic $\mathbf{e}$ whose elements: $e_{ijk} = +1$ if $i,j,k \in \{1,2,3\}$ are cyclic, $e_{jik} = e_{ikj} = e_{kji} = -1$, or $e_{iik} = e_{iji} = e_{ijj} = 0$ otherwise. Equation (A.1) becomes

$$\nabla\times\mathbf{f} = \mathbf{e}:\nabla\mathbf{f} \equiv \sum_i\sum_j\sum_k e_{ijk}\partial_j(\mathbf{f}\cdot\mathbf{e}_k)\mathbf{e}_i, \tag{A.2}$$

allowing us to write (3.1) as

$$\begin{aligned} L \;=\; \tfrac{1}{2}\Big\{ & \rho\dot{\boldsymbol{\xi}}^+\cdot\dot{\boldsymbol{\xi}} \\ & - [\mathbf{B}\cdot(\nabla\boldsymbol{\xi}^+) - \mathsf{I}:(\nabla\boldsymbol{\xi}^+)\mathbf{B} - \boldsymbol{\xi}^+\cdot(\nabla\mathbf{B}) + \boldsymbol{\xi}^+\cdot\mathbf{n}\mathbf{j}\times\mathbf{n}]\cdot(\mathbf{Q} + \xi_n\mathbf{j}\times\mathbf{n}) \\ & - \mathsf{I}:(\nabla\boldsymbol{\xi}^+)\Gamma p\nabla\cdot\boldsymbol{\xi} + 2U\boldsymbol{\xi}^+\cdot(\nabla\psi)\xi \\ & - \mathbf{e}:(\nabla\mathbf{a}^+)\cdot\nabla\times\mathbf{a} + \frac{1}{2\eta}\left(\dot{\mathbf{a}}^+\cdot\mathbf{a} - \mathbf{a}^+\cdot\dot{\mathbf{a}}\right) \\ & - [\mathbf{B}\cdot(\nabla\boldsymbol{\xi}^+) - \mathsf{I}:(\nabla\boldsymbol{\xi}^+)\mathbf{B} - \boldsymbol{\xi}^+\cdot(\nabla\mathbf{B})]\cdot\nabla\times\mathbf{a} \\ & - \mathbf{e}:(\nabla\mathbf{a}^+)\cdot\mathbf{Q} + \boldsymbol{\xi}^+\cdot\mathbf{j}\times(\nabla\times\mathbf{a})\Big\} \end{aligned} \tag{A.3}$$

so that

$$\begin{aligned}\frac{\partial L}{\partial \nabla \boldsymbol{\xi}^{+}} &= \tfrac{1}{2}\{\mathbf{B}\cdot(\mathbf{Q}+\xi_n\mathbf{j}\times\mathbf{n})\,\mathsf{I} - \mathbf{B}(\mathbf{Q}+\xi_n\mathbf{j}\times\mathbf{n}) - \mathsf{I}\,\Gamma p\nabla\cdot\boldsymbol{\xi} \\ &\quad + \mathsf{I}\,\mathbf{B}\cdot\nabla\times\mathbf{a} - \mathbf{B}\nabla\times\mathbf{a}\} \\ \frac{\partial L}{\partial \nabla \mathbf{a}^{+}} &= -\tfrac{1}{2}\mathbf{e}\cdot(\nabla\times\mathbf{a}+\mathbf{Q}) \end{aligned} \tag{A.4}$$

and

$$\begin{aligned}-\frac{\partial L}{\partial \boldsymbol{\xi}^{+}} &= \tfrac{1}{2}\{-(\nabla\mathbf{B})\cdot(\mathbf{Q}+\xi_n\mathbf{j}\times\mathbf{n}) + \mathbf{n}\mathbf{j}\times\mathbf{n}\cdot(\mathbf{Q}+\xi_n\mathbf{j}\times\mathbf{n}) \\ &\quad -2U\nabla\psi\xi - \mathbf{j}\times\nabla\times\mathbf{a} - (\nabla\mathbf{B})\cdot\nabla\times\mathbf{a}\} \\ -\frac{\partial L}{\partial \mathbf{a}^{+}} &= \frac{1}{4\eta}\dot{\mathbf{a}}. \end{aligned} \tag{A.5}$$

The divergence of (A.4) is taken using $\nabla\cdot(\mathbf{B}\cdot\mathbf{Q}\,\mathsf{I}) = (\nabla\mathbf{B})\cdot\mathbf{Q} + (\nabla\mathbf{Q})\cdot\mathbf{B}$, yielding (2.39).

Appendix B

Generalized functions x_L^α, x_R^α, x_+^α and x_-^α

We present here some results of the theory of generalized functions [Gel'fand & Shilov (1964)], focusing in particular on the "regularization" of $|x|^\alpha$, with special emphasis on α negative and non-integer.

Let us introduce the generalized function which satisfies pointwise for $x \neq 0$,

$$x_L^\alpha \equiv \begin{cases} |x|^\alpha & \text{for} \quad x < 0 \\ 0 & \text{for} \quad x > 0 \end{cases}, \tag{B.1}$$

that is x_L^α is confined to negative x, with α being any complex number. Similarly one defines x_R^α such that $x_R^\alpha = 0$ for $x \leq 0$ and x^α for $x > 0$. From (B.1) one has,

$$\int_{-\infty}^{\infty} dx \phi^* x_L^\alpha = \int_{-\infty}^{0} dx \phi^* |x|^\alpha \tag{B.2}$$

which is a convergent integral provided $\mathrm{Re}\{\alpha\} > -1$ and assuming that ϕ is a "well-behaved" test-function which vanishes faster than any power $|x|^\beta$ as $x \to \pm\infty$ so that ϕ is also a suitable test-function for (ϕ, x_R^α) to exist for $\mathrm{Re}\{\alpha\} > -1$. Expression (B.2) can be continued analytically beyond $\mathrm{Re}\{\alpha\} > -1$ using

$$\begin{aligned} (\phi, x_L^\alpha) &= -\frac{1}{\alpha+1}\left(\phi', x_L^{\alpha+1}\right); \ \mathrm{Re}\{\alpha\} > -2 \\ &\vdots \\ &= (-1)^k \frac{\Gamma(\alpha+1)}{\Gamma(\alpha+k+1)}\left(\phi^{(k)}, x_L^{\alpha+k}\right); \ \mathrm{Re}\{\alpha\} > -1-k \end{aligned} \tag{B.3}$$

to the bands $-1 < \mathrm{Re}\{\alpha\} < -2, \cdots, -k < \mathrm{Re}\{\alpha\} < -1-k$ respectively, by applying the differentiation rules of generalized functions: e.g,

$$(\phi, f') = -(\phi', f). \tag{B.4}$$

Gel'fand & Shilov (1964) adopt (B.3) as the *definition* of (ϕ, x_L^α) for $\mathrm{Re}\{\alpha\} < -1$, which constitutes the definition of x_L^α as a canonically regularized generalized function. Procedure (B.3), which can also be applied to x_R^α, is appropriate for values of α which are *non-integer*, for $\Gamma(\alpha+1)$ has poles at $\alpha = -1, -2, \cdots$.

The problem one faces now is to attach a definition to (ϕ, x_L^α) such that (B.3) hold and be convergent for any well-behaved ϕ: ϕ is continuous in value and continuous in derivatives up to $\phi^{(k-1)}$, and such that $(\phi, x_{L,R}^\alpha)$ is given by (B.2) for $\mathrm{Re}\{\alpha\} > -1$. This is called *regularization* and is denoted symbolically by

$$\left(\phi, x_{L,R}^\alpha\right) \equiv \text{r.g.} \int_{-\infty}^{\infty} dx \phi^* x_{L,R}^\alpha. \tag{B.5}$$

In view of (B.2), the integral converges only when the term complementary to $|x|^\alpha$ in the integrand vanishes, as $x \to 0$, at least at the rate of $|x|^k$, $-k < \mathrm{Re}\{\alpha\} < -1-k$. This leads to the regularization:

$$\text{r.g. } \phi(x) \equiv \phi(x) - \phi(0) - x\phi'(0) - \cdots - \frac{x^{k-1}}{(k-1)!}\phi^{(k-1)}(0) \tag{B.6}$$

of ϕ in the finite neighbourhood $x \approx 0$. Each term following $\phi(x)$ in (B.6) contributes to a pole of residue $-(-1)^m \delta^{(m)}(x)/m!$, $m = 0, 1, \cdots k-1$, in (B.5). However, by forming the generalized functions

$$\left.\begin{aligned} x_+^\alpha &\equiv x_R^\alpha + x_L^\alpha \\ x_-^\alpha &\equiv x_R^\alpha - x_L^\alpha \end{aligned}\right\}, \tag{B.7}$$

of even and odd parity respectively [the parity p, $p \in \{+,-\}$, of x_p^α is defined by $(\phi, x_p^\alpha) = 0$ if the parity of ϕ is $-p$: $\phi(x) = -p\phi(-x)$], it is then found that x_+^α has poles at $\alpha = -1, -3, \cdots$ only, whereas the poles of x_-^α are located at $\alpha = -2, -4, \cdots$. Thus the odd distribution x_-^{2m+1} is well-defined for all m, $m = \cdots -1, 0, +1, \cdots$. This is of course the result of having x to any odd-integer being an odd function, usually simply denoted by x^{2m+1}. This remark also applies to x_+^{2m} which is defined for all m, and possesses the even parity as x^{2m} is even.

It is worthwile to point out that, since this formalism is valid for smooth test-functions only, it is therefore not applicable to the problem of regularizing functionals which are quadratic in the singular functions x^{α}.

Appendix C

Frobenius expansion in cylindrical geometry

To familiarize the reader with the Frobenius method, we derive the power expansion for solutions of (4.61) near a singularity occurring where $\mathcal{D}_\theta$ of (4.57) vanishes, that is where the safety factor

$$q_i \equiv \left.\frac{rB_z}{RB_\theta}\right|_{r=r_i} = \frac{m}{n} \tag{C.1}$$

is rational, as in (5.5). We expand

$$f(r) = \sum_{k=0}^{\infty} f_k (r - r_i)^{k+2} \tag{C.2}$$

and

$$g(r) = \sum_{k=0}^{\infty} g_k (r - r_i)^{k} \tag{C.3}$$

so that $f \sim f_0(r-r_i)^2$ and $g \sim g_0$ as $r \to r_i$, in agreement with (4.62) and (4.63). In the zero-β case, one finds that $g_0 = 0$ and $g_1 \neq 0$, [Dewar & Pletzer (1990)], but as we are mainly concerned with the more general, finite-pressure gradient case. Let us assume for the moment that $g_0 \neq 0$. We also restrict ourselves to cases where Eqs.(5.34) are satisfied by requiring $f_0 \neq 0$. Seeking solutions of (4.61) by assuming that the solutions can be expanded in Frobenius series around r_i,

$$\xi(r) = (r - r_i)^\alpha \sum_{k=0}^{\infty} a_k (r - r_i)^k, \tag{C.4}$$

with α being a real number. Accordingly to the rules set in Appendix B; if α is non-integer, x^α is not uniquely defined so that we shall mean either the even x_+^α or

the odd x_-^α generalized function (alternatively we could of course also choose the left-sided x_L^α and right-sided x_R^α representation).

At the lowest order, $k = 0$, Eqs.(C.2), (C.3) and (C.4) lead to the indicial equation $\alpha(\alpha+1)f_0 - g_0 = 0$ whose two roots are

$$\begin{aligned} \alpha^{(s)} &\equiv -\tfrac{1}{2} + \mu, \\ \alpha^{(b)} &\equiv -\tfrac{1}{2} - \mu, \end{aligned} \tag{C.5}$$

where [Dewar & Pletzer (1990)]

$$\mu \equiv \sqrt{\frac{1}{4} + \frac{g_0}{f_0}} \equiv \sqrt{-D_I}. \tag{C.6}$$

Here D_I is the Mercier function of Glasser *et al.* (1975). The plasma is assumed to be stable towards ideal modes, that is $D_I < 0$, so that μ is positive and real. Although μ is usually $< 1/2$ for a cylindrical plasma, we do not restrict ourselves here to this case as we consider cylindrical plasma with hollow pressure-profiles in Ch. 8. The superscript (b) refers to the big solution in the limit $r \to r_i$, while the superscript (s) refers to the small solution in this limit, the corresponding solutions (C.4) being denoted by $\xi^{(b)}$ and $\xi^{(s)}$.

We adopt the normalization

$$a_0^{(s)} = a_0^{(b)} = 1 \tag{C.7}$$

which is consistent with (5.13). Higher-order Frobenius-coefficients

$$a_k^{(s)} = \sum_{k'=0}^{k-1} \frac{g_{k-k'} - (\alpha^{(s)}+k+1)(\alpha^{(s)}+k')f_{k-k'}}{f_0 k(k+2\mu)} a_{k'}^{(s)}, \tag{C.8}$$

$k = 1, 2\ldots$, for the small solution expansion, and

$$a_k^{(b)} = \sum_{k'=0}^{k-1} \frac{g_{k-k'} - (\alpha^{(b)}+k+1)(\alpha^{(b)}+k')f_{k-k'}}{f_0 k(k-2\mu)} a_{k'}^{(b)}, \tag{C.9}$$

$k = 1, 2\ldots$, for the big solution expansion, are obtained by inserting Eqs.(C.2), (C.3) and (C.4) into (4.61) and equating coefficients at each order to zero.

The problems encountered in § 5.2 when $2\mu = k$ are most apparent in the cylindrical case; one can see that the denominator in (C.9) vanishes for some a_k whenever μ is half-integer. As in § 5.5, this situation is very important for it includes

the case of zero pressure-gradient $[p'(r_i) = 0]$ since $g_0 \to 0$ and $\mu \to \frac{1}{2}$ in this limit. In this case, all the $a_k^{(b)}$ for $k > 0$ will diverge as $(1-2\mu)^{-1}$ and become linearly dependent to the $a_{k-1}^{(s)}$'s at this order in $(1-2\mu)^{-1}$. It is then imperative to redefine the big solution using the prescription of (5.39)

$$\xi_p^{(b)} \mapsto \xi_p^{(b)} - s_+(\mu)\xi_p^{(s)} - s_-(\mu)\xi_{-p}^{(s)}, \tag{C.10}$$

where $p = +, -$ (or L, R), and $s_\pm$ are defined at half-integer and integer μ so as to subtract off the divergent part of the big solution, with the interpolation between these values of μ being somewhat arbitrary [Miller & Dewar (1986)]. Note that we must set $s_+ = 0$ when $\mu = 1/2,\ 3/2,\ 5/2,\ \cdots$, while s_- vanishes for $\mu = 1,\ 2,\ 3,\ \cdots$ since in the former case the divergent part has opposite parity to the big solution, while in the latter case it has the same parity.

For μ around $\frac{1}{2}$ we may take $s_+ \equiv 0$ and

$$s_-(\mu) \equiv \frac{f_1 + g_1}{f_0(1-2\mu)}, \tag{C.11}$$

In the limit $\mu \to \frac{1}{2}$ the new big solution becomes

$$\xi_\pm^{(b^*)} = (r - r_i)_\pm^{-1} + \mathcal{O}(r - r_i) + \frac{f_1 + g_1}{f_0}\left(1 + \mathcal{O}(r - r_i)\right) \ln_\mp |r - r_i| \tag{C.12}$$

as $r \to r_i$, where $\ln_+(x)$, denotes the even function $\ln|x|$, whereas $\ln_-(x)$ denotes the odd function $\mathrm{sgn}x\ \ln|x|$. These logarithmic terms come from expanding the identity $x^\epsilon = \exp(\epsilon \ln x)$ to first order in ϵ, where here ϵ is $\pm(\mu - \frac{1}{2})$. We thus recover the usual zero-β solution without having to treat it as a special case necessitating a different *ansatz*, at the expense of using a different definition for the big solution.

Appendix D

Concomitant between big and regular solution

We show in this appendix that the contribution in the concomitant jump (7.13) arising between the big-solution component of $\hat{\mathsf{y}}$ and the regular component of $\check{\mathsf{y}}$ vanishes at all orders of $(x - x_i)$ in the expansion

$$P[\mathsf{y}^{(b)}; \mathsf{y}^{(r)}] = (x - x_i)^{\alpha^{(b)}} \left[P_0 + (x - x_i)P_1 + (x - x_i)^2 P_2 + \cdots\right] \tag{D.1}$$

because the coefficients P_n vanish. Writing (D.1) as

$$P[\mathsf{y}^{(b)}; \mathsf{y}^{(r)}] = < \mathsf{y}^{(b)}, \boldsymbol{\sigma}\mathcal{D}_\theta \mathsf{y}^{(r)} >, \tag{D.2}$$

we immediately find that

$$P_0 = < \mathsf{y}_0^{(b)}, \boldsymbol{\sigma}\mathcal{D}_i \mathsf{y}_0^{(r)} > = 0 \tag{D.3}$$

since $\mathcal{D}_i \mathsf{y}_0^{(b)} = 0$ in virtue of (5.8), with $\mathsf{y}_0^{(b)}$ representing the lowest-order coefficient of the big expansion (5.7). For the purpose of this appendix, it is convenient to multiply (4.54) by the Pauli matrix (7.14), define $\mathsf{B} \equiv \boldsymbol{\sigma}\mathsf{A}$ and expand the quasi-Hamiltonian set of equations in Frobenius terms

$$\left.\begin{aligned} -inq_i'\boldsymbol{\sigma}\alpha_i^{(b)}\mathsf{y}_0^{(b)} + \boldsymbol{\sigma}\mathcal{D}_i(\alpha_i^{(b)} + 1)\mathsf{y}_1^{(b)} &= \mathsf{B}_i\mathsf{y}_0^{(b)} \\ -\tfrac{1}{2}inq_i''\boldsymbol{\sigma}\alpha_i^{(b)}\mathsf{y}_0^{(b)} - inq_i'\boldsymbol{\sigma}(\alpha_i^{(b)} + 1)\mathsf{y}_1^{(b)} + \boldsymbol{\sigma}\mathcal{D}_i(\alpha_i^{(b)} + 2)\mathsf{y}_2^{(b)} &= \mathsf{B}_i'\mathsf{y}_0^{(b)} + \mathsf{B}_i\mathsf{y}_1^{(b)} \\ &\vdots \end{aligned}\right\} \tag{D.4}$$

as done in § 5.2, with $\mathsf{B} = \mathsf{B}_i + (x - x_i)\mathsf{B}_i' + \cdots$. A similar set of equations to (D.4) is found for the regular solution by setting $\alpha = 0$.

To next order in (D.1)

$$\begin{aligned} P_1 &= -inq_i' < \mathsf{y}_0^{(b)}, \boldsymbol{\sigma}\mathsf{y}_0^{(r)} > \; + < \mathsf{y}_1^{(b)}, \boldsymbol{\sigma}\mathcal{D}_i\mathsf{y}_0^{(r)} > \\ &= -\frac{1}{\alpha_i^{(b)} + 1} < [\mathsf{B}_i - inq_i'\boldsymbol{\sigma}]\mathsf{y}_0^{(b)}, \mathsf{y}_0^{(r)} > \end{aligned} \tag{D.5}$$

vanishes ($\alpha_i^{(b)} \neq -1$), for we have

$$\mathsf{B}^\dagger = \mathsf{B} - inq_i'\boldsymbol{\sigma} \tag{D.6}$$

and $\mathsf{B}_i\mathsf{y}_0^{(r)} = \boldsymbol{\sigma}\mathcal{D}_i\mathsf{y}_1^{(r)}$ from (D.4). [It is well-known that for the particular case $\alpha_i^{(b)} = -1$ (D.1) does not vanish as the small and regular solutions degenerate.] In fact, we find after some manipulations involving (D.4) that

$$\begin{aligned} P_2 &= -\frac{1}{(\alpha_i^{(b)} + 1)(\alpha_i^{(b)} + 2)} \Big\{ < \mathsf{y}_0^{(b)}, (\alpha_i^{(b)} + 1)\mathsf{B}_i'\mathsf{y}_0^{(r)} + (\alpha_i^{(b)} + 2)\mathsf{B}_i\mathsf{y}_1^{(r)} > \\ &\quad + (\alpha_i^{(b)} + 1) \; < \mathsf{y}_1^{(b)}, \mathsf{B}_i\mathsf{y}_0^{(r)} > \Big\} \\ &= -\frac{1}{(\alpha_i^{(b)} + 1)(\alpha_i^{(b)} + 2)} \Big\{ -inq_i'(\alpha_i^{(b)} + 1) \; < \mathsf{y}_0^{(b)}, \boldsymbol{\sigma}\mathsf{y}_1^{(r)} > \; + \; < \mathsf{y}_0^{(b)}, \mathsf{B}_i\mathsf{y}_0^{(r)} > \\ &\quad - \; < \mathsf{B}_i^\dagger\mathsf{y}_0^{(b)} + inq_i'\boldsymbol{\sigma}(\alpha_i^{(b)} + 1)\mathsf{y}_0^{(b)}, \mathsf{y}_1^{(r)} > \Big\} \end{aligned} \tag{D.7}$$

also vanishes, this time provided $\alpha_i^{(b)} \neq -1, -2$. This procedure can be continued to arbitrary order to find that

$$P[\mathsf{y}^{(b)}; \mathsf{y}^{(r)}] \equiv 0 \tag{D.8}$$

except when $\alpha_i^{(b)}$ is integer. Equation (D.8) must hold since $P = \text{const}$ is incompatible with $(x - x_i)^{\alpha+k}$ unless const $= 0$. To translate the result (D.8) to $P[\hat{\mathsf{y}}; \mathsf{y}^{(r)}]$ we recall (6.49) that in constructing $\hat{\mathsf{y}}$ we truncate the big-solution expansion at $\mathcal{O}(|x - x_i|^{\alpha_i^{(b)}+k_i+1})$ so that only the Frobenius terms P_0, $P_1 \cdots P_{k_i} = 0$ can be shown to vanish. Therefore $P[\hat{\mathsf{y}}; \mathsf{y}^{(r)}] \to 0$ at a rate exceeding the small solution, which cannot contribute to the concomitant jump (6.41).

Appendix E

Running PEST3.4 on c.nersc.gov

The alterations of PEST3.3 to accommodate the matching-data variational method have been tagged with the string "aplet" in PEST3.4. These have affected mainly the routine ENT33 and more particularly the the source-term computation in the subroutine MATELT. In some repects, the version PEST3.4 is closer to the ideal-stability version PEST2, both sharing the same ideal-energy matrix calculation. However, the following routines have been written to extend PEST3.3 to PEST3.4:

CONCOM.F	for the concomitant jump (matching data).
DELWBB3.F	contribution to the symmetrized energy involving the prescribed solutions only.
DELWRB3.F	contribution to the symmetrized energy involving the response and prescribed solutions.
EXSOLX.F	extraction of the response solution.
FROBE34.F	determination of Frobenius coefficients and evaluation of the source term in the weak form.
NODE2.F	mesh construction.
PLTGRD2.F	tabulation of the ψ surfaces for graphical postprocessing.
SETRHS2.F	evaluation of the source term.
STORRB3.F	Simpson's quadrature routine used in source-term evaluation.

(E.1)

The input files are FOR20, FOR26, FORT.11 (which used to correspond to MAPDSK on the old b-machine) and FORT.43 (which used to be MPOUT1). The last two

routines contain the equilibrium data as produced by the "ZIO" routines (now called BZIO.F). We give here a example of the FOR26 file:

```
multi-tearing input file
 &modes
 lmax=302*4 lmin=302*-4 m=50 mdiv=2 mth=64   n=1.0
  jmax2=9  lsymz=.false.  lfunin=.false. lcirc=.false.
 &end
 &cplots
 lpmax=1  phi=0.0
 &end
 &debugs
 checkv=.false. checkd=.false.  checki=.f.
   check1 = .false. infwal=.false. wall=.true.  ke=.false.
  fast=.true.   symvac=.true.  lebc=.false.
 &end
 &vacdat
 aw=100.  bw=0. nsing=500 epsq=1.e-5 nout=50   delg=.04
 &end
 &shape
 a=-10.0 b=0.5  gext=1.0  f0=0.02 r=20.0
 &end
 &cprofl
 alphar=0.0 betar=0.0  delr=1.0  psi0r=1.0
 alphap=2.5 betap=4.0  dlp=1.0   psi0p=0.0
 betap = 4.0  p0=0.0  gamma=1.66666666667  il=1
 &end
 &vardat
 scale=1.0 varmin=1.0  varmax=4.5  nvar=1
 &end
 &resis
 lmsin=.true.  msin=2 3
```

```
psim(1)=2.0  mm=42 100  dlays=0.015  0.015   nodchk=.false.
maxis=10 fracem=0.25 faclay=.1  .10   lextra=.false. lsing=.true.
lcub=.false.  lmarg = .true.  lpstps=.true.   lsub=.true.
&end
&aplet
laplet=.true. lchkap = .false. lsmoth = .t. lplot = .false.
lplot2 = .f. dlayb = 0.9
alfmsh=1.0 1.8 1.8  1.0 1.0 widmsh=0.1 0.1 0.1 0.0 0.0
xsplus = 0. 0. 0. 0. 0. xsmnus = 0. 0. 0. 0. 0.
&end
&eigdat
liter=.false.
alam=-0.001 dtry=0.01 nsteps=3 epscon=1.e-5 epsmac=1.0e-12
&end
```

as taken from the double-resistive mode case of § 8.4.

The crucial input parameters include LMAX, LMIN and JMAX2, with LMAX – LMIN + 1 giving the number of Fourier modes, LMIN, LMIN + 1, $\cdots$ LMAX. It is strongly recommended to choose LMIN = – LMAX with JMAX2 = LMAX – LMIN + 1, since the latter gives the number of Fourier modes used to invert the surface Green matrix $\mathcal{G}^{-1}$. Therefore, compatibility between LMAX, LMIN and JMAX2 ensures that $(\mathcal{G}^{-1})^{-1} = \mathcal{G}$ is satisfied inspite of the truncation error in the Fourier expansion. In namelist RESIS, MSIN contains the resonant poloidal modes m_i. Setting for instance MSIN = 2 instead of MSIN = 2 3, allows to limit the matching data calculations to the rational surface where $q_i = 2$. The number of mesh nodes is given by MM. Because of Simpson's quadrature rule, PEST3.4 uses only tent functions. Therefore, LCUB should be .FALSE. at all times.

Setting LAPLET = .FALSE. in namelist APLET switches from PEST3.4 to PEST3.3, LCHKAP produces tables of operators (for debugging), LSMOTH suppresses singularities in the source term which are due to some inaccuracy in the equilibrium data. From experience, LSMOTH can be set to .FALSE. in the zero-β cases whereas .TRUE. is essential for the finite-β case. The switch LPLOT deac-

tivates the graphical routines TV80LIB which are not fully supported on machine C and therefore not useful. As a little consolation, LPLOT2 = .TRUE. produces tables which can be easily converted to plots using Mac software for instance. The supports of the prescribed elements are set by DLAYB (< 1), which corresponds to $\delta_i / \min_{j=i\pm1} |x_i - x_j|$. The mesh grading exponents are given by ALFMSH ($\equiv \gamma_i$ of § 7.5) and the width of the scaled zones by WIDMSH ($\equiv w_i$). Finally the two set of parameters XSPLUS and XSMNUS correspond to s_+ and s_- respectively, which allow redefinition of the big solution.